

Dissertation zur Erlangung des Doktorgrades
der Fakultät für Chemie und Pharmazie
der Ludwig-Maximilians-Universität München

Novel Phosphorus (Oxo)Nitriles at Extreme Conditions

Dominik Oskar Baumann

aus

München, Deutschland

2015

Erklärung

Diese Dissertation wurde im Sinne von §7 der Promotionsordnung vom 28. November 2011 von Herrn Prof. Dr. Wolfgang Schnick betreut.

Eidesstattliche Versicherung

Diese Dissertation wurde eigenständig und ohne unerlaubte Hilfe erarbeitet.

München, 05.08.2015

.....

(Dominik Baumann)

Dissertation eingereicht am

07.05.2015

1. Gutachter:

Prof. Dr. Wolfgang Schnick

2. Gutachter:

Prof. Dr. Hubert Huppertz

Mündliche Prüfung am

15.06.2015

To my family

Nature uses only the longest
threads to weave her patterns,
so each small piece of her
fabric reveals the organization
of the entire tapestry.

(Richard Feynman)

Mein ganz besonderer Dank gebührt Prof. Dr. Wolfgang Schnick für die Möglichkeit meine Dissertation in seinem Arbeitskreis anzufertigen. Die vielfältigen Mittel und die Freiheit den Fragestellungen eigenständig auf den Grund zu gehen waren für die Anfertigung dieser Arbeit unverzichtbar. Vielen Dank auch für die Anregungen und lehrreichen Fachgespräche.

Prof. Hubert Huppertz danke ich für die Bereitschaft das Koreferat für diese Arbeit zu übernehmen.

Prof. Dr. Oliver Oeckler, Prof. Dr. Dirk Johrendt, Prof. Dr. Hans-Christian Böttcher, und Prof. Dr. Achim Hartschuh danke ich für ihre Bereitschaft als Teil der Prüfungskommission für die mündliche Prüfung zur Verfügung zu stehen.

Prof. Dr. Oliver Oeckler, Dr. Constantin Hoch und Dr. Thomas Bräuniger möchte ich auch für die vielen interessanten und ausführlichen Fachgespräche und weiteren Unterhaltungen danken.

Besonderer Dank gilt meinem Vorgänger Dr. Stefan Sedlmaier, der mir nicht nur die Thematik näher brachte sondern mir vieles von dem was diese Arbeit erfolgreich gemacht hat beibrachte.

Ebenso danke ich meinen Praktikanten Edgar Uhl, Thomas Hörner, Simon Kloß und Helen Funk, die mich während meiner Zeit mit viel Einsatz unterstützt haben.

Ich danke allen Kollegen mit denen ich an ESRF und DESY zusammenarbeiten und von denen ich viel lernen durfte: Dr. Ashkan Salamat, Dr. Sylvain Petitgirard, Dr. Zuzana Konôpková, Dr. Hanns-Peter Liermann, Dr. Wolfgang Morgenroth und allen voran natürlich Dr. Sebastian Schneider.

Herrn Christian Minke gilt besonderer Dank für die vielen Messungen an Rasterelektronenmikroskop und NMR-Spektrometer auf die ich nie lange warten musste.

Herrn Thomas Miller danke ich für die Betreuung der Pulverdiffraktometer und die Bastelstunden an selbigen, sowie für das Messen vieler Einkristalle, Herrn Wolfgang Wunschheim danke ich für die Instandhaltung der Rechner und das Lösen so manchen Computerproblems.

Frau Olga Lorenz danke ich ganz herzlich für ihre organisatorische Tätigkeit und außergewöhnliche Hilfsbereitschaft bei allen Arten von Problemen.

Ich danke Dr. Tobias Rosenthal und Herrn Lukas Neudert für die zahlreichen Stunden die sie mit meinen Proben am TEM verbracht haben und die damit verbundene Aufklärung der strukturellen Eigenheiten der Phosphoroxonitride.

Dr. Peter Mayer danke ich für die Messung vieler sehr kleiner Einkristalle, Frau Marion Sokoll danke ich für die Aufnahme der IR-Spektren.

Dem Pressenteam, insbesondere Florian Mr. Fixit Pucher, Sebastian Schneider, Stefan Sedlmaier und Alexey Marchuk danke ich für die gute Zusammenarbeit.

Meinen ehemaligen und aktuellen Laborkollegen Florian Pucher, Cora Hecht, Stefan Sedlmaier, Sebastian Schneider, Tobias Rosenthal, Simon Welzmler, Alexey Marchuk, Frank Tambornino, Matthias Wörsching, Eva-Maria Bertschler und Simon Kloth danke ich für die unvergessliche Zeit im Labor D2.110.

Meinen Nachfolgern im Bereich der Nitridophosphate Eva-Maria Bertschler und Simon Kloth wünsche ich alles Gute und viel Spaß für ihre weitere Doktorarbeit.

Ich danke natürlich auch allen bisher nicht erwähnten Mitgliedern der Arbeitskreise Schnick, Johrendt, Lotsch, Schmedt auf der Günne, Oeckler und Hoch für die großartige Stimmung im zweiten Stock.

Meinen Eltern, Geschwistern und meine Freundin Anna kann ich gar nicht genug danken. Ohne euch wäre ich nicht wo ich jetzt bin.

Contents

1	Introduction	1
2	An Unprecedented AB₂ Tetrahedra Network Structure Type in a High-Pressure Phase of Phosphorus Oxonitride PON	17
2.1	Introduction with Results and Discussion	18
2.2	References	22
3	A High-Pressure Polymorph of Phosphorus Oxonitride PON with Coesite Structure	25
3.1	Introduction with Results and Discussion	26
3.2	References	32
4	A High-Pressure Polymorph of Phosphorus Nitride Imide HP₄N₇ Representing a New Framework Topology	37
4.1	Introduction	38
4.2	Experimental Section	39
4.2.1	Synthesis of P ₃ N ₅	39
4.2.2	Synthesis of β-HP ₄ N ₇	40
4.2.3	Spectroscopic Analysis	40
4.2.4	Crystal Structure Analysis	41
4.3	Results and Discussion	41
4.3.1	Synthesis	41

4.3.2	Crystal Structure of β -HP ₄ N ₇	42
4.3.3	Powder X-Ray Diffraction and Rietveld Refinement	48
4.3.4	Spectroscopic Methods	49
4.4	Conclusion	51
4.5	References	51
5	Pentacoordinated Phosphorus in a High-Pressure Polymorph of Phosphorus Nitride Imide P₄N₆(NH)	55
5.1	Introduction with Results and Discussion	56
5.2	References	62
6	Li₁₄(PON₃)₂O – A Non-Condensed Oxonitridophosphate Oxide	67
6.1	Introduction	68
6.2	Results and Discussion	69
6.3	Conclusions	75
6.4	Experimental Section	76
6.4.1	General	76
6.4.2	Powder X-Ray Diffraction	76
6.4.3	Spectroscopic Methods	77
6.5	References	77
7	Summary	81
8	Discussion and Outlook	85
8.1	High-Pressure Phases of Phosphorus Nitrides	85
8.2	Lithium Oxonitridophosphates	89
8.3	References	91
A	Supporting Information for Chapter 2	93

A.1	Experimental Details of the HP/HT-Synthesis of δ -PON	93
A.2	Information on the Data Collection and Structure Elucidation of δ -PON .	94
A.3	Crystallographic Data for δ -PON	95
A.4	Solid-State NMR and FTIR Spectra	98
A.5	Cycle Class Sequence of the δ -PON Network	99
A.6	Symmetry Relationship to a Predicted SiO ₂ Modification	99
A.7	References	101
B	Supporting Information for Chapter 3	103
B.1	Experimental Details of the HP/HT-Synthesis of <i>coe</i> -PON	103
B.2	Information on Data Collection and Structure Elucidation of <i>coe</i> -PON . .	103
B.3	Additional Crystallographic Data for <i>coe</i> -PON	105
B.4	Details of the Rietveld Refinement	107
B.5	Comparison of Coesite SiO ₂ and PON	108
B.6	Solid-State NMR and FTIR Spectra	109
B.7	Detailed Rietveld Plot	110
B.8	Temperature Dependent Powder X-ray Diffraction	111
B.9	Details on the DFT Calculations	112
B.10	References	117
C	Supporting Information for Chapter 4	119
C.1	Additional Crystallographic Data for β -HP ₄ N ₇	119
C.2	Details of the Rietveld Refinement	120
C.3	Solid-State NMR Spectrum	121
C.4	Diffuse Reflectance Spectroscopy	121
C.5	Detailed Rietveld Plot	122
C.6	Temperature Dependent Powder X-ray Diffraction	123

D	Supporting Information for Chapter 5	125
D.1	Experimental Details of the HP/HT-Synthesis of γ -HP ₄ N ₇	125
D.2	Information on the Data Collection and Structure Elucidation of γ -HP ₄ N ₇	126
D.3	Crystallographic Data for γ -HP ₄ N ₇	127
D.4	Details of the Rietveld Refinement	130
D.5	Solid-State NMR and FTIR Spectra	131
D.6	Energy Dispersive X-Ray Spectroscopy	133
D.7	References	133
E	Supporting Information for Chapter 6	135
E.1	Additional Crystallographic Data for Li ₁₄ (PON ₃) ₂ O	135
E.2	⁷ Li Solid-State NMR Spectrum	135
E.3	Detailed Rietveld Plot	136
F	Miscellaneous	137
F.1	List of Publications	137
F.1.1	Publications Within this Thesis	137
F.1.2	Publications Beyond this Thesis	139
F.2	Contributions to Conferences	140
F.3	Deposited Crystallographic Data	142
F.4	Curriculum Vitae	143

List of Figures

1.1	Schematic structure of the Earth.	2
1.2	Phase diagrams of SiO ₂ (a) and PON (b).	5
1.3	Unique nitridophosphate substructures of different dimensionalities.	7
2.1	Observed and calculated powder diffraction pattern of δ -PON as well as position of Bragg reflections and difference profile.	19
2.2	Crystal structure of δ -PON. View along [010].	20
2.3	Topological representation of the crystal structure of δ -PON. Right: section from the crystal structure showing the ladder-like arrangement of 4-rings.	21
3.1	Observed and calculated powder diffraction pattern of <i>coe</i> -PON as well as difference profile. Black vertical bars represent the positions of Bragg reflections.	27
3.2	Crystal structure of <i>coe</i> -PON in polyhedral representation. View along [101].	29
3.3	Atomic arrangement and bond lengths in <i>coe</i> -PON.	29
3.4	Temperature dependent powder X-ray diffraction data for <i>coe</i> -PON in air.	31
4.1	Crystal structure of β -HP ₄ N ₇ in polyhedral representation.	45
4.2	Atomic arrangement of P, N, H and bond lengths in β -HP ₄ N ₇ . Displacement ellipsoids are displayed at the 90 % probability level.	45
4.3	Topological relation between β -HPN ₂ (left) and β -HP ₄ N ₇ (right).	46

4.4	Observed and calculated powder diffraction pattern of β -HP ₄ N ₇ as well as position of Bragg reflections and difference profile.	48
4.5	FTIR spectrum of β -HP ₄ N ₇	49
4.6	³¹ P MAS NMR spectrum of β -HP ₄ N ₇	50
5.1	Crystal structure of γ -P ₄ N ₆ (NH). View along [110].	58
5.2	Coordination polyhedra and bond lengths around the two crystallographically distinct P atoms.	59
5.3	Observed and calculated powder diffraction pattern of γ -P ₄ N ₆ (NH) as well as difference profile. Black and grey vertical bars represent the positions of Bragg reflections of γ -P ₄ N ₆ (NH) and hexagonal BN, respectively.	61
6.1	Crystal structure of Li ₁₄ (PON ₃) ₂ O.	69
6.2	Observed and calculated powder diffraction pattern of Li ₁₄ (PON ₃) ₂ O as well as position of Bragg reflections and difference profile. Reflections from an unknown side phase are marked with asterisks.	71
6.3	Interatomic distances / pm in Li ₁₄ (PON ₃) ₂ O.	73
6.4	FTIR spectrum of Li ₁₄ (PON ₃) ₂ O.	74
6.5	³¹ P solid-state NMR spectrum of Li ₁₄ (PON ₃) ₂ O at 20 kHz MAS.	74
A.1	³¹ P-solid-state NMR-spectrum of δ -PON.	98
A.2	³¹ P-solid-state NMR-spectrum of cristobalite PON.	98
A.3	FTIR spectrum of δ -PON.	99
A.4	Bärnighausen tree showing the symmetry relation between δ -PON and the predicted SiO ₂ phase from the PCOD database.	100
B.1	³¹ P-solid-state NMR spectrum of <i>coe</i> -PON.	109
B.2	FTIR spectrum of <i>coe</i> -PON.	109

B.3	Observed and calculated powder diffraction pattern of <i>coe</i> -PON as well as positions of Bragg reflections and difference profile.	110
B.4	Temperature dependent powder X-ray diffraction for <i>coe</i> -PON.	111
B.5	Different O/N arrangements used for the DFT calculations.	113
B.6	Energy-volume diagram for anion ordering of the energetically lowest models of cristobalite(<i>ctb</i>)-PON and the different coesite(<i>coe</i>)-PON models.	115
B.7	Enthalpy-pressure diagram for the high pressure phase transition of PON from the energetically most stable cristobalite (<i>ctb</i>) model to the different coesite(<i>coe</i>) models as obtained by fitting the Murnaghan equation of state from the energy-volume diagram.	116
C.1	^1H -solid-state NMR-spectrum of $\beta\text{-HP}_4\text{N}_7$	121
C.2	Tauc Plot ($n = \frac{1}{2}$) for $\beta\text{-HP}_4\text{N}_7$	121
C.3	Observed and calculated powder diffraction pattern of $\beta\text{-HP}_4\text{N}_7$ as well as position of Bragg reflections and difference profile.	122
C.4	Temperature dependent powder X-ray diffraction for $\beta\text{-HP}_4\text{N}_7$	123
D.1	^{31}P -solid-state NMR-spectrum of $\gamma\text{-HP}_4\text{N}_7$	131
D.2	^1H -solid-state NMR-spectrum of $\gamma\text{-HP}_4\text{N}_7$	132
D.3	FTIR spectrum of $\gamma\text{-HP}_4\text{N}_7$	132
E.1	^7Li -solid-state NMR-spectrum of $\text{Li}_{14}(\text{PON}_3)_2\text{O}$	135
E.2	Observed and calculated powder diffraction pattern of $\text{Li}_{14}(\text{PON}_3)_2\text{O}$ as well as position of Bragg reflections and difference profile.	136

1 Introduction

Understanding the composition of the Earth and other planets has been a goal for many generations of scientists. The rapid advances in analytical techniques during the 20th century allowed geoscientists and chemists to describe the physical and chemical processes in rocks and create a detailed model of Earth's interior (Figure 1.1). Earth's crust, which extends from the surface to depths of 50–100 km^[1] is the only part of Earth's interior that is experimentally accessible. It is characterized by a large variety of minerals and chemical elements which have separated from the lower layers due to chemical incompatibility.^[2] It is therefore rich in elements that are comparatively rare on a cosmological scale, and has thus fueled the technical progress of humanity for millenia.

In contrast, Earth's mantle, separated from the crust by the Mohorovičić discontinuity,^[3] is presumed to be more homogenous in its composition. The depth combined with the extreme pressures and temperatures have precluded any direct sampling experiments to date. Consequently, most information about the mantle is based on material that has been transported to the surface combined with seismic investigations, which limits knowledge of the deeper layers. Assuming that due to their similar formation processes the overall composition of the Earth and other rocky planets of the inner solar system is similar to that of chondritic meteorites, the chemical composition of the mantle can be roughly inferred.^[4,5] Its overall composition is best described by the hypothetical mineral pyrolite, which has been established by Ringwood.^[6,7]

Current evidence suggests that silicates make up most of Earth's crust and mantle.^[8] They have therefore been the principal target of geochemical research. Due to the immense temperatures and pressures inside the Earth, their behavior at these extreme conditions are of particular importance. In many cases the involved minerals undergo chemical reac-

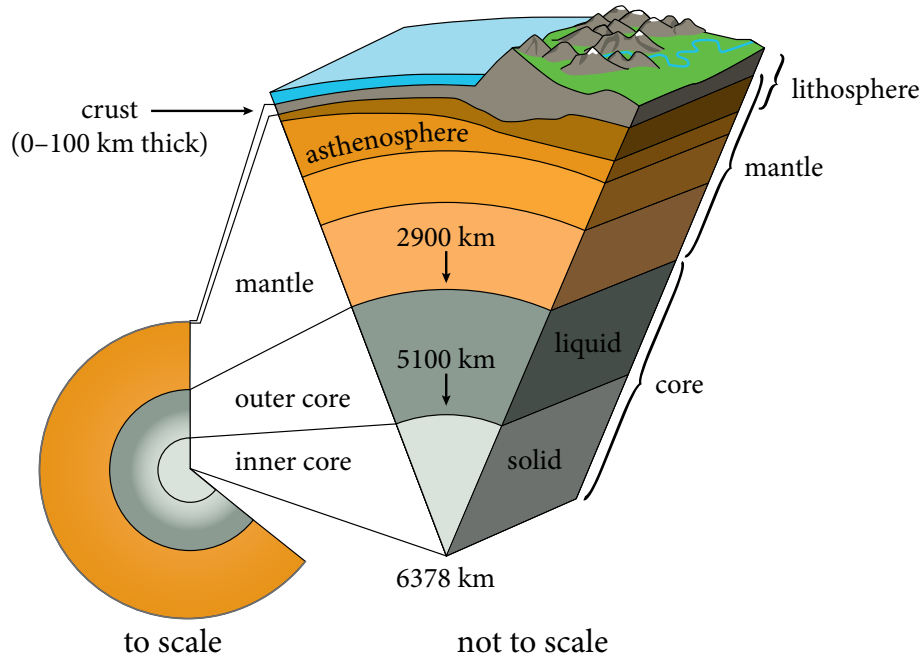


Figure 1.1: Schematic structure of the Earth (adapted from [1]).

tions or phase transitions. This process, called metamorphism, leads to the formation of metamorphic rocks. Many advances in past decades, particularly the development of high-pressure techniques, both hydraulic large volume presses^[9,10] and diamond anvil cells,^[11] combined with new advanced X-ray techniques allowed unprecedented insights into the behavior of minerals at high pressures.^[12]

Most of the silicon in the mantle is believed to be contained in silicates. At the comparatively low pressures of the upper mantle (< 410 km depth; $p < 14$ GPa) it is believed to be composed of mostly olivine ($(\text{Mg,Fe})_2\text{SiO}_4$), garnet ($(\text{Mg,Fe,Ca})_2\text{Al}_3(\text{SiO}_4)_3$), orthopyroxene ($(\text{Mg,Ca})\text{SiO}_3$) and clinopyroxene ($(\text{Mg,Fe})\text{SiO}_3$).^[13] The higher pressure at increasing depth allows orthopyroxene and clinopyroxene to transform into garnet by incorporation of Mg and Si into the octahedral sites.^[14,15] At a depth of approximately 410 km, the beginning of the transition zone, olivine undergoes a phase transformation to wadsleyite, which is indicated by a pronounced seismic discontinuity.^[16] Wadsleyite further transforms to the spinel-type ringwoodite at pressures above 17.5 GPa, corresponding to a depth

of about 520 km.^[17] Below a depth of 660 km at pressures exceeding 23 GPa, the boundary of the lower mantle, ringwoodite and garnet both break down, forming rock-salt structured ferropericlase ((Mg,Fe)O),^[18] magnesium silicate perovskite ((Mg,Fe,Al)(Si,Al)O₃) and calcium silicate perovskite (CaSiO₃).^[19,20] Due to the fact that silicon changes from a fourfold to a sixfold coordination, this transformation results in a large difference in densities, leading to a further seismic discontinuity. Recent evidence suggests that silicate perovskite undergoes another phase transition at the extreme conditions close to the core-mantle boundary (> 2600 km depth; $p > 125$ GPa),^[21] forming a post-perovskite phase in the process. This phase forms a layered structure composed of alternating layers of edge- and corner-sharing SiO₆ octahedra and Mg²⁺ ions.^[22,23] This process might also explain the seismic D'' discontinuity, which is found about 200 km above the core-mantle boundary.^[24]

While SiO₂ itself is not believed to be a major component of the mantle, quartz is considered to be one of the most abundant minerals in the crust, being only surpassed by the feldspar group.^[25] Due to its geological significance as well as industrial importance, extensive research has been performed on its properties and transformations. Since the phase diagram of SiO₂ (Figure 1.2a) is well known, it is possible to draw conclusions on the geological history of rocks by examining the silica crystallites. The high-pressure phases coesite^[26–28] and stishovite,^[29,30] for example, can be used as indicators for rocks having undergone ultrahigh-pressure metamorphism either by subduction or impact events.^[31–33] Similarly, seifertite, an α -PbO₂-structured polymorph of SiO₂, has been found in heavily shocked martian and lunar meteorites.^[34–36] In recent years, further high-pressure phases of SiO₂ have been discovered by synthetic chemists. These include a post-quartz^[37] as well as a pyrite-type^[38,39] modification. Recent theoretical investigations predict the existence of further phases at even higher pressures, such as cotunnite-type (PbCl₂-structured) as well as Fe₂P-type polymorphs.^[40,41] While the pressures necessary to synthesize these

phases exceed even those prevalent in Earth's lower mantle, these findings might still be relevant in understanding the interior of larger terrestrial exoplanets and gas giants.^[42]

Phosphorus is the 12th most abundant element on Earth. Most of Earth's phosphorus is, however, assumed to be accumulated in the core (3500 $\mu\text{g/g}$), whereas its abundance in the mantle and crust is relatively low (90 $\mu\text{g/g}$).^[43] Being a building block of DNA, RNA and ATP, it is an essential nutrient for all life. This makes it particularly suited for use in fertilizers, for which up to 90 % of all mined phosphorus is used. Therefore, systematic investigations into the phosphorus containing minerals and related phases are of great relevance. Phosphate containing rocks, particularly phosphorite, which is mainly composed of the mineral apatite, are mined extensively.^[44,45] Approximately 220 million metric tons of phosphate rock were produced in 2014 worldwide.^[46] While this represents only 0.32 % of the global reserves as estimated by the United States Geological Survey, a steady increase in demand will lead to depletion of the conventional phosphorus sources by 2150. Uncertainty about the true amount of phosphorus rock that can be extracted reliably leads to concerns that *peak phosphorus* will be reached as soon as 2035.^[47,48] Understanding the geological properties of phosphate containing minerals is therefore of extreme economic importance, since it could allow the discovery of new sources of phosphorus.

Another factor that contributed to renewed interest in the solid-state chemistry of phosphorus compounds is its similarity to silicon. Both elements form mostly covalent bonds to O and N and occur in tetrahedral coordination almost exclusively at ambient pressure. Substituting Si with P in conjunction with another element leads to phases that are isoelectronic to silicates. Particularly compounds that are isoelectronic to SiO_2 , such as BPO_4 ,^[49] AlPO_4 ,^[50] GaPO_4 ,^[50] BeSO_4 ^[51,52] and PON ^[53] have attracted interest. Their properties closely resemble that of silica and any insights into their chemical and physical behavior can also partially be transferred to SiO_2 . However, since phosphates are of minor geological importance, their high-pressure chemistry has not yet been exhaustively investigated. Pellicer-Porres *et al.* reported on a CaCl_2 -like modification, which was synthesized in a

laser-heated diamond anvil cell at 76 GPa.^[54] This is the only report of hexacoordinate phosphorus in any polymeric inorganic structure to date.

In the light of this lack of knowledge about phosphates at higher pressures, further research into these and related materials seems reasonable. Pseudobinary and multinary phosphorus nitrides and oxonitrides in particular show great promise for such investigations. Due to the fact that Si and O can be substituted by the isosteric atom combination P–N, they are closely related to silicates. This similarity can be further expanded if the substitution of O^{2-} by the isosteric NH^{2-} is considered. The compounds PON and $\text{PN}(\text{NH})$ are therefore extremely similar to silica SiO_2 .^[55] Both adopt the β -cristobalite structure,^[56–58] which occurs in a high-temperature polymorph of SiO_2 , at ambient conditions. Despite their chemical similarity, marked differences in the behavior of these three compounds emerge at high-pressure conditions (Figure 1.2b). While SiO_2 transforms to coesite^[26–28] at first and to stishovite^[29,30] at significantly higher pressures, PON assumes α -quartz^[59] and moganite-type structures.^[60] $\text{PN}(\text{NH})$ on the other hand transforms to a distortion variant of the β -cristobalite structure above 6 GPa but shows no indication of further transformations up to 18 GPa.^[61]

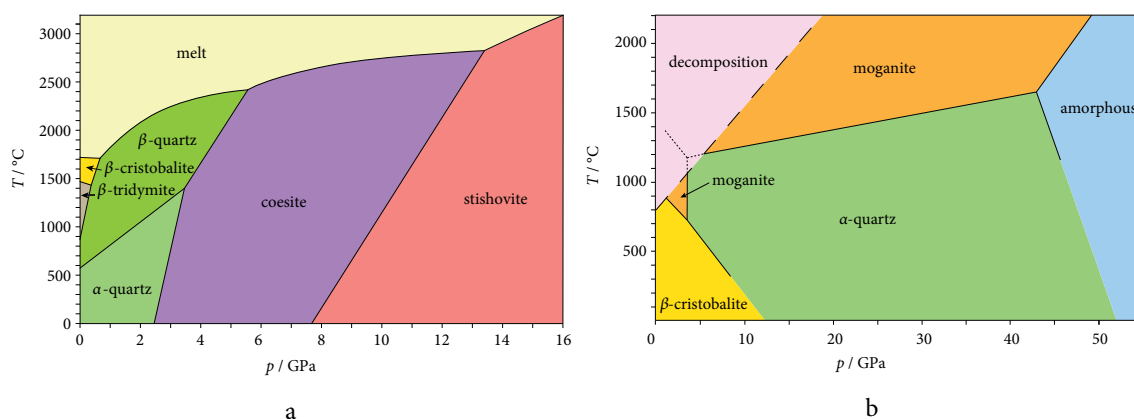


Figure 1.2: Phase diagrams of SiO_2 (a) and PON (b). Adapted from Müller^[62] and Marchand *et al.*,^[56] respectively.

Other (oxo)nitridophosphates display a variety of structure types that is comparable to that of silicates. Low degrees of condensation are found in the *ortho*-nitridophosphate Li_7PN_4 ,^[63,64] which contains the isolated PN_4^{7-} ion. It can formally be derived from imidophosphoric triamide $\text{P}(\text{NH})(\text{NH}_2)_3$ by sevenfold deprotonation. Mg_2PN_3 , Ca_2PN_3 ,^[65,66] Zn_2PN_3 ,^[67] and the oxonitridophosphate $\text{Li}_2\text{PO}_2\text{N}$ ^[68] correspond to a degree of condensation $\kappa = 1/3$, which makes them very similar to single chain inosilicates like pyroxenes. The same degree of condensation is also represented by the cyclo-nitridotriphosphate $\text{Li}_{12}\text{P}_3\text{N}_9$,^[69] which can be considered to be related to the cyclotrisilicates in the benitoite-group.^[70] While there are no examples of silicate-analogous layered (oxo)nitridophosphates, the compound $\text{Li}_{10}\text{P}_4\text{N}_{10}$ shares the same degree of condensation of $2/5$. However, instead of a layered structure that could be expected for this composition, $\text{Li}_{10}\text{P}_4\text{N}_{10}$ is composed of isolated complex P_4O_{10} -like $\text{P}_4\text{N}_{10}^{10-}$ ions (Figure 1.3a).^[71]

The degree of condensation $\kappa = 1/2$, which is representative of framework silicates and zeolites is found in a range of nitridophosphates and oxonitridophosphates. Structurally simple compounds include the aforementioned PON and $\text{PN}(\text{NH})$,^[57,58] as well as the ternary phases LiPN_2 ,^[72] NaPN_2 ,^[73] and CuPN_2 ,^[74] all of which crystallize in the β -cristobalite structure. The alkaline earth nitridophosphates CaP_2N_4 ^[75] and SrP_2N_4 ^[76] adopt a megacalsilite type structure which is also found in CdP_2N_4 .^[77] BeP_2N_4 crystallizes in a variant of the phenakite structure.^[78] However, due to the different occupation of the cation positions, it should be considered a framework nitride ($\kappa = 1/2$), whereas phenakite itself (Be_2SiO_4 , $\kappa = 1/4$) is classified as an *ortho*-silicate.^[79] The lower density types of framework silicates also have nitridophosphate counterparts. NPO ($\text{Li}_{12-x}\text{H}_{x-y+z}[\text{P}_{12}\text{O}_y\text{N}_{24-y}]\text{X}_z$ ($\text{X} = \text{Cl}, \text{Br}$)),^[80,81] NPT ($\text{Ba}_{19}\text{P}_{36}\text{O}_{6+x}\text{N}_{66-x}\text{Cl}_{8+x}$ ($x \approx 4.54$))^[82] and $\text{Ba}_3\text{P}_5\text{N}_{10}\text{X}:\text{Eu}^{2+}$ ($\text{X} = \text{Cl}, \text{Br}, \text{I}$)^[83] represent zeolites with $\kappa = 1/2$, a substance class that is mostly populated by aluminosilicates. $\text{P}_4\text{N}_4(\text{NH})_4(\text{NH}_3)$ ^[84] is similar to clathrasils,^[85] a class of framework silicates with inaccessible pores, the most prominent member of which is melanophlogite.^[86]

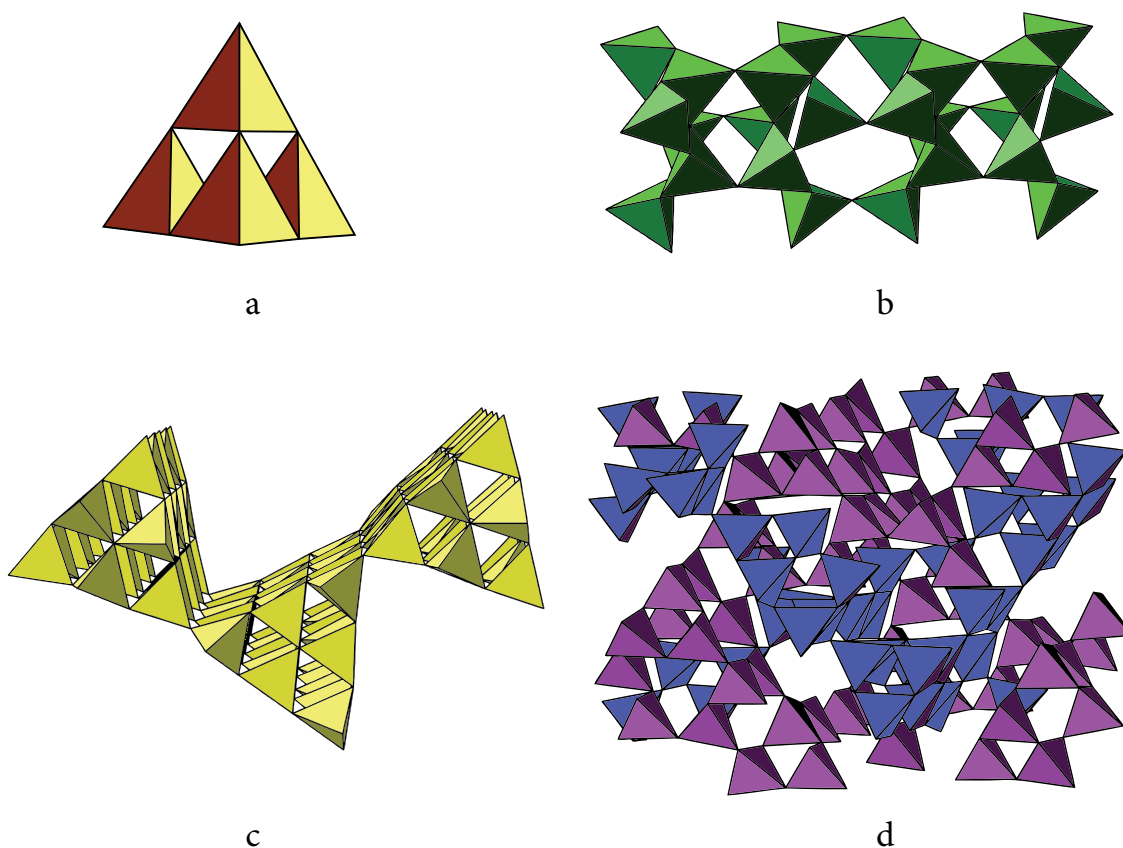


Figure 1.3: Unique nitridophosphate substructures of different dimensionality. **a:** isolated $\text{P}_4\text{N}_{10}^{10-}$ ion in $\text{Li}_{10}\text{P}_4\text{N}_{10}$ (0D); **b:** $\text{P}_{12}\text{N}_{17}\text{O}_9^{9-}$ columns in $\text{Ba}_6\text{P}_{12}\text{N}_{17}\text{O}_9\text{Br}_3$ (1D); **c:** corrugated $\text{P}_3\text{N}_5\text{O}^{2-}$ layers in $\text{SrP}_3\text{N}_5\text{O}$ (2D); **d:** interpenetrating interrupted $\text{P}_6\text{O}_3\text{N}_{10}^{6-}$ networks in $\text{CaMg}_2\text{P}_6\text{O}_3\text{N}_{10}$ (3D).

What separates nitridophosphates from silicates, however, is the higher maximum degree of condensation afforded by the higher charge of N^{3-} compared to O^{2-} . Combined with the higher structural flexibility of N^{3-} , which readily assumes three- and fourfold coordination,^[87] this leads to a wide range of crystal structures that could not be realized in silica-based compounds. The maximum degree of condensation is realized in the parent compound P_3N_5 with a κ of $\frac{3}{5}$. Its high-pressure polymorph $\gamma\text{-P}_3\text{N}_5$ noticeably contains phosphorus both in tetrahedral as well as in quadratic pyramidal coordination.^[88,89] Further frameworks with very high degrees of condensation are formed by the compounds MP_4N_7 ($M = \text{H}, \text{Na}, \text{K}, \text{Rb}, \text{Cs}$)^[90–92] and $\text{M}_3\text{P}_6\text{N}_{11}$ ($M = \text{Na}, \text{K}, \text{Rb}, \text{Cs}$).^[93–95]

Furthermore, combination of N^{3-} with O^{2-} or the isoelectronic NH^{2-} allows for a wide range of unique structure types with unexpected dimensionality. While the degree of condensation of one-dimensional silicates ranges from $\frac{1}{3}$ (e.g. wollastonite CaSiO_3)^[96] to $\frac{2}{5}$ (e.g. agrellite $\text{NaCa}_2\text{Si}_4\text{O}_{10}\text{F}$)^[97] the column-type nitridophosphate $\text{Ba}_6\text{P}_{12}\text{N}_{17}\text{O}_9\text{Br}_3$ ^[98] (Figure 1.3b) is much more condensed ($\kappa = \frac{6}{13} \approx 0.46$). Similarly, the layered oxonitridophosphates $\text{Sr}_3\text{P}_6\text{O}_6\text{N}_8$ ^[99] and $\text{Ba}_3\text{P}_6\text{O}_6\text{N}_8$ ^[100] ($\kappa = \frac{3}{7} \approx 0.43$) exhibit a degree of condensation between those of classical layered silicates and framework structures. $\text{SrP}_3\text{N}_5\text{O}$ ^[101] (Figure 1.3c) as well as the imidonitridophosphates $\text{MgH}_4\text{P}_6\text{N}_{11}$ and $\text{CaH}_4\text{P}_6\text{N}_{11}$ ^[102] even exhibit a degree of condensation of $\frac{1}{2}$, which is normally found in framework silicates. The structural diversity of phosphorus oxonitrides is also evident in the interrupted framework compounds $\text{H}_3\text{P}_8\text{O}_8\text{N}_9$ ($\kappa = \frac{8}{17}$)^[103] and $\text{CaMg}_2\text{P}_6\text{O}_3\text{N}_{10}$ ($\kappa = \frac{6}{13}$)^[104] which are comprised of both all-side vertex sharing Q^4 - as well as only threefold-linking Q^3 tetrahedra. Interestingly, $\text{CaMg}_2\text{P}_6\text{O}_3\text{N}_{10}$ features two independent $\text{P}_6\text{O}_3\text{N}_{10}^{6-}$ networks, which are interpenetrating (Figure 1.3d).

The multitude of possible crystal structures, which has been illustrated above, allows for (oxo)nitridophosphates to display many properties that could allow technical application. Nitridic zeolites like NPO and NPT could potentially be used in industrial applications dominated by silica based zeolites such as gas separation or catalysis, whereas alkaline earth nitridophosphates, such as $\text{Ba}_3\text{P}_5\text{N}_{10}\text{X}:\text{Eu}^{2+}$ ($\text{X} = \text{Cl}, \text{Br}, \text{I}$) and MP_2N_4 ($\text{M}=\text{Ca}, \text{Sr}, \text{Ba}$)^[75] have already been shown to be capable luminescent materials. The high lithium ion conductivity of some oxonitridophosphates, such as $\text{Li}_2\text{PO}_2\text{N}$ or *LiPON*,^[105] which is already commercially used as an electrolyte in thin film cells,^[106] makes them promising materials for the construction of next generation solid-state lithium-ion batteries. Possible high-pressure phases of phosphorus nitrides, particularly those containing hexacoordinate phosphorus, might display useful mechanical properties, particularly high hardness and bulk modulus. Similar behavior has been observed for SiO_2 ^[107–109] and Si_3N_4 ,^[110–112] the high-

pressure polymorphs of which are considered to be among the hardest oxides and nitrides, respectively.

The main objectives of this thesis were the synthesis and structural characterization of high-pressure phases of nitridophosphates as well as new lithium oxonitridophosphates. This includes establishing suitable reaction conditions in both the pressure and the temperature regime. The emphasis of the synthetic parts lies on the establishment of new synthesis pathways to phases that are otherwise not readily accessible. This includes developing new synthetic strategies such as high-temperature deprotonation syntheses, the use of amorphous precursor compounds or in situ synthesis of high-pressure phases. Several methods are used in conjunction to identify and structurally characterize the compounds. X-ray diffraction on powders and single crystals is used as the main means of structure determination. It is supplemented by ^{31}P , ^1H and ^7Li MAS NMR as well as FTIR spectroscopy in order to offset the inherent limitations of the method. One of the aims of this thesis is also the comparison of the newly determined crystal structures to other new or well-known structure types. To this end, topological analyses were carried out and structural relations established. Furthermore, DFT calculations are used to determine the stability regions of different phases.

References

- [1] W. J. Kious, R. I. Tilling, *This Dynamic Earth: The Story of Plate Tectonics*, United States Geological Survey, Reston, VA, USA, **1996**, p. 4.
- [2] A. W. Hofmann, *Earth Planet. Sci. Lett.* **1988**, 90, 297.
- [3] R. Carbonell, A. Levander, R. Kind, *Tectonophysics* **2013**, 609, 353.
- [4] W. McDonough, S.-S. Sun, *Chem. Geol.* **1995**, 120, 223.

-
- [5] C. J. Allègre, J.-P. Poirier, E. Humler, A. W. Hofmann, *Earth Planet. Sci. Lett.* **1995**, 134, 515.
- [6] A. E. Ringwood, *J. Geophys. Res.* **1962**, 67, 857.
- [7] A. E. Ringwood, *J. Geophys. Res.* **1962**, 67, 4473.
- [8] A. E. Ringwood, *Geochim. Cosmochim. Acta* **1991**, 55, 2083.
- [9] H. Hall in *Chemical Experimentation Under Extreme Conditions, Techniques of Chemistry*, (Eds.: A. Weissberger, B. Rossiter), John Wiley & Sons, Hoboken, NJ, USA, **1980**.
- [10] H. Huppertz, *Z. Kristallogr.* **2004**, 219, 330.
- [11] R. Boehler, *Rev. Geophys.* **2000**, 38, 221.
- [12] F. J. Manjón, D. Errandonea, *Phys. Status Solidi B* **2009**, 246, 9.
- [13] D. J. Frost, *Elements* **2008**, 4, 171.
- [14] A. E. Ringwood, *Earth Planet. Sci. Lett.* **1967**, 2, 255.
- [15] G. R. Helffrich, B. J. Wood, *Nature* **2001**, 412, 501.
- [16] T. Katsura, H. Yamada, O. Nishikawa, M. Song, A. Kubo, T. Shinmei, S. Yokoshi, Y. Aizawa, T. Yoshino, M. J. Walter, E. Ito, K.-I. Funakoshi, *J. Geophys. Res.: Solid Earth* **2004**, 109, B02209.
- [17] T. Yoshino, G. Manthilake, T. Matsuzaki, T. Katsura, *Nature* **2008**, 451, 326.
- [18] A.-L. Auzende, J. Badro, F. J. Ryerson, P. K. Weber, S. J. Fallon, A. Addad, J. Siebert, G. Fiquet, *Earth Planet. Sci. Lett.* **2008**, 269, 164.
- [19] E. Knittle, R. Jeanloz, *Science* **1987**, 235, 668.
- [20] M. Murakami, Y. Ohishi, N. Hirao, K. Hirose, *Nature* **2012**, 485, 90.
- [21] G. Fiquet, F. Guyot, J. Badro, *Elements* **2008**, 4, 177.

-
- [22] M. Murakami, K. Hirose, K. Kawamura, N. Sata, Y. Ohishi, *Science* **2004**, *304*, 855.
- [23] T. Tsuchiya, J. Tsuchiya, K. Umemoto, R. M. Wentzcovitch, *Earth Planet. Sci. Lett.* **2004**, *224*, 241.
- [24] A. R. Oganov, S. Ono, *Nature* **2004**, *430*, 445.
- [25] F. R. Spellman, M. L. Stoudt, *The Handbook of Geoscience*, Scarecrow Press, Plymouth, UK, **2013**.
- [26] L. Coes Jr., *Science* **1953**, *118*, 131.
- [27] L. S. Ramsdell, *Am. Mineral.* **1955**, *40*, 975.
- [28] T. Zoltai, M. J. Buerger, *Z. Kristallogr.* **1959**, *111*, 129.
- [29] W. Sinclair, A. E. Ringwood, *Nature* **1978**, *272*, 714.
- [30] R. J. Hill, M. D. Newton, G. V. Gibbs, *J. Solid State Chem.* **1983**, *47*, 185.
- [31] D. C. Smith, *Nature* **1984**, *310*, 641.
- [32] C. Chopin, *Contrib. Mineral. Petrol.* **1984**, *86*, 107.
- [33] S. R. Bohlen, D. H. Lindsley, *Ann. Rev. Earth Planet. Sci.* **1987**, *15*, 397.
- [34] P. Dera, C. T. Prewitt, N. Z. Boctor, R. J. Hemley, *Am. Mineral.* **2002**, *87*, 1018.
- [35] A. E. Goresy, P. Dera, T. G. Sharp, C. T. Prewitt, M. Chen, L. Dubrovinsky, B. Wopenka, N. Z. Boctor, R. J. Hemley, *Eur. J. Mineral.* **2008**, *20*, 523.
- [36] M. Miyahara, S. Kaneko, E. Ohtani, T. Sakai, T. Nagase, M. Kayama, H. Nishido, N. Hirao, *Nat. Commun.* **2008**, *4*, 1737.
- [37] J. Haines, J. M. Léger, F. Gorelli, M. Hanfland, *Phys. Rev. Lett.* **2001**, *87*, 155503–1.
- [38] Y. Kuwayama, K. Hirose, N. Sata, Y. Ohishi, *Science* **2005**, *309*, 923.
- [39] Y. Kuwayama, K. Hirose, N. Sata, Y. Ohishi, *Phys. Chem. Minerals* **2011**, *38*, 591.
- [40] A. Metsue, T. Tsuchiya, *Phys. Chem. Minerals* **2012**, *39*, 177.

-
- [41] S. Wu, K. Umemoto, M. Ji, C.-Z. Wang, K.-M. Ho, R. M. Wentzcovitch, *Phys. Rev. B: Condens. Matter Mater. Phys.* **2011**, 83, 184102.
- [42] T. Tsuchiya, J. Tsuchiya, *Proc. Natl. Acad. Sci. U. S. A.* **2011**, 108, 1252.
- [43] W. F. McDonough in *Earthquake Thermodynamics and Phase Transformation in the Earth's Interior*, (Eds.: R. Teisseyre, E. Majewski), Academic Press, San Diego, CA, USA, **2001**.
- [44] *Phosphate Deposits of the World, Proterozoic and Cambrian Phosphorites, Vol. 1*, (Eds.: P. J. Cook, J. H. Shergold), Cambridge University Press, Cambridge, UK, **2005**.
- [45] *Phosphate Deposits of the World, Phosphate Rock Resources, Vol. 2*, (Eds.: A. J. G. Notholt, R. P. Sheldon, D. F. Davidson), Cambridge University Press, Cambridge, UK, **2005**.
- [46] S. Jewell, S. M. Kimball, *Mineral Commodity Summaries 2015*, United States Geological Survey, Reston, VA, USA, **2015**, p. 118.
- [47] J. R. Herring, R. J. Fantel, *Nonrenewable Resour.* **1993**, 2, 226.
- [48] D. Cordell, J.-O. Drangert, S. White, *Global Environmental Change* **2009**, 19, 292.
- [49] G. E. Schulze, *Naturwissenschaften* **1933**, 21, 562.
- [50] R. C. L. Mooney, *Acta Crystallogr.* **1956**, 9, 728.
- [51] A. Grund, *Tschermaks Mineral. Petrogr. Mitt.* **1955**, 5, 227.
- [52] P. Kokkoros, *Tschermaks Mineral. Petrogr. Mitt.* **1956**, 6, 116.
- [53] A. L. Sauze, J. Haines, C. Chateac, J. M. Leger, R. Marchand, *Mater. Sci. Forum* **2000**, 325–326, 77.
- [54] J. Pellicer-Porres, A. M. Saitta, A. Polian, J. P. Itié, M. Hanfland, *Nat. Mater.* **2007**, 6, 698.

-
- [55] A. Le Sauze, J. Haines, C. Chateac, J. M. Leger, R. Marchand, *Mater. Sci. Forum* **2000**, 325-326, 77.
- [56] J. M. Léger, J. Haines, C. Chateau, G. Bocquillon, M. W. Schmidt, S. Hull, F. Gorelli, A. Lesauze, R. Marchand, *Phys. Chem. Minerals* **2001**, 28, 388.
- [57] W. Schnick, J. Lücke, *Z. Anorg. Allg. Chem.* **1992**, 610, 121.
- [58] N. Jacobs, R. Nymwegen, S. Doyle, T. Wroblewski, W. Kockelmann, *Z. Anorg. Allg. Chem.* **1997**, 623, 1467.
- [59] J. M. Léger, J. Haines, L. S. de Oliveira, C. Chateau, A. L. Sauze, R. Marchand, S. Hull, *J. Phys. Chem. Solids* **1999**, 60, 145.
- [60] J. Haines, C. Chateau, J. M. Léger, A. L. Sauze, N. Diot, R. Marchand, S. Hull, *Acta Crystallogr. Sect. B: Struct. Sci.* **1999**, 55, 677.
- [61] A. Marchuk, F. J. Pucher, F. W. Karau, W. Schnick, *Angew. Chem. Int. Ed.* **2014**, 53, 2469; *Angew. Chem.* **2014**, 126, 2501.
- [62] U. Müller, *Anorganische Strukturchemie*, Vieweg + Teubner, Wiesbaden, Germany, **2008**, p. 187.
- [63] J. Brice, J. Motte, A. El Maslout, J. Aubry, *C. R. Seances Acad. Sci. Ser. C* **1971**, 273, 744.
- [64] W. Schnick, J. Lücke, *J. Solid State Chem.* **1990**, 87, 101.
- [65] W. Schnick, V. Schultz-Coulon, *Angew. Chem. Int. Ed. Engl.* **1993**, 32, 280; *Angew. Chem.* **1993**, 105, 308.
- [66] V. Schultz-Coulon, W. Schnick, *Z. Anorg. Allg. Chem.* **1997**, 623, 69.
- [67] S. Sedlmaier, M. Eberspächer, W. Schnick, *Z. Anorg. Allg. Chem.* **2011**, 637, 362.
- [68] K. Senevirathne, C. S. Day, M. D. Gross, A. Lachgar, N. Holzwarth, *Solid State Ionics* **2013**, 233, 95.

- [69] W. Schnick, *Angew. Chem. Int. Ed. Engl.* **1993**, 32, 806; *Angew. Chem.* **1993**, 105, 846.
- [70] F. Liebau, *Structural Chemistry of Silicates*, Springer, Berlin, **1985**.
- [71] W. Schnick, U. Berger, *Angew. Chem. Int. Ed. Engl.* **1991**, 30, 830; *Angew. Chem.* **1991**, 103, 857.
- [72] W. Schnick, J. Lücke, *Z. Anorg. Allg. Chem.* **1990**, 588, 19.
- [73] K. Landskron, S. Schmid, W. Schnick, *Z. Anorg. Allg. Chem.* **2001**, 627, 2469.
- [74] F. J. Pucher, F. Hummel, W. Schnick, *Eur. J. Inorg. Chem.* **2015**, 1886.
- [75] F. J. Pucher, A. Marchuk, P. J. Schmidt, D. Wiechert, W. Schnick, *Chem. Eur. J.* **2015**, 21, 6443.
- [76] F. W. Karau, L. Seyfarth, O. Oeckler, J. Senker, K. Landskron, W. Schnick, *Chem. Eur. J.* **2007**, 13, 6841.
- [77] F. Karau, doctoral thesis, Ludwig-Maximilians-Universität München, **2007**.
- [78] F. Pucher, S. Römer, F. Karau, W. Schnick, *Chem. Eur. J.* **2010**, 16, 7208.
- [79] L. W. Bragg, W. H. Zachariasen, *Z. Kristallogr. Kristallgeom. Kristallphys. Kristallchem.* **1930**, 72, 518.
- [80] S. Correll, O. Oeckler, N. Stock, W. Schnick, *Angew. Chem. Int. Ed.* **2003**, 42, 3549; *Angew. Chem.* **2003**, 115, 3674.
- [81] S. Correll, N. Stock, O. Oeckler, J. Senker, T. Nilges, W. Schnick, *Z. Anorg. Allg. Chem.* **2004**, 630, 2205.
- [82] S. J. Sedlmaier, M. Döblinger, O. Oeckler, J. Weber, J. S. auf der Günne, W. Schnick, *J. Am. Chem. Soc.* **2011**, 133, 12069.
- [83] A. Marchuk, W. Schnick, *Angew. Chem. Int. Ed.* **2015**, 54, 2383; *Angew. Chem.* **2015**, 127, 2413.

-
- [84] F. Karau, W. Schnick, *Angew. Chem. Int. Ed.* **2006**, 45, 4505; *Angew. Chem.* **2006**, 118, 4617.
- [85] F. Liebau, *Zeolites* **1983**, 3, 191.
- [86] M. Gies, *Z. Kristallogr.* **1983**, 164, 247.
- [87] M. Zeuner, S. Pagano, W. Schnick, *Angew. Chem. Int. Ed.* **2011**, 50, 7754; *Angew. Chem.* **2011**, 123, 7898.
- [88] K. Landskron, H. Huppertz, J. Senker, W. Schnick, *Angew. Chem. Int. Ed.* **2001**, 40, 2643; *Angew. Chem.* **2001**, 113, 2713.
- [89] K. Landskron, H. Huppertz, J. Senker, W. Schnick, *Z. Anorg. Allg. Chem.* **2002**, 628, 1465.
- [90] S. Horstmann, E. Irran, W. Schnick, *Angew. Chem. Int. Ed. Engl.* **1997**, 36, 1992; *Angew. Chem.* **1997**, 109, 2085.
- [91] S. Horstmann, E. Irran, W. Schnick, *Z. Anorg. Allg. Chem.* **1998**, 624, 221.
- [92] K. Landskron, E. Irran, W. Schnick, *Chem. Eur. J.* **1999**, 5, 2548.
- [93] A. Vitola, J. Ronis, T. Millers, *Latv. PSR Zinat. Akad. Vestis Kim. Ser.* **1990**, 1, 35.
- [94] H. Jacobs, R. Nymwegen, *Z. Anorg. Allg. Chem.* **1997**, 623, 429.
- [95] K. Landskron, W. Schnick, *J. Solid State Chem.* **2001**, 156, 390.
- [96] F. J. Trojer, *Z. Kristallogr. Kristallgeom. Kristallphys. Kristallchem.* **1968**, 127, 291.
- [97] S. Ghose, C. Wan, *Am. Mineral.* **1979**, 64, 563.
- [98] E. Mugnaioli, S. J. Sedlmaier, O. Oeckler, U. Kolb, W. Schnick, *Eur. J. Inorg. Chem.* **2012**, 121.
- [99] S. J. Sedlmaier, J. Schmedt auf der Günne, W. Schnick, *Dalton Trans.* **2009**, 4081.
- [100] S. J. Sedlmaier, D. Weber, W. Schnick, *Z. Kristallogr. - New Cryst. Struct.* **2012**, 227, 1.

- [101] S. J. Sedlmaier, E. Mugnaioli, O. Oeckler, U. Kolb, W. Schnick, *Chem. Eur. J.* **2011**, *17*, 11258.
- [102] A. Marchuk, V. R. Celinski, J. Schmedt auf der G nne, W. Schnick, *Chem. Eur. J.* **2015**, *21*, 5836.
- [103] S. J. Sedlmaier, V. R. Celinski, J. Schmedt auf der G nne, W. Schnick, *Chem. Eur. J.* **2012**, *18*, 4358.
- [104] A. Marchuk, L. Neudert, O. Oeckler, W. Schnick, *Eur. J. Inorg. Chem.* **2014**, 3427.
- [105] J. Bates, N. Dudney, G. Gruzalski, R. Zuhr, A. Choudhury, C. Luck, J. Robertson, *J. Power Sources* **1993**, *43*, 103.
- [106] P. Knauth, *Solid State Ionics* **2009**, *180*, 911.
- [107] W. Sinclair, A. E. Ringwood, *Nature* **1978**, *272*, 714.
- [108] R. J. Hill, M. D. Newton, G. V. Gibbs, *J. Solid State Chem.* **1983**, *47*, 185.
- [109] J. M. L ger, J. Haines, M. Schmidt, J. P. Petit t, A. S. Pereira, J. A. H. da Jornada, *Nature* **1996**, *383*, 401.
- [110] A. Zerr, G. Miehe, G. Serghiou, M. Schwarz, E. Kroke, R. Riedel, H. Fue  , P. Kroll, R. Boehler, *Nature* **1999**, *400*, 340.
- [111] M. Schwarz, G. Miehe, A. Zerr, E. Kroke, B. T. Poe, H. Fuess, R. Riedel, *Adv. Mater.* **2000**, *12*, 883.
- [112] J. Z. Jiang, F. Kragh, D. J. Frost, K. St hl, H. Lindelov, *J. Phys.: Condens. Matter* **2001**, *13*, L515.

2 An Unprecedented AB₂ Tetrahedra Network Structure Type in a High-Pressure Phase of Phosphorus Oxonitride PON

Dominik Baumann, Stefan J. Sedlmaier, Wolfgang Schnick

published in: *Angew. Chem. Int. Ed.* **2012**, *51*, 4707. DOI: 10.1002/anie.201200811

published in: *Angew. Chem.* **2012**, *121*, 4785. DOI: 10.1002/ange.201200811

Reprinted (adapted) with permission from *Angewandte Chemie*. Copyright 2012 John Wiley and Sons.

Abstract

Restructuring: An unprecedented framework structure made up of tetrahedra has been discovered in a novel high-pressure polymorph of the phosphorus oxonitride PON by treating a single-source precursor at 12 GPa and 1250 °C. It is the first polymorph of PON that does not crystallize in a structure type known from SiO₂.

2.1 Introduction with Results and Discussion

Compounds exhibiting AB₂-type tetrahedral network structures are versatile materials and of great technical importance. First of all microporous zeolites are known for their outstanding absorption properties and catalytic behavior and are therefore extensively used in industrial, agricultural, and laboratory environments.^[1] However, the importance of dense AB₂-networks should not be underestimated. SiO₂ and to a minor extent GaPO₄ are applied in piezoelectric devices, such as pressure sensors and microbalances,^[2] while quartz-like compounds in general, including phosphates like AlPO₄ and BPO₄, can also be used for second-harmonic generation (SHG) purposes.^[3,4] Due to the variety of applications, widespread research into novel AB₂-type structures was conducted, including the prediction of more than two million unique prospective crystal structures for zeolites.^[5,6] However, only a minute subset of possible structures has been realized to date. In this search for new structure types we have directed our attention to the system P-O-N, which is isoelectronic to silica. The inclusion of nitrogen provides additional structural flexibility which theoretically opens up an even wider range of possibly structure types. The few known compounds in this system include the first nitridic zeolites NPO^[7,8] and Ba₁₉P₃₆O_{6+x}N_{66-x}Cl_{8+x} ($x \approx 4.54$)^[9] as well as the nitridic clathrate P₄N₄(NH)₄(NH₃)^[10] and the polymorphs of PON exhibiting cristobalite-,^[11] quartz-,^[12] and moganite-type^[13] structures. Glassy compounds in the system Li-Ca-P-N also exhibit desirable properties, such as a high hardness and refractive index.^[14,15] The great potential for novel structure types in this system is offset by difficulties in preparation, such as thermal decomposition, low reactivity, and a low degree of crystallinity. In order to circumvent the mentioned problems we developed a novel synthetic approach, utilizing an amorphous single-source precursor. Here, we report on a new high-pressure phase of phosphorus oxonitride PON. Since this is the fourth known polymorph of PON, we propose the name δ -PON. Unlike the quartz and moganite polymorphs, it is not directly accessible by treating cristobalite-

type PON at high-pressure/high-temperature conditions. This hints at the possibility of δ -PON being thermodynamically metastable at these conditions. Instead we prepared δ -PON by carrying out the final thermal condensation step of an amorphous phosphorus oxonitride imide under high pressure employing the multianvil technique.^[16–20] The starting material was subjected to a temperature around 1350 °C at 12 GPa for 120 min in a Walker-type module. The product could be obtained as a hard, colorless solid.

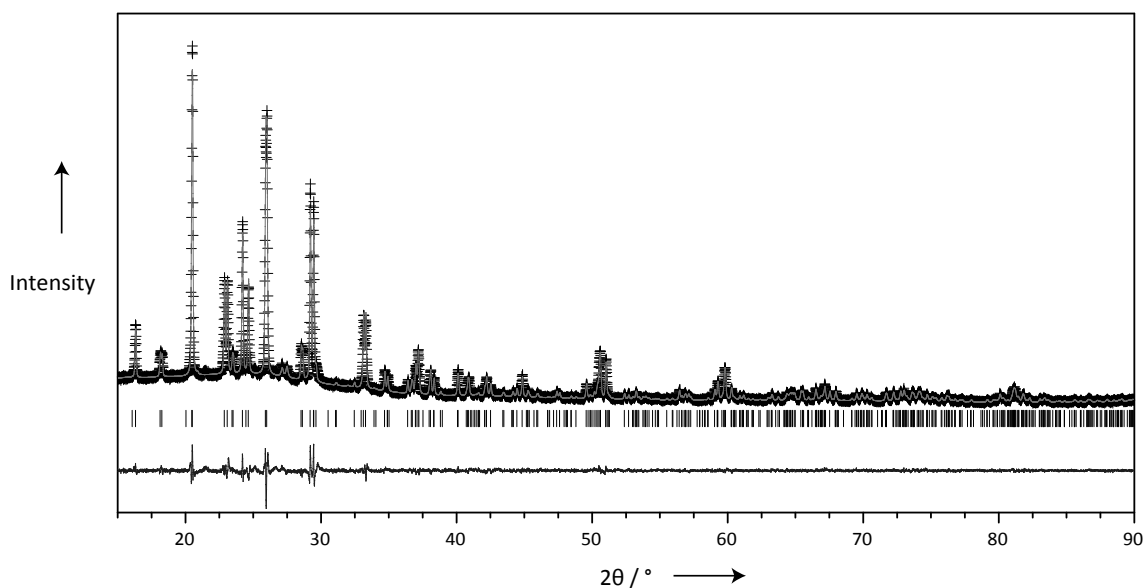


Figure 2.1: Observed (crosses) and calculated (gray line) powder diffraction pattern of δ -PON as well as position of Bragg reflections (vertical lines) and difference profile (dark gray line).

The crystal structure of δ -PON was elucidated ab initio with X-ray powder diffraction data in space group $P2_1/c$ (no. 14).^[21] Final refinement was carried out employing the Rietveld method (Figure 2.1). Energy dispersive X-ray spectroscopy showed the presence of P, O and N, while no other elements were detected. The product was further characterized using FTIR and solid-state NMR spectroscopy.

The crystal structure of δ -PON exhibits a three-dimensional network composed of all-side vertex sharing $P(O,N)_4$ tetrahedra representing an unprecedented topology (Figure 2.2). The arrangement of the tetrahedra is characterized of condensed 4-, 6- and 8-rings which is expressed by the cycle class sequence according to Klee^[22,23] (Table S5). The com-

parison with the cycle class sequences of the other polymorphs shows that δ -PON is not topologically equivalent to any of the known phases. The arrangement of P(O,N)₄ tetrahedra into 4- and 6-rings is reminiscent to that of moganite PON but due to the difference in framework topologies no crystallographic group-subgroup relation between the two phases is existent. One type of the two crystallographically independent 4-rings forms ladder-like chains along [010] (Figure 2.3), which are surrounded by 6-rings. The topology of this framework (Figure 2.3) indicated by the vertex symbol $(4_1 6_2 8_3)(4_1 6_4 8_1)(4_2 6_3 8)_2$ (determined by the TOPOS Software)^[24,25] is different from those of all other PON polymorphs and has not been found in any other known compound as yet. Therefore δ -PON can be considered a truly novel structure type and correspondingly supplements the few known AB₂-structure types. However a SiO₂-modification with the same topology in space group *Aea*2 has been predicted and can be found in the Predicted Crystallography Open Database (PCOD; entry 3102887).^[26]

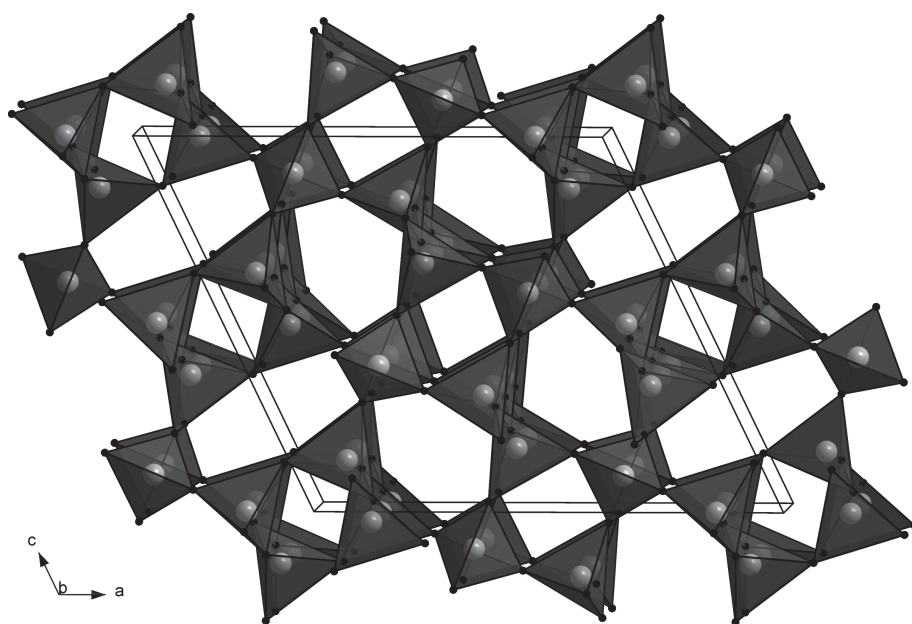


Figure 2.2: Crystal structure of δ -PON. View along [010] (P: light grey; O/N: black).

P–(O,N) bond lengths vary between 152 and 165 pm, with their variance and the mean bond length being slightly larger than in the other known polymorphs of PON. The bond-

ing angles at the bridging atoms range from 128 to 147° which is comparable to other PON phases. Deviations from the regular tetrahedral angle vary slightly with values between 104 and 118°. Detailed information on bond lengths and angles can be found in the supporting information (Tables S3 & S4). The electrostatic plausibility of the crystal structure was assessed using the MAPLE (Madelung part of lattice energy) concept.^[27,28] The partial MAPLE values of the atomic sites (O/N = 4460 – 4778, P = 13941 – 14878 kJ mol⁻¹) as well as the overall MAPLE-value (23809 kJ mol⁻¹) are in good agreement with those calculated for the other PON polymorphs. Notably, the partial MAPLE values of the anion sites are between the literature values for nitrogen (4600 – 6000 kJ mol⁻¹) and oxygen (2400 – 2800 kJ mol⁻¹)^[29] giving a strong indication for anion disorder.

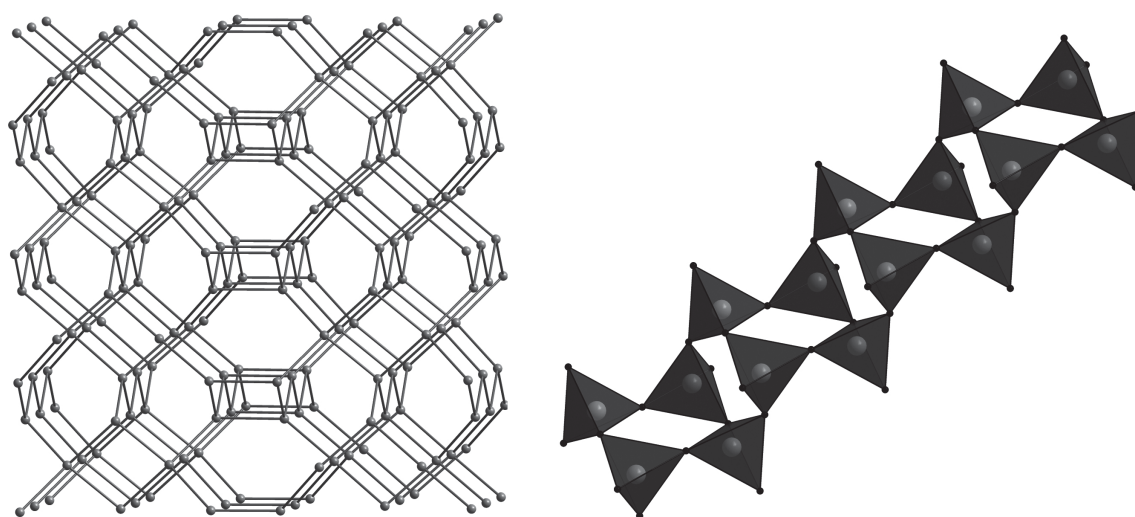


Figure 2.3: Topological representation of the crystal structure of δ -PON. Right: section from the crystal structure showing the ladder-like arrangement of 4-rings.

Since neutron diffraction studies on the known polymorphs of PON by Marchand *et. al.* did not show any evidence for O/N-order, we assume similar disorder in δ -PON. To corroborate this hypothesis δ -PON was characterized further by recording a ³¹P solid-state NMR spectrum. The chemical shift of $\delta_{\text{iso}} = -32.1$ ppm is close to those found for cristobalite-PON ($\delta_{\text{iso}} = -26.3$ ppm, see spectrum in the supplementary information) and H₃P₈O₈N₉ ($\delta_{\text{iso}} = -31.9$ ppm).^[30] As expected for a phase with statistical O/N-distribution,

the FWHM of the signal is so high that the four individual signals expected for the four crystallographically distinct P-atoms cannot be resolved. To rule out the possibility of δ -PON being in fact a phosphorus oxonitride imide, the absence of stoichiometric amounts of hydrogen was confirmed by ¹H solid-state NMR spectroscopy as well as FTIR spectroscopy.

With δ -PON we have found the first polymorph of PON which does not crystallize in a structure type known from SiO₂. This novel AB₂ structure type had only been predicted theoretically so far. With the high-pressure high-temperature condensation of a newly developed amorphous phosphorus oxonitride imide precursor, a powerful synthetic approach towards new high-pressure phases of PON has been established. This could possibly lead to further high-pressure polymorphs of PON, allowing a structural diversity approaching that of SiO₂. This promising synthesis approach could also be applied to many other systems, possibly facilitating the discovery of a range of novel networks with interesting properties. The high-pressure approach in combination with the inclusion of nitrogen in the framework allows an even wider range of possible frameworks, even including triply coordinated nitrogen atoms or edge-sharing tetrahedra.^[31] Even the synthesis of stishovite-like polymorphs with interesting materials properties showing higher coordination numbers of P may be possible.

2.2 References

- [1] F. A. Mumpton, *Proc. Natl. Acad. Sci. U. S. A.* **1999**, 96, 3463.
- [2] H. Thanner, P. W. Krempel, W. Wallnöfer, P. M. Worsch, *Vacuum* **2002**, 67, 687.
- [3] S. Defregger, G. F. Engel, P. W. Krempel, *Phys. Status Solidi B* **1990**, 162, 311.
- [4] Z. Li, Z. Lin, Y. Wu, P. Fu, Z. Wang, C. Chen, *Chem. Mater.* **2004**, 16, 2906.

-
- [5] M. M. J. Treacy, I. Rivin, E. Balkovsky, K. Randall, M. Foster, *Microporous Mesoporous Mater.* **2004**, *74*, 121.
- [6] M. D. Foster, M. M. J. Treacy, Database of Hypothetical Zeolite Structures, **2010**, <http://www.hypotheticalzeolites.net> (visited on 03/2012).
- [7] S. Correll, O. Oeckler, N. Stock, W. Schnick, *Angew. Chem. Int. Ed.* **2003**, *42*, 3549; *Angew. Chem.* **2003**, *115*, 3674.
- [8] S. Correll, N. Stock, O. Oeckler, J. Senker, T. Nilges, W. Schnick, *Z. Anorg. Allg. Chem.* **2004**, *630*, 2205.
- [9] S. J. Sedlmaier, M. Döblinger, O. Oeckler, J. Weber, J. S. auf der Günne, W. Schnick, *J. Am. Chem. Soc.* **2011**, *133*, 12069.
- [10] F. Karau, W. Schnick, *Angew. Chem. Int. Ed.* **2006**, *45*, 4505; *Angew. Chem.* **2006**, *118*, 4617.
- [11] J. M. Léger, J. Haines, C. Chateau, G. Bocquillon, M. W. Schmidt, S. Hull, F. Gorelli, A. Lesauze, R. Marchand, *Phys. Chem. Minerals* **2001**, *28*, 388.
- [12] J. M. Léger, J. Haines, L. S. de Oliveira, C. Chateau, A. L. Sauze, R. Marchand, S. Hull, *J. Phys. Chem. Solids* **1999**, *60*, 145.
- [13] J. Haines, C. Chateau, J. M. Léger, A. L. Sauze, N. Diot, R. Marchand, S. Hull, *Acta Crystallogr. Sect. B: Struct. Sci.* **1999**, *55*, 677.
- [14] T. Grande, J. R. Holloway, P. F. McMillan, C. A. Angell, *Nature* **1994**, *369*, 43.
- [15] T. Grande, S. Jacob, J. R. Holloway, P. F. McMillan, C. A. Angell, *J. Non-Cryst. Solids* **1995**, *184*, 151.
- [16] N. Kawai, S. Endo, *Rev. Sci. Instrum.* **1970**, *41*, 1178.
- [17] D. Walker, M. A. Carpenter, C. M. Hitch, *Am. Mineral.* **1990**, *75*, 1020.
- [18] D. Walker, *Am. Mineral.* **1991**, *76*, 1092.

- [19] D. C. Rubie, *Phase Transitions* **1999**, 68, 431.
- [20] H. Huppertz, *Z. Kristallogr.* **2004**, 219, 330.
- [21] Crystal data for δ -PON: formula: PON, $M = 60.98 \text{ g mol}^{-1}$, space group $P2_1/c$ (no. 14), $a = 12.2472(2)$, $b = 4.83618(6)$, $c = 10.8604(2) \text{ \AA}$, $\beta = 115.8026(8)^\circ$, $V = 579.12(2) \text{ \AA}^3$, $Z = 16$, Cu-K $_{\alpha 1}$ radiation ($\lambda = 1.5406 \text{ \AA}$), $T = 298(2) \text{ K}$, step size: 0.01° , 474 reflections, 90 parameters, $R_p = 0.03806$, $wR_p = 0.04910$, $\chi^2 = 1.447$, $R_{\text{Bragg}} = 0.012128$, background: shifted Chebyshev, 32 background parameters.
- Further details of the crystal structure investigation may be obtained from Fachinformationszentrum Karlsruhe, 76344 Eggenstein-Leopoldshafen, Germany (fax: (+49)7247-808-666; e-mail: crysdata@fiz-karlsruhe.de, on quoting the depository number CSD-423589.
- [22] W. E. Klee, *Z. Kristallogr.* **1987**, 179, 67.
- [23] A. Beukemann, W. E. Klee, *Z. Kristallogr.* **1994**, 209, 709.
- [24] V. A. Blatov, M. O’Keeffe, D. M. Proserpio, *CrystEngComm* **2010**, 12, 44.
- [25] V. A. Blatov, *IUCr CompComm Newsletter* **2006**, 7, 4.
- [26] A. L. Bail, *Phys. Chem. Chem. Phys.* **2010**, 12, 8521.
- [27] R. Hoppe, *Angew. Chem. Int. Ed. Engl.* **1966**, 5, 95; *Angew. Chem.* **1966**, 78, 52.
- [28] R. Hoppe, *Angew. Chem. Int. Ed. Engl.* **1970**, 9, 25; *Angew. Chem.* **1970**, 82, 7.
- [29] M. Zeuner, S. Pagano, W. Schnick, *Angew. Chem. Int. Ed.* **2011**, 50, 7754; *Angew. Chem.* **2011**, 123, 7898.
- [30] S. J. Sedlmaier, V. R. Celinski, J. Schmedt auf der G nne, W. Schnick, *Chem. Eur. J.* **2012**, 18, 4358.
- [31] W. Schnick, *Angew. Chem. Int. Ed. Engl.* **1993**, 32, 806; *Angew. Chem.* **1993**, 105, 846.

3 A High-Pressure Polymorph of Phosphorus Oxonitride PON with Coesite Structure

Dominik Baumann, Robin Niklaus, Wolfgang Schnick

published in: *Angew. Chem. Int. Ed.* **2015**, *54*, 4388. DOI: 10.1002/anie.201410526

published in: *Angew. Chem.* **2015**, *12*, 4463. DOI: 10.1002/ange.201410526

Reprinted (adapted) with permission from *Angewandte Chemie*. Copyright 2015 John Wiley and Sons.

Abstract

The chemical and physical properties of phosphorus oxonitride (PON) closely resemble those of silica, to which it is isosteric. A new high-pressure phase of PON is reported herein. This polymorph, synthesized by using the multianvil technique, crystallizes in the coesite structure. This represents the first occurrence of this very dense network structure outside of SiO₂. Phase-pure coesite PON (*coe*-PON) can be synthesized in bulk at pressures above 15 GPa. This compound was thoroughly characterized by means of powder X-ray diffraction, DFT calculations, and FTIR and MAS NMR spectroscopy, as well as temperature-dependent diffraction. These results represent a major step towards the exploration of the phase diagram of PON at very high pressures and the possible synthesis of a stishovite-type PON containing hexacoordinate phosphorus.

3.1 Introduction with Results and Discussion

Owing to its unique properties, silica (SiO_2) has been of great interest for physicists, chemists, and geoscientists for many decades. This is partly due to its properties and the resultant applications, such as nonlinear optical properties^[1] or piezoelectricity,^[2] but it is also to a large extent due to the wide variety of crystal structures found for this material.^[3] With SiO_2 being the parent compound of the major components of the crust and mantle of the Earth,^[4–6] precise knowledge of the phase diagram of silica leads to a detailed understanding of many geological processes. The high-pressure polymorph coesite was artificially synthesized^[7] and studied in detail^[8,9] before it was first discovered in nature as a product of meteorite impacts.^[10] Subsequent investigations showed that the presence of coesite in rocks can serve as an indicator of the material having undergone ultrahigh-pressure metamorphism.^[11–13] This enables a detailed understanding of the geological history of these rocks. Similarly, the polymorphs stable at even higher pressures, namely stishovite^[14,15] and seifertite,^[16,17] can be used as indicators of previous impact events. Stishovite has additionally drawn particular interest because of remarkable mechanical properties. It held the record for the hardest oxide^[18] until it was surpassed by cotunnite-type TiO_2 in 2001.^[19]

In order to gain a more detailed understanding of the high-pressure behavior of silica related phases we have investigated the phase diagram of phosphorus oxonitride PON, which is isosteric to SiO_2 ^[20] and its analogues $\text{PN}(\text{NH})$ ^[21] and AlPO_4 .^[22] Owing to the similar ionic radii (Si^{4+} : 26 pm, P^{5+} : 17 pm; O^{2-} : 135 pm, N^{3-} : 146 pm)^[23] some of the polymorphs exhibited by silica can also be found in PON. At ambient pressure PON adopts a β -cristobalite-type structure and has no known high-temperature polymorphs.^[24] The high-pressure phases include quartz-^[25] and moganite-type polymorphs.^[26] In the case of silica, moganite has only been found in microscopic quantities in nature, whereas it is synthetically accessible in bulk quantities for PON. Recently, we were able to synthesize an-

other polymorph of phosphorus oxonitride that crystallizes in a unique structure type that had not been observed in any other compound before.^[27] This indicates that the diversity of possible structure types for PON could possibly even exceed that for SiO_2 . A particular factor that could extend the range of possible AB_2 -structures in PON is the fact that the nitride ion is able to connect more than two neighboring $\text{P}(\text{O},\text{N})_4$ tetrahedra.^[28] Notable examples that contain triply bridging nitrogen are α - and β - HP_4N_7 ,^[29–31] $\text{P}_4\text{N}_6\text{O}$ ^[32] as well as the layered oxonitridophosphate $\text{Sr}_3\text{P}_6\text{O}_6\text{N}_8$.^[33]

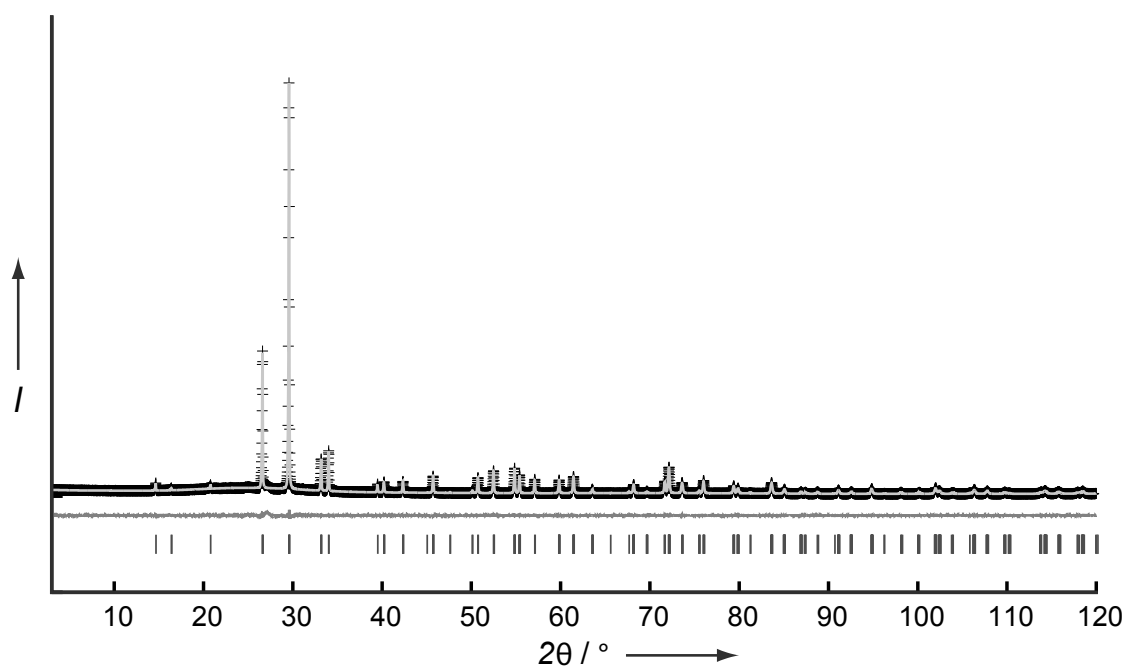


Figure 3.1: Observed (crosses) and calculated (light gray line) powder diffraction pattern of *coe*-PON as well as difference profile (dark gray line). Black vertical bars represent the positions of Bragg reflections.

Herein, we report the discovery of a new polymorph of PON that crystallizes in the coesite structure type, for which we propose the name coesite PON or *coe*-PON. This high-pressure phase was synthesized in a modified Walker-type multianvil assembly. The starting material cristobalite-type PON was treated at 15.5 GPa and approximately 1300 °C for 60 min. The product could then be isolated as a colorless crystalline solid. Energy-dispersive X-ray (EDX) spectroscopy was used to establish the absence of any

elements other than P, O, and N. The crystal structure was elucidated from powder X-ray diffraction data.^[34] Structure solution was performed by using the charge-flipping algorithm.^[35–37] Both structure solution and Rietveld refinement were carried out by using TOPAS-Academic 4.1.^[38] Rietveld refinement also showed no signs of any amorphous or crystalline side phases (Figure 3.1). The unit cell of *coe*-PON ($a = 6.95903(8)$, $b = 12.0610(2)$, $c = 6.96821(8)$ Å, $\beta = 120.0348(7)^\circ$) displays remarkable lattice pseudosymmetry, appearing hexagonal at first glance. The symmetry of the structure itself, however, is monoclinic, a fact that has similarly been observed for coesite SiO₂.^[9]

The crystal structure (Figure 3.2) closely resembles that of coesite. The compound is composed of a three-dimensional network of all-side vertex-sharing P(O,N)₄ tetrahedra. As with the other known polymorphs of PON, there was no indication of any ordering of the anion positions. We thus assume a statistical disorder of the anions. In the case of cristobalite PON, this was confirmed by neutron diffraction experiments.^[39] The topological identity of the networks of coesite SiO₂ and PON is also illustrated by topological analysis with TOPOS.^[40,41] Both compounds are described by the point symbol $(4^2.6.8^2.9)(4^2.6^3.8)$.

According to the nomenclature established by Liebau, the crystal structure of *coe*-PON can be described as loop-branched dreier single chains that are interconnected to form a three-dimensional network. This leads to a loop-branched dreier framework $\{\text{IB}_\infty^3\}[\text{P}_4(\text{O,N})_8]$ similar to that found in feldspars.^[42]

The P–(O,N) bond lengths are in the range of 154 to 164 pm (Figure 3.3). A similarly large variance in the interatomic distances has been observed in δ -PON.^[27] The P(O,N)₄ tetrahedra are slightly distorted, but to a lesser degree than those in δ -PON. The P–(O,N)–P angles around most of the anion sites range from 137 to 147° and are therefore very similar to those found in coesite SiO₂. The angle P1–(O,N)1–P1, however, exhibits an intriguing value of 180°. Since this same angle occurs in coesite SiO₂ as well and differs greatly from the value of 140° for a strain-free Si–O–Si bond, it has been discussed in detail by

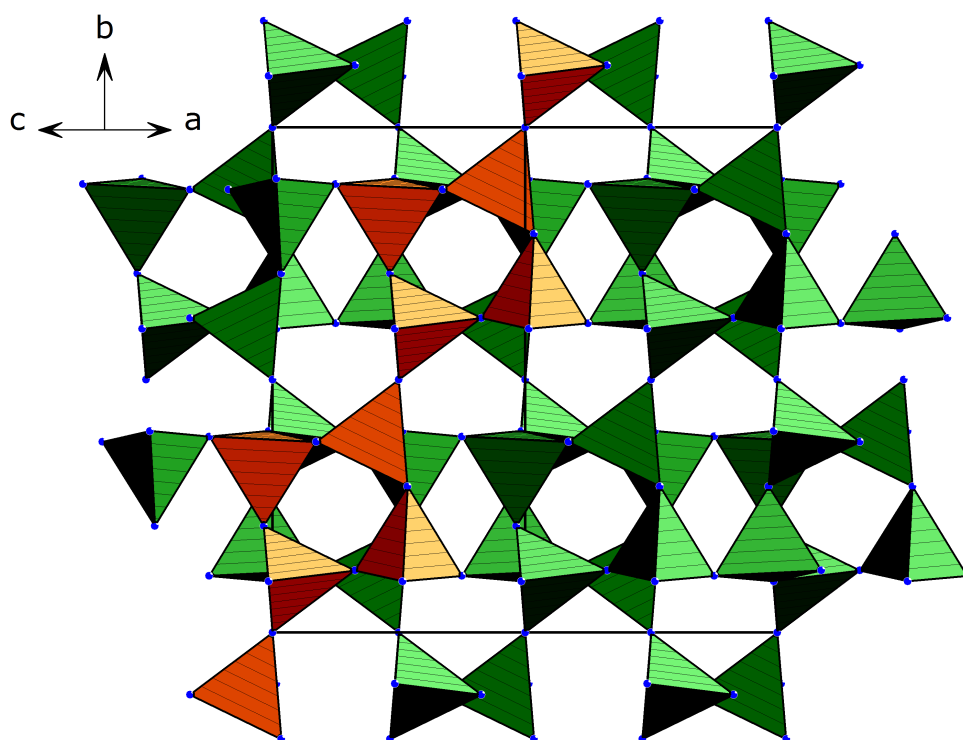


Figure 3.2: Crystal structure of *coe*-PON in polyhedral representation. View along [101]. One fundamental chain is highlighted in orange.

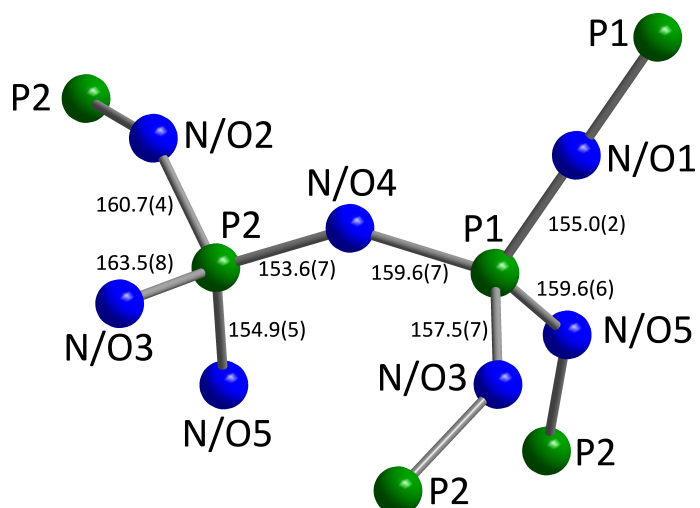


Figure 3.3: Atomic arrangement and bond lengths in *coe*-PON. Bond lengths are denoted in pm.

Liebau.^[42] He came to the conclusion that this angle is not an artifact caused by the fact that the bridging atom resides on an inversion center but is intrinsic to the crystal structure. In order to show the same for *coe*-PON, we also performed the structure solution in the noncentrosymmetric space group *Cc*. This did not lead to a significant deviation of this angle from 180°, thus indicating that the structural model in space group *C2/c* is correct. Another possible cause of an apparent angle of 180° could be static or dynamic disorder of the bridging atom around the crystallographic site. Such an effect, which can also be described as a coupled rotation of the involved tetrahedra, has been discussed for β -cristobalite.^[43] This would, however, lead to a significantly increased displacement parameter for the anion site. Since the B_{eq} value for (O,N)1 is similar to those of the other anion sites, this phenomenon is unlikely for *coe*-PON.

In order to quantify the similarity between the crystal structures of coesite SiO₂ and coesite PON, the two were compared by using the COMPSTRU program of the Bilbao Crystallographic Server.^[44] The calculated arithmetic mean of the distance between equivalent atomic sites amounts to just 4.4 pm. This leads to a measure of similarity^[45] (Δ) of 0.014, thus indicating that the two crystal structures are in fact very closely related.

DFT calculations were employed to validate our experimental findings. Owing to the statistical O/N disorder, energy-volume curves were calculated for all six chemically reasonable arrangements of O and N. For comparison, the energy-volume curves for cristobalite PON with the lowest energy O/N arrangements were also determined. Details of the calculations and ordered structural models can be found in the Supporting Information. The corresponding enthalpy–pressure diagram (Figure B.7 in the Supporting Information) shows that coesite PON is expected to be more stable than the ambient pressure polymorph above 7.5–10.5 GPa, which is in good agreement with the pressure of 15.5 GPa used in the synthesis. The predicted bulk modulus for *coe*-PON is in the range of 151 to 170 GPa.

The high-pressure high-temperature conditions used for the synthesis, combined knowledge of the phase diagram of closely related SiO₂, strongly suggest that *coe*-PON is a high-

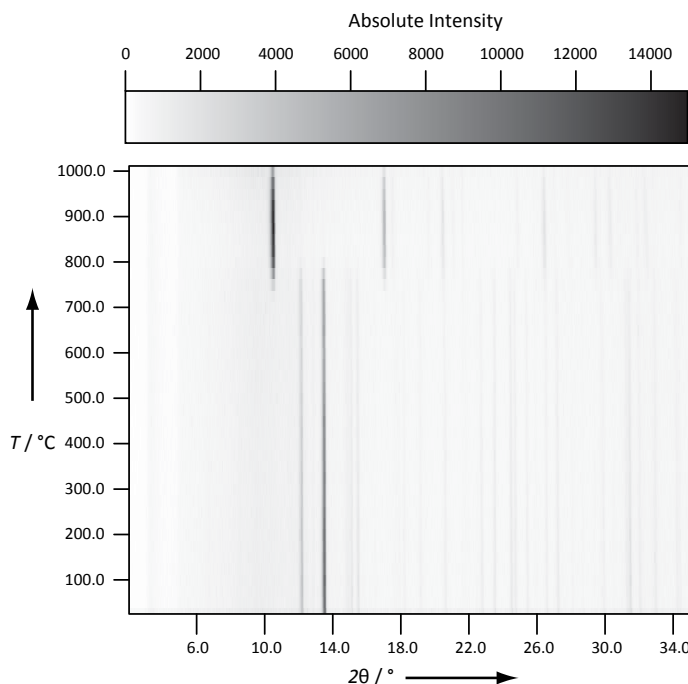


Figure 3.4: Temperature dependent powder X-ray diffraction data for *coe*-PON in air. The transformation to cristobalite PON starts at 750 °C.

pressure phase of phosphorus oxonitride and therefore metastable at ambient pressure. In order to corroborate this hypothesis, we performed temperature-dependent powder X-ray diffraction up to 1000 °C. The results (Figure 3.4) show that at ambient pressures, *coe*-PON transforms back into the cristobalite polymorph above 750 °C. This result indicates that temperatures above 700 °C are needed to initiate reconstructive transformations in phosphorus oxonitride, which is consistent with our laboratory experience. At 975 °C, the first signs of thermal decomposition can be observed.

In order to corroborate the results of the structure solution, a ^{31}P MAS NMR spectrum was acquired (Figure B.1). The spectrum shows two rather broad peaks at -48 and -66 ppm that can be attributed to the two crystallographic P sites. The broad signals can be explained by statistical O/N disorder. This leads to a range of distinct local environments around the P nuclei. Since the NMR signal is an average over all of the P sites in the sample, this leads to a broadening of the NMR signals. A similar effect has been observed in the case of δ -

PON.^[27] In order to rule out the presence of NH groups in the sample, which could in theory replace the isoelectronic O²⁻, an FTIR spectrum of the sample was collected (Figure B.2). It showed no signs of the characteristic N–H vibrations around 3000 cm⁻¹, which is a strong indication of the absence of hydrogen in the sample.

The discovery of *coe*-PON provides new insight into the high-pressure chemistry of phosphorus oxonitride. Previous investigations up to a pressure of 70 GPa with diamond anvil cells at room temperature showed no reconstructive transformations to new high-pressure phases,^[46] while experiments in laser-heated diamond anvil cells at 20 GPa led to the formation of the already known moganite PON. The new results presented herein show that it is indeed possible to obtain further high-pressure phases of PON through a combined high-temperature high-pressure approach by using the multianvil technique. The formation of a coesite-type phase shows that the similarity between SiO₂ and PON extends to higher pressures. However, the pressure needed for the transformation of PON (15.5 GPa) is significantly higher than that for SiO₂ (3.5 GPa).^[7] It is plausible that this similarity could extend to the extreme pressure phases known for silica. Stishovite-type PON containing hexacoordinate phosphorus might thus be accessible, albeit at even higher pressures than for stishovite SiO₂. The possibility of synthesizing and recovering compounds containing pentacoordinate phosphorus has already been shown for the closely related systems P₃N₅^[47,48] and P₄N₆(NH).^[49]

3.2 References

- [1] P. A. Franken, A. E. Hill, C. W. Peters, G. Weinreich, *Phys. Rev. Lett.* **1961**, 7, 118.
- [2] G. W. Pierce, *Proc. Am. Acad. Arts Sci.* **1923**, 59, 81.
- [3] N. R. Keskar, J. R. Chelikowsky, *Phys. Rev. B* **1992**, 46, 1.
- [4] D. L. Anderson, *Science* **1989**, 243, 367.

-
- [5] W. McDonough, S.-S. Sun, *Chem. Geol.* **1995**, *120*, 223.
- [6] C. J. Allègre, J.-P. Poirier, E. Humler, A. W. Hofmann, *Earth Planet. Sci. Lett.* **1995**, *134*, 515.
- [7] L. Coes Jr., *Science* **1953**, *118*, 131.
- [8] L. S. Ramsdell, *Am. Mineral.* **1955**, *40*, 975.
- [9] T. Zoltai, M. J. Buerger, *Z. Kristallogr.* **1959**, *111*, 129.
- [10] E. C. T. Chao, E. M. Shoemaker, B. M. Madsen, *Science* **1960**, *132*, 220.
- [11] D. C. Smith, *Nature* **1984**, *310*, 641.
- [12] C. Chopin, *Contrib. Mineral. Petrol.* **1984**, *86*, 107.
- [13] S. R. Bohlen, D. H. Lindsley, *Ann. Rev. Earth Planet. Sci.* **1987**, *15*, 397.
- [14] W. Sinclair, A. E. Ringwood, *Nature* **1978**, *272*, 714.
- [15] R. J. Hill, M. D. Newton, G. V. Gibbs, *J. Solid State Chem.* **1983**, *47*, 185.
- [16] P. Dera, C. T. Prewitt, N. Z. Boctor, R. J. Hemley, *Am. Mineral.* **2002**, *87*, 1018.
- [17] A. E. Goresy, P. Dera, T. G. Sharp, C. T. Prewitt, M. Chen, L. Dubrovinsky, B. Wopenka, N. Z. Boctor, R. J. Hemley, *Eur. J. Mineral.* **2008**, *20*, 523.
- [18] J. M. Léger, J. Haines, M. Schmidt, J. P. Petitet, A. S. Pereira, J. A. H. da Jornada, *Nature* **1996**, *383*, 401.
- [19] L. S. Dubrovinsky, N. A. Dubrovinskaia, V. Swamy, J. Muscat, N. M. Harrison, R. Ahuja, B. Holm, B. Johansson, *Nature* **2001**, *410*, 653.
- [20] A. L. Sauze, J. Haines, C. Chateac, J. M. Leger, R. Marchand, *Mater. Sci. Forum* **2000**, *325–326*, 77.
- [21] J. Liebig, F. Wöhler, *Liebigs Ann. Chem.* **1843**, *11*, 139.
- [22] A. F. Wright, A. J. Leadbetter, *Philos. Mag.* **1975**, *31*, 1391.

- [23] R. D. Shannon, *Acta Crystallogr. Sect. A: Cryst. Phys. Diffr. Theor. Gen. Crystallogr.* **1976**, 32, 751.
- [24] J. M. Léger, J. Haines, C. Chateau, G. Bocquillon, M. W. Schmidt, S. Hull, F. Gorelli, A. Lesauze, R. Marchand, *Phys. Chem. Minerals* **2001**, 28, 388.
- [25] J. M. Léger, J. Haines, L. S. de Oliveira, C. Chateau, A. L. Sauze, R. Marchand, S. Hull, *J. Phys. Chem. Solids* **1999**, 60, 145.
- [26] J. Haines, C. Chateau, J. M. Léger, A. L. Sauze, N. Diot, R. Marchand, S. Hull, *Acta Crystallogr. Sect. B: Struct. Sci.* **1999**, 55, 677.
- [27] D. Baumann, S. J. Sedlmaier, W. Schnick, *Angew. Chem. Int. Ed.* **2012**, 51, 4707; *Angew. Chem.* **2012**, 124, 4785.
- [28] W. Schnick, *Angew. Chem. Int. Ed. Engl.* **1993**, 32, 806; *Angew. Chem.* **1993**, 105, 846.
- [29] S. Horstmann, E. Irran, W. Schnick, *Angew. Chem. Int. Ed. Engl.* **1997**, 36, 1992; *Angew. Chem.* **1997**, 109, 2085.
- [30] S. Horstmann, E. Irran, W. Schnick, *Z. Anorg. Allg. Chem.* **1998**, 624, 221.
- [31] D. Baumann, W. Schnick, *Inorg. Chem.* **2014**, 53, 7977.
- [32] J. Ronis, B. Bondars, A. Vitola, T. Millers, J. Schneider, F. Frey, *J. Solid State Chem.* **1995**, 115, 265.
- [33] S. Sedlmaier, J. S. auf der Günne, W. Schnick, *Dalton Trans.* **2009**, 4081.
- [34] Crystal data for *coe*-PON: $a = 6.95903(8)$, $b = 12.0610(2)$, $c = 6.96821(8)$ Å, $\beta = 120.0348(7)^\circ$, $V = 506.33(2)$ Å³, space group *C2/c* (no. 15), $Z = 16$; Stoe StadiP powder diffractometer with MYTHEN 1K Si strip detector, Cu-K_{α1} radiation ($\lambda = 1.54059$ Å, Ge(111) monochromated), $T = 298(2)$ K, 7800 data points, 385 measured reflections, 65 parameters, peak shape modelled by fundamental parameters approach,^[50, 51] background function: shifted Chebychev (21 coefficients), $\chi^2 =$

- 2.111, $R_{\text{wp}} = 0.04069$, $R_{\text{exp}} = 0.01927$, $R_{\text{Bragg}} = 0.00657$; Further details of the crystal structure investigation can be obtained from the Fachinformations-Zentrum Karlsruhe, 76344 Eggenstein-Leopoldshafen, Germany (fax: (+49)7247-808-666; email: crysdata@fiz-karlsruhe.de) on quoting the depository number CSD-428382.
- [35] G. Oszlányi, A. Sütő, *Acta Crystallogr. Sect. A: Found. Crystallogr.* **2004**, *60*, 134.
- [36] G. Oszlányi, A. Sütő, *Acta Crystallogr. Sect. A: Found. Crystallogr.* **2008**, *64*, 123.
- [37] A. A. Coelho, *Acta Crystallogr. Sect. A: Found. Crystallogr.* **2007**, *63*, 400.
- [38] A. Coelho, *TOPAS-Academic Version 4.1*, Coelho Software: Brisbane, **2007**.
- [39] L. Boukbir, R. Marchand, Y. Laurent, P. Bacher, G. Roult, *Ann. Chim. Fr.* **1989**, *14*, 475.
- [40] V. A. Blatov, M. O’Keeffe, D. M. Proserpio, *CrystEngComm* **2010**, *12*, 44.
- [41] V. Blatov, A. Shevchenko, D. Proserpio, *Cryst. Growth Des.* **2014**, *14*, 3576.
- [42] F. Liebau, *Structural Chemistry of Silicates*, Springer, Berlin, **1985**.
- [43] T. R. Welberry, L. Hua, R. L. Withers, *J. Appl. Crystallogr.* **1989**, *22*, 87.
- [44] E. Tasci, G. de la Flor, D. Orobengoa, C. Capillas, J. Perez-Mato, M. Aroyo, *EPJ Web Conf.* **2012**, *22*, 00009.
- [45] G. Bergerhoff, M. Berndt, K. Brandenburg, T. Degen, *Acta Crystallogr. Sect. B: Struct. Sci.* **1999**, *55*, 147.
- [46] K. J. Kingma, R. E. Gerald Pacalo, P. F. McMillan in *Properties of Earth and Planetary Materials at High Pressure and Temperature*, (Eds.: M. H. Manghnani, T. Yagi), American Geophysical Union, Washington, D. C., **1998**, pp. 105–119.
- [47] K. Landskron, H. Huppertz, J. Senker, W. Schnick, *Angew. Chem. Int. Ed.* **2001**, *40*, 2643; *Angew. Chem.* **2001**, *113*, 2713.

- [48] K. Landskron, H. Huppertz, J. Senker, W. Schnick, *Z. Anorg. Allg. Chem.* **2002**, 628, 1465.
- [49] D. Baumann, W. Schnick, *Angew. Chem. Int. Ed.* **2014**, 53, 14490; *Angew. Chem.* **2014**, 126, 14718.
- [50] R. W. Cheary, A. Coelho, *J. Appl. Crystallogr.* **1992**, 25, 109.
- [51] R. W. Cheary, A. A. Coelho, J. P. Cline, *J. Res. Natl. Inst. Stand. Technol.* **2004**, 109, 1.

4 A High-Pressure Polymorph of Phosphorus Nitride Imide HP_4N_7 Representing a New Framework Topology

Dominik Baumann, Wolfgang Schnick

published in: *Inorg. Chem.* **2014**, *53*, 7977. DOI: 10.1021/ic500767f 10.1021/ic500767f

Reprinted (adapted) with permission from *Inorganic Chemistry*. Copyright 2014 American Chemical Society.

Abstract

A new polymorph of phosphorus nitride imide HP_4N_7 has been synthesized under high-pressure/high-temperature conditions from P_3N_5 and NH_4Cl at 6 GPa and temperatures between 800 and 1300 °C. Its crystal structure was elucidated using single crystal X-ray diffraction data. $\beta\text{-HP}_4\text{N}_7$ (space group $C2/c$, no. 15, $Z = 4$, $a = 12.873(2)$ Å, $b = 4.6587(4)$ Å, $c = 8.3222(8)$ Å, $\beta = 102.351(3)^\circ$, $R_1 = 0.0485$, $wR_2 = 0.1083$) crystallizes in a new framework structure type that is made up of all-side vertex-sharing PN_4 tetrahedra. The topology of the network is represented by the point symbol $(3^2.4^2.5^2.6^3.7)(3^4.4^4.5^4.6^3)$, and it has not been identified in other compounds so far. Structural differences between the two polymorphs of HP_4N_7 as well as the topological relationship to the recently discovered high-pressure polymorph $\beta\text{-HPN}_2$ are discussed. Additionally, FTIR and solid-state NMR spectroscopy are used to corroborate the results of the structure determination.

4.1 Introduction

Compounds that comprise tetrahedral framework structures are of high interest both from a scientific point of view as well as concerning their broad technical applicability. Archetypal tetrahedral framework structures are formed by silicates and related compounds like aluminosilicates or aluminophosphates.^[1–3] Prominent applications of such materials include sorption and catalysis in the case of zeolites^[4] as well as optical materials and piezoelectrics, particularly in the case of quartz.^[5] Properties of these functional materials are intrinsically facilitated by their respective crystal structures. Accordingly, the discovery of new tetrahedral framework structures both with new topologies or new elemental compositions is an important issue for material scientists.^[5]

The emerging interest in nitridosilicates during the last few years can in part be attributed to their broad structural variety as well as their high chemical and thermal stability. The latter qualities stem from the inclusion of the nitride ion N^{3-} , which in nitridosilicates can link up to four tetrahedral centers as opposed to two in the case of oxosilicates.^[6] Undoubtedly, this structural variability expands greatly the range of possible crystal structures and furthermore allows higher degrees of condensation than would be possible in oxosilicates. In recent years we could show that the substance class of (oxo)nitridophosphates rivals even the structural diversity of nitridosilicates. Silica analogous phosphorus oxonitride PON forms a high-pressure polymorph the structure of which was predicted for SiO_2 but has never been observed.^[7] Other representatives in this system include porous compounds such as the first nitridic zeolites NPO^[8,9] and NPT^[10] as well as the clathrate $\text{P}_4\text{N}_4(\text{NH})_4(\text{NH}_3)$.^[11] Glassy compounds in the system Li-Ca-P-N have displayed remarkable values for hardness and refractive index.^[12,13] Existing applications of phosphorus nitrides like PON and HPN_2 are mainly in the field of flame retardation.^[14,15] Theoretically predicted cubic BeP_2N_4 is expected to show superior mechanical properties,^[16] possibly making it a suitable material for high performance tools. As these examples show, further

research on new nitridophosphate frameworks is likely to lead to the discovery of novel compounds exhibiting interesting properties.

The synthesis of nitridophosphates can be markedly facilitated by the use of high-pressure techniques. On the one hand this approach allows suppression of thermal decomposition of the products which occurs typically at high temperatures necessary for synthesis. On the other hand – according to the pressure-coordination rule^[17] – very high pressures allow access to structures featuring higher coordination numbers,^[18] one of the most prominent examples being the mineral stishovite.^[19] In the case of phosphorus nitrides a higher coordination number of phosphorus has been realized in γ - P_3N_5 , where two thirds of the P atoms are coordinated by nitrogen in the form of a square pyramid.^[20,21] An increase in coordination number often leads to a significantly increased hardness, making such type of compounds interesting for material scientists.^[18] In this contribution we demonstrate the high structural flexibility of nitridophosphate frameworks by characterizing an entirely new topology realized in a high-pressure polymorph of phosphorus nitride imide β - HP_4N_7 .

4.2 Experimental Section

4.2.1 Synthesis of P_3N_5

P_3N_5 was obtained by reaction of P_4S_{10} with dry ammonia gas according to the literature.^[22] P_4S_{10} (8.0 g, 36 mmol, 99 %, Sigma-Aldrich) was placed inside an open ended silica glass tube (length 30 cm) which was inserted into a silica glass flow tube. The reactant was saturated with streaming dry ammonia (99.98%, Air Liquide) for 4 h at room temperature and subsequently heated to 850 °C for 8 h. After cooling the brown reaction product was washed subsequently with deionized water, ethanol and acetone.

4.2.2 Synthesis of $\beta\text{-HP}_4\text{N}_7$

$\beta\text{-HP}_4\text{N}_7$ was synthesized under high-pressure/high-temperature conditions in a modified Walker-type multianvil assembly using a 1000 t hydraulic press (Voggenreiter, Mainleus, Germany). P_3N_5 (48 mg, 0.295 mmol) and NH_4Cl (4 mg, 0.075 mmol, 99.5 %, Sigma-Aldrich) were thoroughly ground in an agate mortar, tightly packed into a cylindrical boron nitride crucible (Henze, Kempten, Germany) and centered in a 18/11 MgO octahedron. A detailed description of the assembly can be found in the literature.^[23–27] The sample was compressed between eight truncated tungsten carbide cubes (Hawedia, Marklkofen, Germany) to a pressure of 6 GPa at room temperature during 164 min. It was subsequently heated to 800 °C during 15 min, held at this temperature for 240 min and cooled to room temperature during 30 min. Finally, it was decompressed during 600 min. After isolation and grinding the sample was obtained as a light gray air-stable powder. Excess NH_4Cl was removed by washing the sample with deionized water, ethanol and acetone. Single crystals suitable for X-ray diffraction were obtained by heating the reaction mixture to 1300 °C within 15 min, holding the temperature for 60 min and cooling within 15 min.

4.2.3 Spectroscopic Analysis

The chemical composition of the sample was established by energy dispersive X-ray spectroscopy using a JSM 6500F scanning electron microscope (Jeol) with an Oxford Instruments 7418 Si/Li EDX detector. FTIR spectra were collected employing KBr disks with the use of an IFS 66 v/S spectrometer (Bruker). Solid-state MAS NMR experiments were carried out on an Avance III spectrometer (Bruker) at a field strength of 11.7 T with a 2.5 mm probe at a spinning rate of 20 KHz. ^1H and ^{31}P chemical shift values are referenced to 0.1% TMS in CDCl_3 (Sigma Aldrich) as an external reference. Diffuse reflectance UV-Vis spectroscopy was carried out on a Cary 500 spectrometer (Varian) equipped with a praying mantis diffuse reflectance accessory.

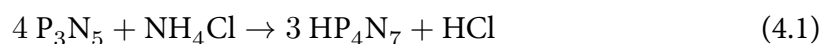
4.2.4 Crystal Structure Analysis

Single crystal X-ray diffraction analysis was carried out on a Bruker D8 Quest diffractometer equipped with a microfocus X-ray source (Mo- K_α radiation) at 140 K. A crystal of the size $0.035 \times 0.065 \times 0.070$ mm was chosen from the coarsely ground sample under paraffin oil. The crystal structure was solved ab initio using the charge-flipping algorithm as implemented in the program Superflip.^[28–30] Subsequent full-matrix least squares refinement was carried on F^2 out using SHELXL-97.^[31] The position of the hydrogen site was extracted from difference fourier maps. The N–H distance was restrained to 0.9 Å. Due to the low absorption coefficient and the very small crystal size no absorption correction was applied. Powder X-ray diffraction data was collected in parafocusing Debye-Scherrer geometry on a Stadi P diffractometer (Stoe, Darmstadt, Germany) using Ge(111)-monochromated Cu- $K_{\alpha 1}$ radiation and a linear position sensitive detector. The ground sample was enclosed in a glass capillary (diameter 0.3 mm). Rietveld refinement was carried out using TOPAS-Academic 4.^[32] The peak shape was modeled using the fundamental parameters approach (direct convolution of source emission profiles, axial instrument contributions and crystallite size and microstrain effects).^[33,34]

4.3 Results and Discussion

4.3.1 Synthesis

As previously reported the synthesis of phase pure α -HP₄N₇ was accomplished with the use of the moisture sensitive molecular precursor (NH₂)₂P(S)NP(NH₂)₃.^[35,36] Under ambient pressure the simple reaction between phosphorus nitride and ammonium chloride (Eq. 4.1) does not yield a pure product.



However, at high pressures this reaction proceeds cleanly and yields pure samples of $\beta\text{-HP}_4\text{N}_7$. This high pressure polymorph can be synthesized in a multianvil assembly at pressures between 5 and 8 GPa at temperatures ranging from 750 to 1400 °C. Purest samples have been obtained at 750 °C with constant heating for 240 min. Higher reaction temperatures lead to the formation of significant amounts of side phases but promote crystal growth. Therefore single crystals for structure determination were grown at 1300 °C, whereas bulk samples were synthesized at 800 °C. The purpose of using NH_4Cl in this synthesis is twofold. Primarily, it acts as reactant and H^+ -donor. However, recently we have demonstrated that NH_4Cl functions as an effective mineralizer for the synthesis of nitridophosphates.^[37] With this synthetic approach the product is obtained in form of a gray sintered pellet that yields a light gray air stable powder after grinding. Single crystals of $\beta\text{-HP}_4\text{N}_7$ form colorless platelets. An atomic ratio of $\text{P}:\text{N} = 4:6.9$ was determined by energy dispersive X-ray (EDX) analysis, which is in good agreement with the sum formula HP_4N_7 . Oxygen was only detectable in trace amounts in the sample.

4.3.2 Crystal Structure of $\beta\text{-HP}_4\text{N}_7$

The crystal structure of $\beta\text{-HP}_4\text{N}_7$ was determined from single crystal X-ray diffraction data. The reflections were indexed with a monoclinic unit cell ($a = 12.873(2)$, $b = 4.6587(4)$, $c = 8.3222(8)$ Å, $\beta = 102.351(3)^\circ$).^[38] Structure solution was performed assuming space group $C2/c$ (15), as indicated by the systematic absences. All heavy atom positions were determined during structure solution. The position of the hydrogen atom was unequivocally localized from difference Fourier maps during structure refinement. The single crystallographic hydrogen atom site leads to two adjacent positions in the unit cell coupled by an inversion center. Their respective distances indicate a mutual exclusive occupation, represented by a fixed occupation factor of 0.5 during structure refinement. Due to the small diffraction contribution of hydrogen it cannot be decided whether a symmetry reduction (loss of centrosymmetry towards Cc) leading to an ordered structure model with respect

Table 4.1: Crystallographic data and details of the structure refinement for β -HP₄N₇.

formula	β -HP ₄ N ₇
crystal size / mm ³	$0.035 \times 0.065 \times 0.070$
molar mass / g · mol ⁻¹	222.96
crystal system	monoclinic
space group	<i>C2/c</i> (no. 15)
T / K	140(2)
radiation, λ / pm	Mo-K α , 71.073
<i>a</i> / Å	12.873(2)
<i>b</i> / Å	4.6587(4)
<i>c</i> / Å	8.3222(8)
β / °	102.351(3)
<i>V</i> / Å ³	487.55(8)
<i>Z</i>	4
calculated density / g · cm ⁻³	3.037
absorption coefficient / mm ⁻¹	1.459
measured reflections	8803
independent reflections	1218
observed reflections	909
refined parameters	55
GOF	1.046
final R indices [<i>I</i> > 2s(<i>I</i>)]	$R_1 = 0.0485$ $wR_2 = 0.0984$ ^[a]
final R indices (all data)	$R_1 = 0.0769$ $wR_2 = 0.1083$ ^[a]

[a] $w = 1/[\sigma^2(F_o^2) + (0.0458 P)^2 + 2.3837 P]$, with $P = (F_o^2 + 2F_c^2) / 3$

Table 4.2: Atomic coordinates and isotropic equivalent displacement parameters for $\beta\text{-HP}_4\text{N}_7$.

atom	Wyckoff symbol	x	y	z	$U_{\text{iso}} / \text{\AA}^2$	occupancy
P1	$8f$	0.18029(5)	0.2114(2)	0.22415(7)	0.0038(2)	1
P2	$8f$	0.10496(5)	0.3067(2)	$-0.13583(7)$	0.0041(2)	1
N1	$4e$	0	0.1987(6)	$-\frac{1}{4}$	0.0063(7)	1
N2	$8f$	0.1025(2)	0.1964(4)	0.0467(3)	0.0061(5)	1
N3	$8f$	0.1384(2)	0.3666(4)	0.3650(2)	0.0051(4)	1
N4	$8f$	0.2947(2)	0.3702(4)	0.2069(2)	0.0049(4)	1
H1	$8f$	0.051(4)	0.065(11)	0.035(9)	0.01(2)	0.5

Table 4.3: Selected interatomic distances / \AA and angles / $^\circ$ in $\beta\text{-HP}_4\text{N}_7$.

P1–N2	1.599(2)	P2–N1–P2	142.2(2)
P1–N3	1.568(2)	P1–N2–P2	136.2(2)
P1–N4	1.682(2)	P1–N3–P2	125.3(2)
P1–N4'	1.697(2)	P1–N4–P1	119.3(2)
P2–N1	1.560(2)	P1–N4–P2	123.3(2)
P2–N2	1.610(2)	P1–N4–P2'	117.3(2)
P2–N3	1.581(2)		
P2–N4	1.739(2)		
N2–H1	0.89(5)		
N2...H1	2.29(5)		

to the hydrogen atoms is required. Crystallographic data for $\beta\text{-HP}_4\text{N}_7$ are summarized in Table 4.1. Details on the atomic positions as well as selected bond lengths and angles are listed in Tables 4.2 and 4.3, respectively.

The crystal structure of $\beta\text{-HP}_4\text{N}_7$ (Figure 4.1) consists of a three-dimensional network of all-side vertex-sharing PN_4 tetrahedra. In contrast to the ambient pressure modification there are no edge-sharing tetrahedra. The framework is characterized by the existence of 3-, 4- and 5-rings. The six-membered rings are large enough to provide space for the single

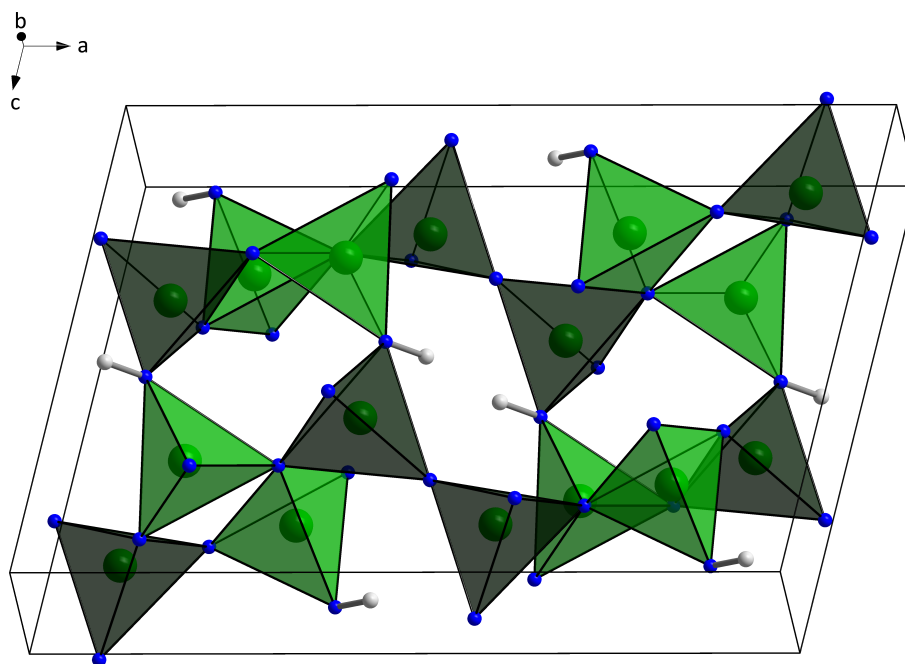


Figure 4.1: Crystal structure of β -HP₄N₇ in polyhedral representation (P1: light green, P2: dark green, N: blue, H: white).

hydrogen atom, which is covalently bound to half of the nitrogen atoms pointing into the ring.

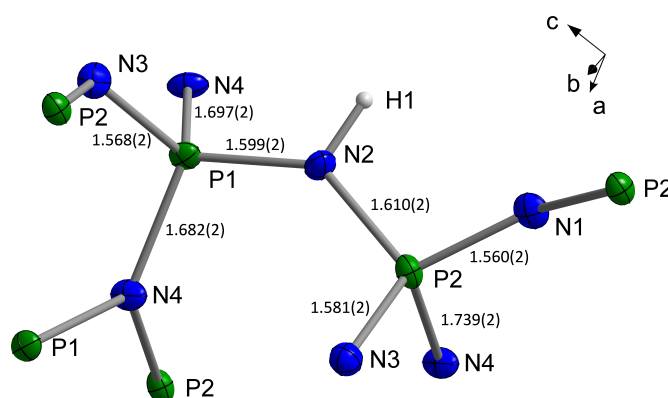


Figure 4.2: Atomic arrangement of P, N, H and bond lengths in β -HP₄N₇. Displacement ellipsoids are displayed at the 90 % probability level.

Figure 4.2 illustrates the coordination of the atoms in $\beta\text{-HP}_4\text{N}_7$. Both P atoms are coordinated tetrahedrally by nitrogen, with bond angles P–N–P $103.7(1)\text{--}120.8(2)^\circ$ slightly deviating from the regular tetrahedral angle. The N bridges are linking either two or three PN_4 tetrahedra, respectively. The position of the H atoms is corroborated by the fact that P–N bonds around the protonated N2 are significantly longer than those of the unprotonated N1 and N3. Bond lengths around the triply coordinating N4 are even larger ranging from $1.682(2)$ to $1.739(2)$ Å, which is consistent with the values observed in other nitridophosphates such as $\alpha\text{-HP}_4\text{N}_7$ or MP_4N_7 ($M = \text{Na}, \text{K}, \text{Rb}, \text{Cs}$).^[39] The bond angles around N4 are very close to 120° , which is indicative of an almost regular trigonal planar coordination. In contrast to $\alpha\text{-HP}_4\text{N}_7$ no edge sharing of tetrahedra occurs in this framework. Nevertheless, the phase transition leads to an increase in density of 6.0 %. Therefore, the increase of density due to the tilting of the tetrahedra offsets the loss of shared tetrahedra edges and leads to an overall higher density of $\beta\text{-HP}_4\text{N}_7$. This difference in densities stabilizes this crystal structure at high pressures.

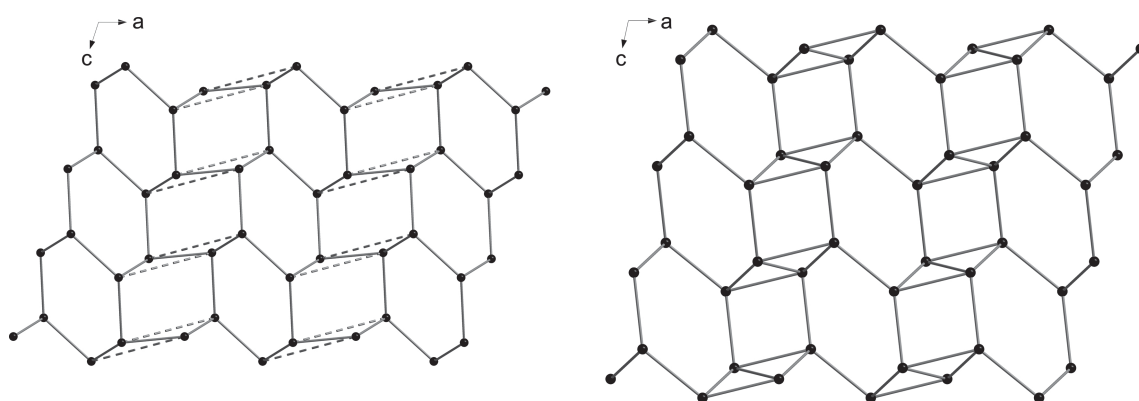


Figure 4.3: Topological relation between $\beta\text{-HPN}_2$ (left) and $\beta\text{-HP}_4\text{N}_7$ (right). Only P atoms (black spheres) are displayed for clarity. Each connecting line represents a P–N–P bond. New bonds formed by formal condensation are indicated by dashed lines.

In order to characterize the framework topology of the network the point symbol $(3^2.4^2.5^2.6^3.7)$ ($3^4.4^4.5^4.6^3$) was calculated by the program TOPOS.^[40,41] This network topology is distinct from that of $\beta\text{-HP}_4\text{N}_7$, the isosteric $\text{P}_4\text{N}_6\text{O}$,^[42] as well as the related

nitridophosphates MP_4N_7 ($M = \text{Na, K, Rb, Cs}$)^[39] and has in fact not been observed in any compound so far. The change in topology also indicates that the transition from $\alpha\text{-HP}_4\text{N}_7$ to $\beta\text{-HP}_4\text{N}_7$ is reconstructive. It has been illustrated in the past that the structure of ambient pressure HP_4N_7 can be derived from the structure of less condensed $\beta\text{-HPN}_2$. This process involves formal release of NH_3 and the simultaneous formation of new P–N–P linkages. Analogously, Figure 4.3 illustrates the formal topotactic condensation of the recently discovered high-pressure polymorph $\beta\text{-HPN}_2$ leading to $\beta\text{-HP}_4\text{N}_7$. The dashed lines indicate new connections formed during this process. During condensation half of the six-membered rings are preserved, while the other half forms the 3- and 4-rings due to additional linkages.

In order to confirm the electrostatic consistency of the crystal structure lattice energy calculations were performed using the MAPLE (Madelung part of lattice energy) software.^[43,44] Both the overall as well as the partial MAPLE values for $\beta\text{-HP}_4\text{N}_7$, listed in Table 4.4, are in good agreement with those of the ambient pressure polymorph. The small difference of 0.3 % between both polymorphs confirms that the crystal structure of $\beta\text{-HP}_4\text{N}_7$ described here is electrostatically valid. All the partial MAPLE values for the atomic sites also fall in the range described in the literature.^[6]

Table 4.4: Results of MAPLE calculations for $\alpha\text{-HP}_4\text{N}_7$ and $\beta\text{-HP}_4\text{N}_7$. All values are in $\text{kJ} \cdot \text{mol}^{-1}$.

MAPLE Value	$\alpha\text{-HP}_4\text{N}_7$	$\beta\text{-HP}_4\text{N}_7$
overall	104636	104316
P atoms	15691–17079	16054–16814
N ^[2] atoms	5050–5679	4980–5498
N ^[3] atoms	6047–6163	6215

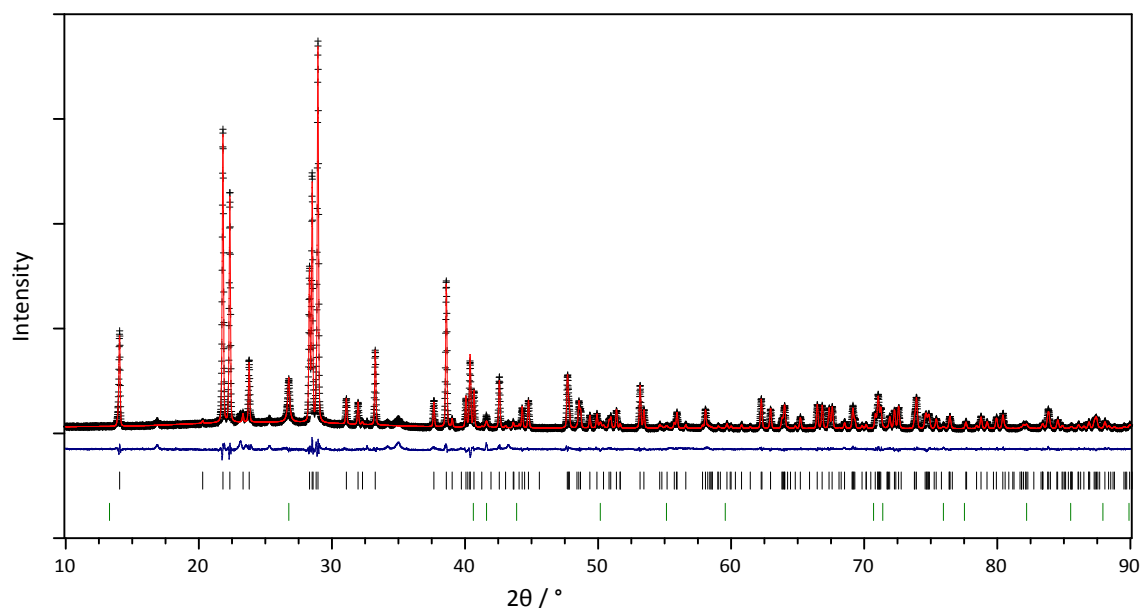


Figure 4.4: Observed (crosses) and calculated (red line) powder diffraction pattern of $\beta\text{-HP}_4\text{N}_7$ as well as position of Bragg reflections (black: $\beta\text{-HP}_4\text{N}_7$; green: BN) and difference profile (blue line).

4.3.3 Powder X-Ray Diffraction and Rietveld Refinement

In order to determine the bulk composition of the sample and evaluate the possible presence of side phases a powder diffraction pattern was collected. Rietveld refinement was performed using the TOPAS-Academic package. The powder pattern and resulting difference curves are displayed in Figure 4.5. The refinement shows that the sample is composed of 89 % of $\beta\text{-HP}_4\text{N}_7$ and 11 % of the crucible material BN. A few weak reflections could not be attributed to any known phase. Their position does not correspond to any possible superstructure of $\beta\text{-HP}_4\text{N}_7$. Therefore these peaks are likely due to small amounts of an unknown impurity. The refinement also confirms the structure determined by single crystal structure analysis. Further details on the Rietveld refinement can be found in the supporting information. In order to ascertain the thermodynamic stability of $\beta\text{-HP}_4\text{N}_7$, high temperature powder X-ray diffraction was performed. No phase transition could be determined up to the maximum temperature of 800 °C. This could suggest that $\beta\text{-HP}_4\text{N}_7$

could be the thermodynamically stable phase at ambient pressure. However, due to the large difference in densities, it is more likely that phase transition to the ambient pressure phase is kinetically hindered below 800 °C.

4.3.4 Spectroscopic Methods

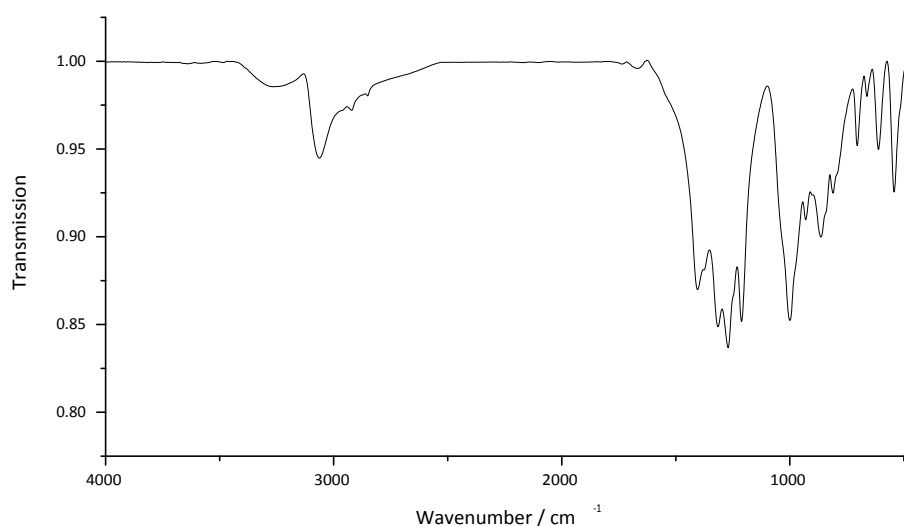


Figure 4.5: FTIR spectrum of β -HP₄N₇.

Due to the fact that HP₄N₇ and P₄N₆O are isoelectronic X-ray diffraction is insufficient to prove the identity of the title compound. In order to unequivocally determine the presence of hydrogen in the sample FTIR and solid-state NMR spectroscopy was performed. As expected, the FTIR spectrum of β -HP₄N₇ (Figure 4.4) bears a strong similarity to that of β -HP₄N₇. The strong N–H stretching band at 3000 cm⁻¹ shows that the sample contains significant amounts of imidic hydrogen (N–H groups). Further bands at 1050–1500 cm⁻¹ and 600–1000 cm⁻¹ correspond to P=N–P and P–NH–P asymmetric stretching modes, respectively.^[35,36,45] Additional indication of the presence of stoichiometric amounts of hydrogen can be obtained from the ¹H solid-state NMR spectrum shown in Figure C.1 in the supporting information.

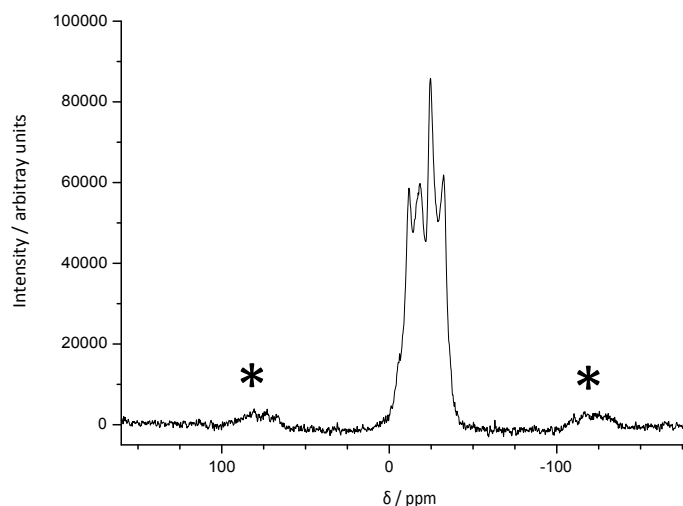


Figure 4.6: ^{31}P MAS NMR spectrum of $\beta\text{-HP}_4\text{N}_7$. Rotational sidebands are marked with asterisks.

Information about the local chemical environments of the P atoms can be derived from the ^{31}P solid-state NMR spectrum, which is displayed in Figure 4.6. The sample exhibits four distinct signals, which correspond to four different atomic environments. This seems to be contradictory with the fact that the single crystal structure only shows two distinct P sites. However, this discrepancy can be explained by the nature of the H atom. Since only one of the two adjacent hydrogen sites can be occupied simultaneously, inversion symmetry is violated locally and the P sites split into four distinct atomic environments. Due to the extremely small influence of the hydrogen atom on the total electron density the effect of this phenomenon is not detectable using X-ray crystallography. The chemical shifts of the signals (-11.8 ppm, -18.4 ppm, -24.6 ppm, -32.5 ppm) are close to the shift reported for $\beta\text{-HP}_4\text{N}_7$ and fall into the range expected for highly condensed nitridophosphates.

In order to gain insight into the gray color of the sample the band gap of the sample was investigated using diffuse reflectance UV-VIS spectroscopy. The Tauc plot (Figure C.1) shows that the band gap of $\beta\text{-HP}_4\text{N}_7$ is higher than 4.5 eV. Thus the color of the sample is not intrinsic, but rather due to small amounts of a dark impurity.

4.4 Conclusion

A new polymorph of phosphorus nitride imide HP_4N_7 has been synthesized by reaction of P_3N_5 and NH_4Cl at high-pressure high-temperature conditions. We were able to thoroughly characterize the compound by means of single crystal X-ray diffraction, FTIR and solid-state NMR spectroscopy. The compound crystallizes in an entirely new structure type with a framework topology that has not been observed so far. This structure consists of a three-dimensional framework of all-side vertex-sharing PN_4 tetrahedra. We could show that this structure can be derived from that of the high-pressure phase of HPN_2 by formal topotactic condensation. Considering the variety of different polymorphs in the closely related phosphorus oxonitride PON, the discovery of a phase transition in HP_4N_7 at moderate pressures could be indicative of the existence of further polymorphs at higher pressures. The structural flexibility displayed by HP_4N_7 makes it an interesting candidate for high-pressure synthesis of potential phases containing five- or sixfold coordinated phosphorus.

4.5 References

- [1] D. Taylor, *Mineral. Mag.* **1983**, 47, 319.
- [2] D. Taylor, *Mineral. Mag.* **1984**, 48, 65.
- [3] S. T. Wilson, B. M. Lok, C. A. Messina, T. R. Cannan, E. M. Flanigen, *J. Am. Chem. Soc.* **1982**, 104, 1146.
- [4] F. A. Mumpton, *Proc. Natl. Acad. Sci. U. S. A.* **1999**, 96, 3463.
- [5] G. H. Beall, *Rev. Mineral* **1994**, 29, 469.
- [6] M. Zeuner, S. Pagano, W. Schnick, *Angew. Chem. Int. Ed.* **2011**, 50, 7754; *Angew. Chem.* **2011**, 123, 7898.

- [7] D. Baumann, S. Sedlmaier, W. Schnick, *Angew. Chem. Int. Ed.* **2012**, *51*, 4707; *Angew. Chem.* **2012**, *124*, 4785.
- [8] S. Correll, O. Oeckler, N. Stock, W. Schnick, *Angew. Chem. Int. Ed.* **2003**, *42*, 3549; *Angew. Chem.* **2003**, *115*, 3674.
- [9] S. Correll, N. Stock, O. Oeckler, J. Senker, T. Nilges, W. Schnick, *Z. Anorg. Allg. Chem.* **2004**, *630*, 2205.
- [10] S. J. Sedlmaier, M. Döblinger, O. Oeckler, J. Weber, J. S. auf der Günne, W. Schnick, *J. Am. Chem. Soc.* **2011**, *133*, 12069.
- [11] F. Karau, W. Schnick, *Angew. Chem. Int. Ed.* **2006**, *45*, 4505; *Angew. Chem.* **2006**, *118*, 4617.
- [12] T. Grande, J. R. Holloway, P. F. McMillan, C. A. Angell, *Nature* **1994**, *369*, 43.
- [13] T. Grande, S. Jacob, J. R. Holloway, P. F. McMillan, C. A. Angell, *J. Non-Cryst. Solids* **1995**, *184*, 151.
- [14] S. V. Levchik, G. F. Levchik, A. I. Balabanovich, E. D. Weil, M. Klatt, *Angew. Makromol. Chem.* **1999**, *264*, 48.
- [15] E. D. Weil, N. G. Patel, *Fire Mater.* **1994**, *18*, 1.
- [16] W. Y. Ching, S. Aryal, P. Rulis, W. Schnick, *Phys. Rev. B: Condens. Matter Mater. Phys.* **2011**, *83*, 155109–1.
- [17] A. Neuhaus, *Chimia* **1964**, *18*, 93.
- [18] F. J. Manjón, D. Errandonea, *Phys. Status Solidi B* **2009**, *246*, 9.
- [19] W. Sinclair, A. E. Ringwood, *Nature* **1978**, *272*, 714.
- [20] K. Landskron, H. Huppertz, J. Senker, W. Schnick, *Angew. Chem. Int. Ed.* **2001**, *40*, 2643; *Angew. Chem.* **2001**, *113*, 2713.

-
- [21] K. Landskron, H. Huppertz, J. Senker, W. Schnick, *Z. Anorg. Allg. Chem.* **2002**, 628, 1465.
- [22] A. Stock, H. Grüneberg, *Ber. Dtsch. Chem. Ges.* **1907**, 40, 2573.
- [23] H. Huppertz, *Z. Kristallogr.* **2004**, 219, 330.
- [24] N. Kawai, S. Endo, *Rev. Sci. Instrum.* **1970**, 41, 1178.
- [25] D. Walker, M. A. Carpenter, C. M. Hitch, *Am. Mineral.* **1990**, 75, 1020.
- [26] D. Walker, *Am. Mineral.* **1991**, 76, 1092.
- [27] D. C. Rubie, *Phase Transitions* **1999**, 68, 431.
- [28] L. Palatinus, G. Chapuis, *J. Appl. Crystallogr.* **2007**, 40, 786.
- [29] G. Oszlányi, A. Sütő, *Acta Crystallogr. Sect. A: Found. Crystallogr.* **2005**, 61, 147.
- [30] G. Oszlányi, A. Sütő, *Acta Crystallogr. Sect. A: Found. Crystallogr.* **2004**, 60, 134.
- [31] G. M. Sheldrick, *Acta Crystallogr. Sect. A: Found. Crystallogr.* **2008**, 64, 112.
- [32] A. Coelho, *TOPAS-Academic Version 4.1*, Coelho Software: Brisbane, **2007**.
- [33] J. Bergmann, R. Kleeberg, A. Haase, B. Breidenstein, *Mater. Sci. Forum* **2000**, 347-349, 303.
- [34] R. W. Cheary, A. A. Coelho, J. P. Cline, *J. Res. Natl. Inst. Stan.* **2004**, 109, 1.
- [35] S. Horstmann, E. Irran, W. Schnick, *Angew. Chem. Int. Ed. Engl.* **1997**, 36, 1992; *Angew. Chem.* **1997**, 109, 2085.
- [36] S. Horstmann, E. Irran, W. Schnick, *Z. Anorg. Allg. Chem.* **1998**, 624, 221.
- [37] A. Marchuk, F. J. Pucher, F. W. Karau, W. Schnick, *Angew. Chem. Int. Ed.* **2014**, 53, 2469; *Angew. Chem.* **2014**, 126, 2501.

- [38] Further details of the crystal structure investigation can be obtained from the Fach-informations-Zentrum Karlsruhe, 76344 Eggenstein-Leopoldshafen, Germany (fax: (+49)7247-808-666; email: crysdata@fiz-karlsruhe.de) on quoting the depository number CSD-427230.
- [39] K. Landskron, E. Irran, W. Schnick, *Chem. Eur. J.* **1999**, 5, 2548.
- [40] V. A. Blatov, M. O’Keeffe, D. M. Proserpio, *CrystEngComm* **2010**, 12, 44.
- [41] V. A. Blatov, *IUCr CompComm Newsletter* **2006**, 7, 4.
- [42] J. Ronis, B. Bondars, A. Vitola, T. Millers, J. Schneider, F. Frey, *J. Solid State Chem.* **1995**, 115, 265.
- [43] R. Hoppe, *Angew. Chem. Int. Ed. Engl.* **1966**, 5, 95; *Angew. Chem.* **1966**, 78, 52.
- [44] R. Hoppe, *Angew. Chem. Int. Ed. Engl.* **1970**, 9, 25; *Angew. Chem.* **1970**, 82, 7.
- [45] J. Lücke, W. Schnick, *Z. Anorg. Allg. Chem.* **1992**, 610, 121.

5 Pentacoordinated Phosphorus in a High-Pressure Polymorph of Phosphorus Nitride Imide $P_4N_6(NH)$

Dominik Baumann, Wolfgang Schnick

published in: *Angew. Chem. Int. Ed.* **2014**, 53, 14490. DOI: 10.1002/anie.201406086

published in: *Angew. Chem.* **2014**, 126, 14718. DOI: 10.1002/ange.201406086

Reprinted (adapted) with permission from *Angewandte Chemie*. Copyright 2014 John Wiley and Sons.

Abstract

Coordination numbers higher than usual are often associated with superior mechanical properties. In this contribution we report on the synthesis of the high-pressure polymorph of highly condensed phosphorus nitride imide $P_4N_6(NH)$ representing a new framework topology. This is the first example of phosphorus in trigonal-bipyramidal coordination being observed in an inorganic network structure. We were able to obtain single crystals and bulk samples of the compound employing the multi-anvil technique. γ - $P_4N_6(NH)$ has been thoroughly characterized using X-ray diffraction, solid-state NMR and FTIR spectroscopy. The synthesis of γ - $P_4N_6(NH)$ gives new insights into the coordination chemistry of phosphorus at high pressures. The synthesis of further high-pressure phases with higher coordination numbers exhibiting intriguing physical properties seems within reach.

5.1 Introduction with Results and Discussion

Unusually high coordination numbers of cations, particularly in covalent network structures, are often associated with interesting physical properties. The latter include high density, enhanced bulk modulus, and extraordinary mechanical hardness, all of which are of particular relevance for engineering applications.^[1,2] According to the pressure-coordination rule, high coordination numbers are likely to occur in high-pressure polymorphs.^[3] Therefore, explorative high-pressure synthesis is a highly valuable tool for the discovery of novel materials with intriguing properties.^[4] Perhaps one of the most notable examples of an increase in coordination number at high pressures is observed in the case of SiO_2 , which transforms to the six-coordinated stishovite structure type at pressures exceeding 9 GPa.^[5,6] This phase has long been considered the hardest known oxide^[7] and has only recently been surpassed by cotunnite-type TiO_2 .^[8] Recent investigations show that above 46 GPa silica analogous $AlPO_4$ adopts a $CaCl_2$ -like structure containing PO_6 octahedra.^[9] Similar phase transformations take place in Earth's mantle, most prominently in magnesium silicate $MgSiO_3$. High-pressure studies show that this mineral undergoes phase transitions to perovskite^[10] and post-perovskite^[11] structures at extreme pressures, both of which contain hexacoordinated Si atoms. Knowledge of these phase transitions greatly supports understanding of processes in planetary interiors. Increased coordination numbers also lead to interesting properties in nitride materials. Cubic boron nitride already enjoys widespread application as a high-temperature abrasive due to its extreme hardness.^[12,13] Silicon nitride Si_3N_4 is of high technological importance due to its mechanical and thermal properties.^[14] It can be converted to its cubic high-pressure polymorph γ - Si_3N_4 at elevated pressures.^[15,16] This high-pressure polymorph crystallizes in a spinel-type structure composed of SiN_4 tetrahedra as well as SiN_6 octahedra and displays a remarkably high hardness, which even surpasses that of stishovite.^[17] In the case of phosphorus nitrides an increased coordination number has to date only been observed in γ - P_3N_5 , which also shows an in-

creased hardness compared to the ambient pressure phase.^[18,19] In the latter compound chains of edge-sharing quadratic PN_5 -pyramids are linked by PN_4 tetrahedra to form a three-dimensional network. Even though a trigonal bipyramidal coordination is expected to be close in energy to a pyramidal one, no example for this coordination type has been found in inorganic network structures yet. Molecular species displaying this coordination geometry include PF_5 ,^[20,21] $\text{P}(\text{N}_3)_5$ ^[22] as well as phosphazenes.^[23] It has also been proposed to occur in the theoretically predicted high-pressure polymorph δ' - P_3N_5 .^[24] In this contribution we report on a new high-pressure polymorph of phosphorus nitride imide $\text{P}_4\text{N}_6(\text{NH})$, which contains phosphorus in trigonal-bipyramidal coordination. To date only the ambient pressure polymorph α - $\text{P}_4\text{N}_6(\text{NH})$ ^[25,26] as well as the high-pressure phase β - $\text{P}_4\text{N}_6(\text{NH})$,^[27] both of which contain only PN_4 tetrahedra, have been reported. Since this is the third reported polymorph of this compound we propose the name γ - $\text{P}_4\text{N}_6(\text{NH})$.

We were able to synthesize γ - $\text{P}_4\text{N}_6(\text{NH})$ by the reaction of P_3N_5 and NH_4Cl . The starting materials were treated at approximately 1200 °C for 120 min at a pressure of 14 GPa. The synthesis conditions were achieved using a modified Walker-type multianvil assembly and a 1000 t hydraulic press.^[28–32] The product was obtained as an air-stable colorless crystalline solid. The product contained crystals large enough to be suitable for single crystal X-ray diffraction. The formation of single crystals can be attributed to the presence of NH_4Cl acting as a mineralizer during the synthesis. This property has previously been utilized in the synthesis of the phosphorus nitrides β -HPN₂^[33] and β - $\text{P}_4\text{N}_6(\text{NH})$.^[27] The product was successively washed with deionized water, ethanol and acetone to remove excess NH_4Cl .

The composition of the obtained sample was analyzed using energy-dispersive X-ray (EDX) spectroscopy. The analysis confirmed the atomic ratio P:N of 4:7 and other than trace amounts of oxygen showed no signs of other elements being present in the sample. Details of the EDX results can be found in the supporting information.

The crystal structure of γ - $\text{P}_4\text{N}_6(\text{NH})$ was solved from single crystal X-ray diffraction data in the monoclinic space group $C2/c$ (no. 15) using direct methods.^[34] All the heavy

atom positions could be found during structure solution and were refined anisotropically. Due to its low scattering power and the small crystal size the H atoms could not be located. The crystal structure shows that γ - $P_4N_6(NH)$ is composed of a three-dimensional network of PN_4 tetrahedra and trigonal PN_5 bipyramids (Figure 5.1). The PN_5 bipyramids are connected via shared edges to form infinite strands along $[110]$ and $[1\bar{1}0]$. These are arranged in a mesh-like pattern and are mutually interconnected by bowtie-like P_2N_7 double tetrahedra.

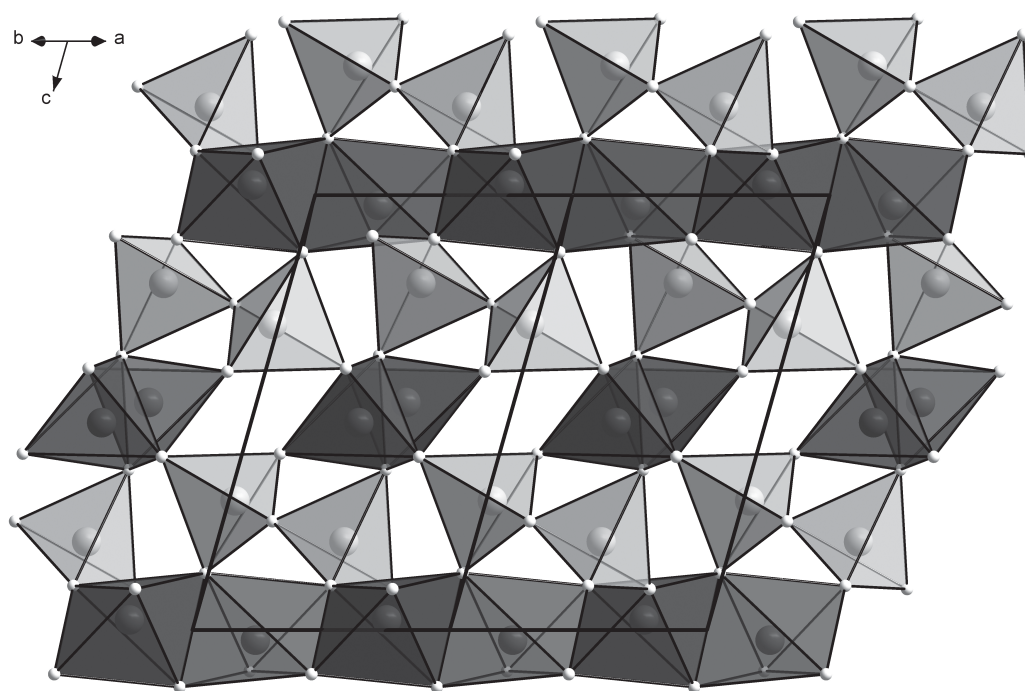


Figure 5.1: Crystal structure of γ - $P_4N_6(NH)$. View along $[110]$ (P: light/dark gray; N: white).

The framework topology can be unambiguously described with the point symbol $(3^2.4^6.5^6.6)$ $(3^4.4^8.5^7.6^2)$ as determined with the TOPOS software package.^[35,36] Due to the different coordination numbers of the P atom, the network topology is different to those of the other polymorphs. Therefore the phase transition leading to γ - $P_4N_6(NH)$

is necessarily a reconstructive one. The phase transition is associated with a considerable change in the crystal density. The change in density for the transition from β - to γ - $\text{P}_4\text{N}_6(\text{NH})$ results in a much higher difference in densities (18.9 %) than the transition from α - to β - $\text{P}_4\text{N}_6(\text{NH})$ (5.5 %). This behavior is expected due to the change in phosphorus coordination during the former transition.

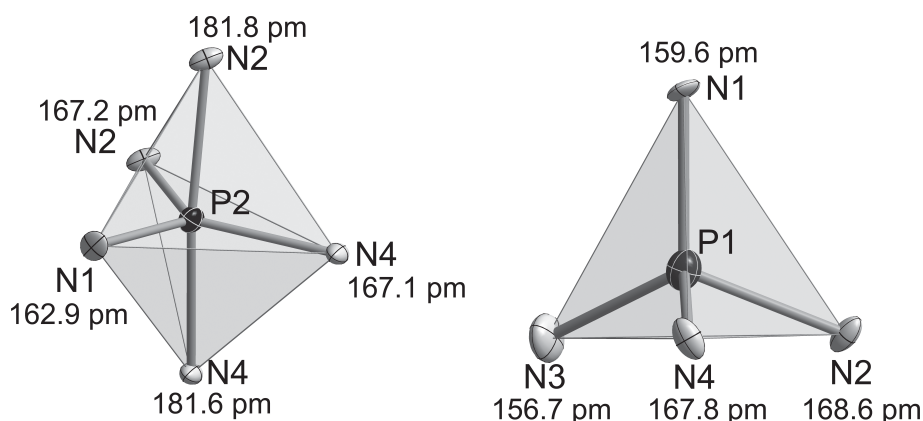


Figure 5.2: Coordination polyhedra and bond lengths around the two crystallographically distinct P atoms; ellipsoids are drawn with a probability factor of 90 %.

The bonds around the tetrahedrally coordinated phosphorus atom (Figure 5.2) vary in the range between 156 and 169 pm which is consistent with the values found in other nitridophosphates. Due to its higher coordination number, the bonds to the threefold coordinated nitrogen atoms N2 and N4 are about 10 pm longer than those to the doubly bridging nitrogen atoms N1 and N3. Tetrahedral angles (102 – 111°) show a slight deviation from the regular value. As would be expected,^[37] the bonds around the trigonal bipyramidal phosphorus show a larger variation, with the axial bonds (182 pm) being markedly longer than the equatorial ones (163–167 pm). In the equatorial plane the bond to N1 is shorter than those to the triply coordinated N4 and N2. The equatorial N atoms form an almost equilateral triangle with no N–P–N angle deviating more than 0.7° from the regular value of 120° . However, the axial nitrogen ligands display a distinct kink in the N–P–N arrangement, as evidenced by the angle of $170.5(2)^\circ$. This effect is presumably caused by the high

steric demand of this very dense network structure. While the location of the imidic H atom could not be directly determined from the structure analysis, crystal chemical considerations show that it is likely bound to N1. N2 and N4 already link three P atoms in a trigonal planar arrangement, thus unlikely representing NH-groups. The bond length P1–N1 is 2.9 pm longer than that to N3, which is likely due to the proton being bound to N1. Detailed information on bond lengths and angles can be found in the supporting information.

In order to verify the electrostatic consistency of the structure model, lattice energy calculations were performed using the program MAPLE (Madelung part of lattice energy).^[38,39] The overall MAPLE value for γ - $P_4N_6(NH)$ is in excellent agreement with that of β - $P_4N_6(NH)$, differing by less than 0.02 %. The partial MAPLE values of the atomic sites (P = 17030–16537; N = 4910–5673 kJ mol^{−1}) are in the range found in other nitridophosphates. The MAPLE values for N show a marked difference between N^[2] and N^[3], similar to what has been reported in literature.^[40] The imidic N1 displays the lowest partial MAPLE value. The same pattern has been observed in β - $P_4N_6(NH)$, further corroborating our hypothesis on the location of the proton.

The accuracy of the structure model as well as the phase purity of the sample has further been established by means of Rietveld refinement of the powder pattern (Figure 5.3). The results corroborate the established crystal structure and show that other than 0.45(4) weight percent of the crucible material BN, no side phases are present.

³¹P solid-state NMR spectroscopy (Figure D.1) shows two signals, which can be attributed to the two distinct atomic environments in γ - $P_4N_6(NH)$. The signal at −17.4 ppm is in a range typical for tetrahedrally coordinated phosphorus nitrides. The second signal is at a distinct chemical shift of −103.0 ppm. The only other example of a chemical shift in this range for phosphorus nitrides has been found in the case of γ - P_3N_5 , where the signal was attributed to tetragonal pyramidally coordinated phosphorus. Thus the general trend seems to be that higher coordination numbers shift the ³¹P signals significantly towards

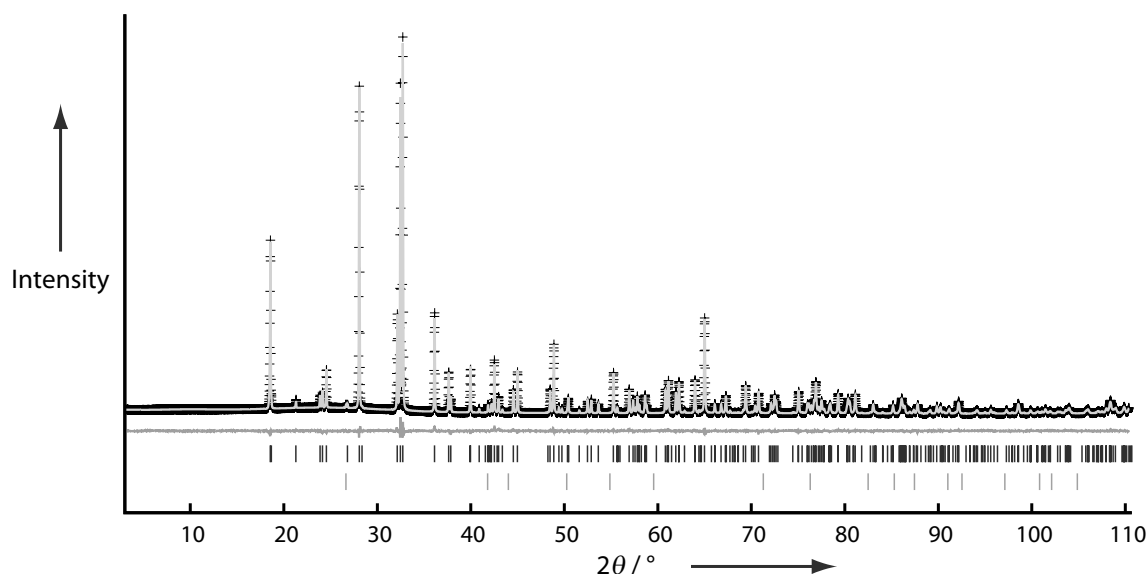


Figure 5.3: Observed (crosses) and calculated (light gray line) powder diffraction pattern of $\gamma\text{-P}_4\text{N}_6(\text{NH})$ as well as difference profile (dark gray line). Black and grey vertical bars represent the positions of Bragg reflections of $\gamma\text{-P}_4\text{N}_6(\text{NH})$ and hexagonal BN, respectively.

high fields. In order to gain more insight into the location of the hydrogen atom, a ^1H solid-state NMR spectrum (Figure D.2) was collected. It displays one single sharp peak at 10.6 ppm, corresponding to a single hydrogen site in the crystal structure.

The FTIR spectrum of the sample is reminiscent of that of the other polymorphs, as well as the less condensed phosphorus nitride imide PNNH.^[41] A broad absorption around 3000 cm^{-1} can be attributed to the N–H valence bond. Additionally, two groups of bands can be seen below 1500 cm^{-1} . The group in the range $1400\text{--}1200\text{ cm}^{-1}$ is caused by asymmetric P–N–P stretching modes. The second group between 600 and 1200 cm^{-1} can be attributed to symmetric P–N–P stretching modes.

With $\gamma\text{-P}_4\text{N}_6(\text{NH})$, we obtained the first inorganic network structure containing phosphorus in trigonal-bipyramidal coordination and the second one with pentacoordinated phosphorus at all. We were able to thoroughly characterize this compound by means of single crystal and powder X-ray diffraction as well as solid-state NMR and FTIR spectroscopy. The location of the H atom can be inferred with reasonable certainty. This shows

that in the pressure range attainable with the multianvil technique structures containing higher coordinated phosphorus are accessible. Therefore similar structures of related nitridophosphates like MP_4N_7 ^[42] and $M_3P_6N_{11}$ ($M = Na, K, Rb, Cs$)^[43–45] should be accessible. Similarly, this gives an indication that silica analogous phosphorus oxonitride PON could have a high-pressure polymorph containing pentacoordinated phosphorus, potentially representing a new AB_2 -type net. These findings could indicate that even compounds containing hexacoordinated phosphorus could be accessible in macroscopic amounts using multianvil techniques. Likely candidates are the theoretically predicted δ - P_3N_5 and δ' - P_3N_5 ^[24] as well as spinel type BeP_2N_4 .^[46]

5.2 References

- [1] F. J. Manjón, D. Errandonea, *Phys. Status Solidi B* **2009**, *246*, 9.
- [2] E. Horvath-Bordon, R. Riedel, A. Zerr, P. F. McMillan, G. Auffermann, Y. Prots, W. Bronger, R. Kniep, P. Kroll, *Chem. Soc. Rev.* **2006**, *35*, 987.
- [3] G. Demazeau, H. Huppertz, J. A. Alonso, R. Pöttgen, E. Moran, J. P. Attfield, Z. *Naturforsch. B: J. Chem. Sci.* **2006**, *61*, 1457.
- [4] E. Kroke, *Angew. Chem. Int. Ed.* **2002**, *41*, 77; *Angew. Chem.* **2002**, *114*, 81.
- [5] W. Sinclair, A. E. Ringwood, *Nature* **1978**, *272*, 714.
- [6] R. J. Hill, M. D. Newton, G. V. Gibbs, *J. Solid State Chem.* **1983**, *47*, 185.
- [7] J. M. Léger, J. Haines, M. Schmidt, J. P. Petitet, A. S. Pereira, J. A. H. da Jornada, *Nature* **1996**, *383*, 401.
- [8] L. S. Dubrovinsky, N. A. Dubrovinskaia, V. Swamy, J. Muscat, N. M. Harrison, R. Ahuja, B. Holm, B. Johansson, *Nature* **2001**, *410*, 653.
- [9] J. Pellicer-Porres, A. M. Saitta, A. Polian, J. P. Itié, M. Hanfland, *Nat. Mater.* **2007**, *6*, 698.

-
- [10] E. Knittle, R. Jeanloz, *Science* **1987**, 235, 668.
- [11] M. Murakami, K. Hirose, K. Kawamura, N. Sata, Y. Ohishi, *Science* **2004**, 304, 855.
- [12] J. R. H. Wentorf *J. Chem. Phys.* **1961**, 34, 809.
- [13] L. Vel, G. Demazeau, J. Etourneau, *Mater. Sci. Eng. B* **1991**, 10, 149.
- [14] F. L. Riley, *J. Am. Ceram. Soc.* **2000**, 83, 245.
- [15] A. Zerr, G. Miehe, G. Serghiou, M. Schwarz, E. Kroke, R. Riedel, H. Fueß, P. Kroll, R. Boehler, *Nature* **1999**, 400, 340.
- [16] M. Schwarz, G. Miehe, A. Zerr, E. Kroke, B. T. Poe, H. Fuess, R. Riedel, *Adv. Mater.* **2000**, 12, 883.
- [17] J. Z. Jiang, F. Kragh, D. J. Frost, K. Ståhl, H. Lindelov, *J. Phys.: Condens. Matter* **2001**, 13, L515.
- [18] K. Landskron, H. Huppertz, J. Senker, W. Schnick, *Angew. Chem. Int. Ed.* **2001**, 40, 2643; *Angew. Chem.* **2001**, 113, 2713.
- [19] K. Landskron, H. Huppertz, J. Senker, W. Schnick, *Z. Anorg. Allg. Chem.* **2002**, 628, 1465.
- [20] H. Kurimura, S. Yamamoto, T. Egawa, K. Kuchitsu, *J. Mol. Struct.* **1986**, 140, 79.
- [21] D. Mootz, M. Wiebcke, *Z. Anorg. Allg. Chem.* **1987**, 545, 39.
- [22] W. Buder, A. Schmidt, *Z. Anorg. Allg. Chem.* **1975**, 415, 263.
- [23] R. O. Day, A. Schmidpeter, R. R. Holmes, *Inorg. Chem.* **1983**, 22, 3696.
- [24] P. Kroll, W. Schnick, *Chem. Eur. J.* **2002**, 8, 3530.
- [25] S. Horstmann, E. Irran, W. Schnick, *Angew. Chem. Int. Ed. Engl.* **1997**, 36, 1992; *Angew. Chem.* **1997**, 109, 2085.
- [26] S. Horstmann, E. Irran, W. Schnick, *Z. Anorg. Allg. Chem.* **1998**, 624, 221.

- [27] D. Baumann, W. Schnick, *Inorg. Chem.* **2014**, 53, 7977.
- [28] N. Kawai, S. Endo, *Rev. Sci. Instrum.* **1970**, 41, 1178.
- [29] D. Walker, M. A. Carpenter, C. M. Hitch, *Am. Mineral.* **1990**, 75, 1020.
- [30] D. Walker, *Am. Mineral.* **1991**, 76, 1092.
- [31] D. C. Rubie, *Phase Transitions* **1999**, 68, 431.
- [32] H. Huppertz, *Z. Kristallogr.* **2004**, 219, 330.
- [33] A. Marchuk, F. J. Pucher, F. W. Karau, W. Schnick, *Angew. Chem. Int. Ed.* **2014**, 53, 2469; *Angew. Chem.* **2014**, 126, 2501.
- [34] Crystal data for γ - $P_4N_6(NH)$: crystal size: $0.011 \times 0.026 \times 0.026$ mm³, space group $C2/c$ (no. 15), $a = 6.8018(4)$, $b = 7.2204(5)$, $c = 8.9572(6)$ Å, $\beta = 111.231(2)^\circ$, $V = 410.05(5)$ Å³, $Z = 4$, $\rho_{\text{diffn}} = 3.612$ g cm⁻³, Bruker D8 Venture, Mo-K α radiation ($\lambda = 71.073$ pm), multi-scan absorption correction, 5565 reflections, 628 independent reflections, $R_{\text{int}} = 0.0273$, least-squares refinement on F^2 , R -values (all data / $F_o^2 \geq 2\sigma(F_o^2)$): $R_1 = 0.0301/0.0252$, $wR_2 = 0.0814/0.0788$, GooF = 1.197 for 555 observed reflections ($F_o^2 \geq 2\sigma(F_o^2)$) and 51 parameters. Further details on the crystal structure investigations may be obtained from the Fachinformationszentrum Karlsruhe, 76344 Eggenstein-Leopoldshafen, Germany (fax (+49)7247-808-666; E-Mail: crysdata@fiz-karlsruhe.de), on quoting the depository number CSD-427650.
- [35] V. A. Blatov, M. O'Keeffe, D. M. Proserpio, *CrystEngComm* **2010**, 12, 44.
- [36] V. A. Blatov, *IUCr CompComm Newsletter* **2006**, 7, 4.
- [37] D. E. C. Corbridge, *Phosphorus*, Elsevier, Amsterdam, **1990**, p. 994.
- [38] R. Hoppe, *Angew. Chem. Int. Ed. Engl.* **1966**, 5, 95; *Angew. Chem.* **1966**, 78, 52.
- [39] R. Hoppe, *Angew. Chem. Int. Ed. Engl.* **1970**, 9, 25; *Angew. Chem.* **1970**, 82, 7.

-
- [40] M. Zeuner, S. Pagano, W. Schnick, *Angew. Chem. Int. Ed.* **2011**, 50, 7754; *Angew. Chem.* **2011**, 123, 7898.
 - [41] J. Gobeau, R. Pantzer, *Z. Anorg. Allg. Chem.* **1972**, 390, 25.
 - [42] K. Landskron, E. Irran, W. Schnick, *Chem. Eur. J.* **1999**, 5, 2548.
 - [43] J. Ronis, B. Y. Bondars, A. A. Vitola, T. Millers, *Latv. PSR Zinat. Akad. Vestis Kim. Ser.* **1990**, 299.
 - [44] H. Jacobs, R. Nymwegen, *Z. Anorg. Allg. Chem.* **1997**, 623, 429.
 - [45] K. Landskron, W. Schnick, *J. Solid State Chem.* **2001**, 156, 390.
 - [46] W. Y. Ching, S. Aryal, P. Rulis, W. Schnick, *Phys. Rev. B: Condens. Matter Mater. Phys.* **2011**, 83, 155109–1.

6 $\text{Li}_{14}(\text{PON}_3)_2\text{O}$ – A Non-Condensed Oxonitridophosphate Oxide

Dominik Baumann, Wolfgang Schnick

published in: *Eur. J. Inorg. Chem.* 2015, 617. DOI: 10.1002/ejic.201403125

Reprinted (adapted) with permission from *European Journal of Inorganic Chemistry*. Copyright 2015 John Wiley and Sons.

Abstract

$\text{Li}_{14}(\text{PON}_3)_2\text{O}$ was synthesized by reaction of phosphoric triamide $\text{PO}(\text{NH}_2)_3$ with LiNH_2 at 550 °C. It crystallizes in a trigonal structure ($P\bar{3}$ (no. 147), $a = 5.6880(5)$, $c = 8.0855(8)$ Å, $V = 226.55(5)$ Å³, $Z = 1$) that can be described as a defect variant of the antiferite structure type. The crystal structure was elucidated from X-ray powder diffraction data and corroborated by FTIR and solid-state NMR spectroscopy. $\text{Li}_{14}(\text{PON}_3)_2\text{O}$ is composed of non-condensed PON_3^{2-} tetrahedra and O^{2-} ions that are surrounded by tetrahedrally coordinated Li^+ . This is the first example of an *ortho*-oxonitridophosphate.

6.1 Introduction

Over the past few decades nitridophosphates and oxonitridophosphates gained renewed interest due to their large structural variability. The parent compounds P_3N_5 ,^[1,2] PON ^[3] and $\text{PN}(\text{NH})$ ^[4] have been mentioned in literature since the 18th century. However, owing to intrinsic difficulties in crystal growth, their comprehensive structural description was not possible until the advent of modern powder diffraction techniques.^[5–8]

Due to the fact that both PON and $\text{PN}(\text{NH})$ are isoelectronic to SiO_2 ,^[9] (oxo)nitridophosphates and silicates often display similar structural features. Many of the well-studied structures of SiO_2 have also been found in PON , such as the cristobalite,^[10] quartz^[11] and coesite structure types.^[12] Structures comparable to layer and chain silicates are found in the compounds $\text{Sr}_2\text{P}_6\text{O}_6\text{N}_8$ ^[13] and $M_2\text{PN}_3$ ($M = \text{Ca}, \text{Mg}, \text{Zn}$).^[14,15] The high structural flexibility of (oxo)nitridophosphates may partly be caused by the fact that more than two tetrahedra can be linked by the nitride ion. And it is expressed by remarkable building blocks such as the star-shaped $\text{N}(\text{PO}_3)_3^{6-}$ ion^[16] or the adamantane analogous $\text{P}_4\text{N}_{10}^{10-}$ ion in $\text{Li}_{10}\text{P}_4\text{N}_{10}$.^[17] However, with Li_7PN_4 there is only one example of a nitridophosphate containing isolated tetrahedra.^[18] This is in stark contrast with the varied and extensive range of known *ortho*-silicates. Presumably, Li^+ is specifically capable for stabilization of highly charged *ortho*-anions like PN_4^{7-} .

Lithium oxonitridophosphates in particular have attracted attention as possible lithium ion conductors. They already enjoy application in the form of amorphous LiPON thin films.^[19] A variety of possible structural candidates for $\text{Li}_2\text{PO}_2\text{N}$ have been predicted on the basis of ab initio calculations by Holzwarth et al.,^[20] which closely resemble those verified by experiment.^[21]

In this contribution we report on the successful preparation of $\text{Li}_{14}(\text{PON}_3)_2\text{O}$, the first *ortho*-oxonitridophosphate, containing isolated PON_3^{2-} tetrahedra beside O^{2-} ions, synthesized using a molecular precursor.

6.2 Results and Discussion

Nearly phase pure samples of $\text{Li}_{14}(\text{PON}_3)_2\text{O}$ were obtained by high-temperature reaction of phosphoric triamide $\text{PO}(\text{NH}_2)_3$ and LiNH_2 in evacuated silica glass ampoules. Samples are microcrystalline, colorless and sensitive to moisture.

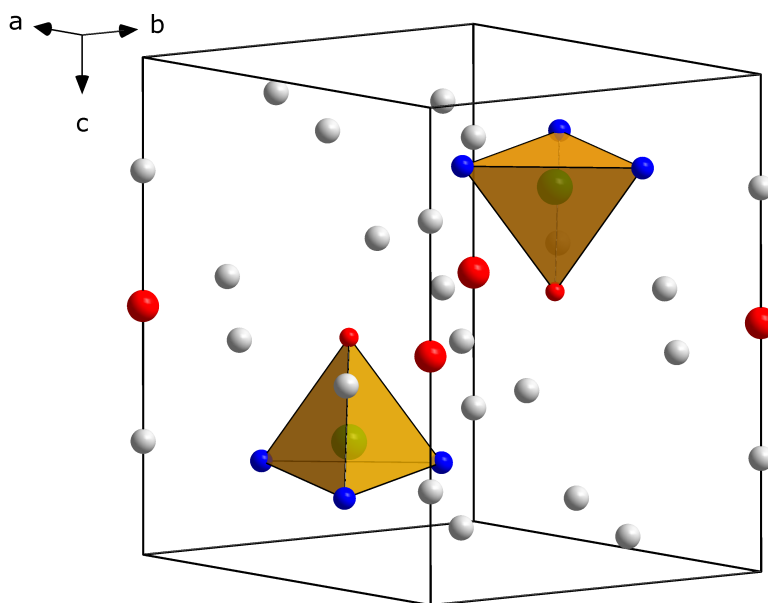


Figure 6.1: Crystal structure of $\text{Li}_{14}(\text{PON}_3)_2\text{O}$ (P: green, O: red, N: blue, Li: white).

The crystal structure of $\text{Li}_{14}(\text{PON}_3)_2\text{O}$ (Figure 6.1) was elucidated ab initio with the charge-flipping algorithm using X-ray powder diffraction data (Figure 6.2). The presence of elements other than Li, P, O and N was ruled out on the basis of energy dispersive X-ray (EDX) spectroscopy. Rietveld refinement showed only small amounts of an unidentified side phase. Assignment of the anion positions to O and N in an ordered way was carried out on the basis of their isotropic displacement parameters. Different distributions lead to significantly abnormal values, thus giving a strong indication that the structural model is correct. Additionally, this distribution of O and N leads to an electrically neutral structure as well as the occurrence of the expected PON_3^{6-} ion. The positions of Li^+ were determined from difference Fourier maps.

Table 6.1: Crystal data for $\text{Li}_{14}(\text{PON}_3)_2\text{O}$.

formula	$\text{Li}_{14}(\text{PON}_3)_2\text{O}$
formula mass / $\text{g} \cdot \text{mol}^{-1}$	291.16
crystal system / space group	trigonal, $P\bar{3}$ (no. 147)
lattice parameters / \AA	$a = 5.6880(5)$ $c = 8.0855(8)$
cell volume / \AA^3	226.55(5)
formula units per cell Z	1
X-ray density / $\text{g} \cdot \text{cm}^{-3}$	2.147
linear absorption coefficient / cm^{-1}	43.39
radiation	Cu- $\text{K}_{\alpha 1}$ ($\lambda = 154.059 \text{ pm}$)
monochromator	Ge(111)
diffractometer	Stoe StadiP
detector 2θ -range / $^\circ$	5–110.51
temperature / K	297(2)
data points	7035
number of observed reflections	198
number of parameters	52
constraints	0
program used	TOPAS Academic
structure solution	charge-flipping
structure refinement	Rietveld-Method
profile function	fundamental parameters model
background function	shifted Chebychev
R_{wp}	0.07553
R_{exp}	0.01776
R_{p}	0.04576
R_{Bragg}	0.01539
χ^2	4.252

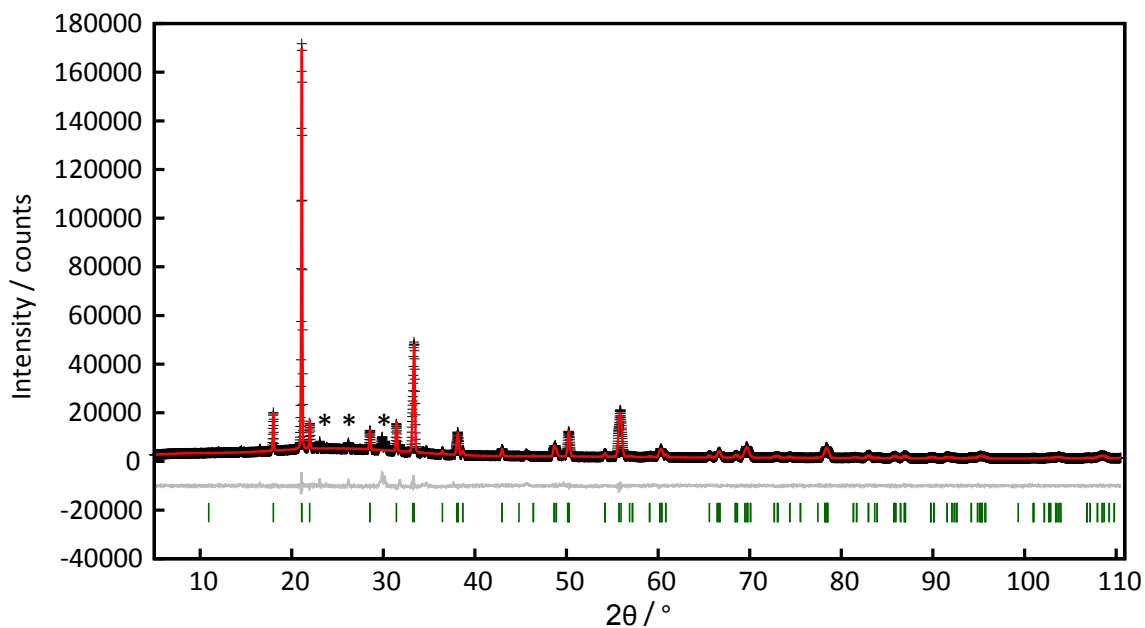


Figure 6.2: Observed (crosses) and calculated (red line) powder diffraction pattern of $\text{Li}_{14}(\text{PON}_3)_2\text{O}$ as well as position of Bragg reflections (green) and difference profile (gray line). Reflections from an unknown side phase are marked with asterisks.

Table 6.2: Atomic coordinates and isotropic equivalent displacement parameters for $\text{Li}_{14}(\text{PON}_3)_2\text{O}$.

atom	Wyckoff symbol	x	y	z	$U_{\text{iso}} / \text{\AA}^2$
P1	$2d$	$\frac{1}{3}$	$\frac{2}{3}$	0.2379(6)(7)	0.0074(6)
O1	$1b$	$\frac{1}{3}$	$\frac{2}{3}$	0.4482(9)	0.029(2)
O2	$2d$	0	0	$\frac{1}{2}$	0.044(4)
N1	$6g$	0.057(2)	0.6919(8)	0.1736(8)	0.023(2)
Li1	$6g$	0.045(3)	0.636(3)	0.909(2)	0.034(5)
Li2	$6g$	0.293(3)	0.291(3)	0.411(2)	0.037(4)
Li3	$2c$	0	0	0.77(1)	0.17(2)

$\text{Li}_{14}(\text{PON}_3)_2\text{O}$ crystallizes in the trigonal space group $P\bar{3}$ with the lattice parameters $a = 5.6880(5)$ and $c = 8.0855(8)$ Å. Further crystallographic data are summarized in Table 6.1 and atomic positions and isotropic displacement parameters are given in Table 6.2. The crystal structure (Figure 6.2) is isotypic to $\text{Li}_{14}\text{Cr}_2\text{N}_8\text{O}$ ^[22,23] and $\text{Na}_{14}\text{Mn}_2\text{O}_9$,^[24] albeit with a different anion arrangement. The crystal structure can be understood as a defect variant of the antiferite structure type. O^{2-} and N^{3-} ions are arranged in a slightly distorted cubic closest packing, while 16/18 of the tetrahedral voids are occupied by P^{5+} and Li^+ respectively. For every tetrahedral void occupied by P, one of the adjacent tetrahedral voids along [001] is unoccupied. Due to the occurrence of isolated PON_3^{6-} tetrahedra as well as isolated O^{2-} ions, $\text{Li}_{14}(\text{PON}_3)_2\text{O}$ can be considered a lithium oxonitridophosphate oxide. As detailed by Rabenau *et al.*, the cubic cell of the antiferite structure of Li_2O can be transformed to the trigonal cell found in $\text{Li}_{14}(\text{PON}_3)_2\text{O}$.^[22]

Transforming the unit cell of Li_2O in this manner results in a trigonal cell with lattice parameters $a = 5.6510$ and $c = 7.9917$ Å. These values and consequently the cell volume of 221.01 Å^3 are very close to the values found for $\text{Li}_{14}(\text{PON}_3)_2\text{O}$ ($a = 5.6880$ and $c = 8.0855$ Å, $V = 226.55 \text{ Å}^3$). The slightly larger cell dimensions of the title compound are presumably due to the slightly larger ionic radius of N^{3-} (146 pm) compared to O^{2-} (138 pm).^[25] The "isolated" oxygen atom O2 is coordinated by 8 Li atoms in the form of a slightly distorted cube, whereas, due to the incomplete filling of the tetrahedral voids, O1 and N1 are coordinated in the shape of a cube with one of its vertices removed. This coordination polyhedron resembles a strongly distorted capped trigonal bipyramid.

Atomic arrangements and bond lengths in $\text{Li}_{14}(\text{PON}_3)_2\text{O}$ are displayed in Figure 6.3. Bond lengths around P are 170.0(9) to O and 172.8(7) pm to N respectively. These values are comparable to the value 173.3 pm found in closely related Li_7PN_4 ,^[18] but significantly longer than those found in $\text{PO}(\text{NH}_2)_3$,^[26] which can be explained by the higher charge of the PON_3^{2-} ion. With values between $107.5(3)$ and $111.4(3)^\circ$, O/N–P–O/N-angles differ only slightly from the regular tetrahedral angle. Bond lengths around Li differ greatly due

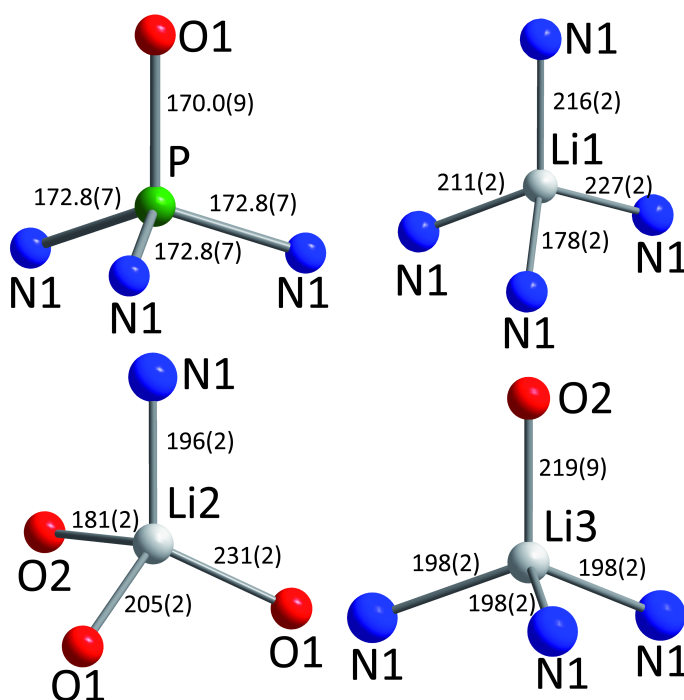


Figure 6.3: Interatomic distances / pm in $\text{Li}_{14}(\text{PON}_3)_2\text{O}$.

to the different properties of the coordinating anions. Distances between Li and the isolated O2 (181–220 pm) and N1 (178–227 pm) are shorter than those to O1 (205–231 pm). The variation of these distances may be due to the more covalent nature of the P–N-bonds and its small variability in length, which leads to a distortion of the $\text{Li}(\text{O},\text{N})_4$ tetrahedra.

In order to prove complete deprotonation of $\text{PO}(\text{NH}_2)_3$ to PON_3^{2-} , and the consequential absence of H as described by the structural model, FTIR spectroscopy was performed. The spectrum (Figure 6.4) shows only a very weak signal in the region where N–H-vibrations are expected, which can be explained by surface hydrolysis of the sample. However, the presence of stoichiometric amounts of hydrogen in the sample seems to be unlikely. P–O and P–N vibrations are visible in the region between 500 and 1000 cm^{-1} .

Solid-state NMR spectroscopy was used to corroborate the crystal structure model. The ^{31}P NMR spectrum shows a single strong resonance at 44.3 ppm. Small peaks between 25 and 0 ppm are caused by trace amounts of a side phase present in the sample. The

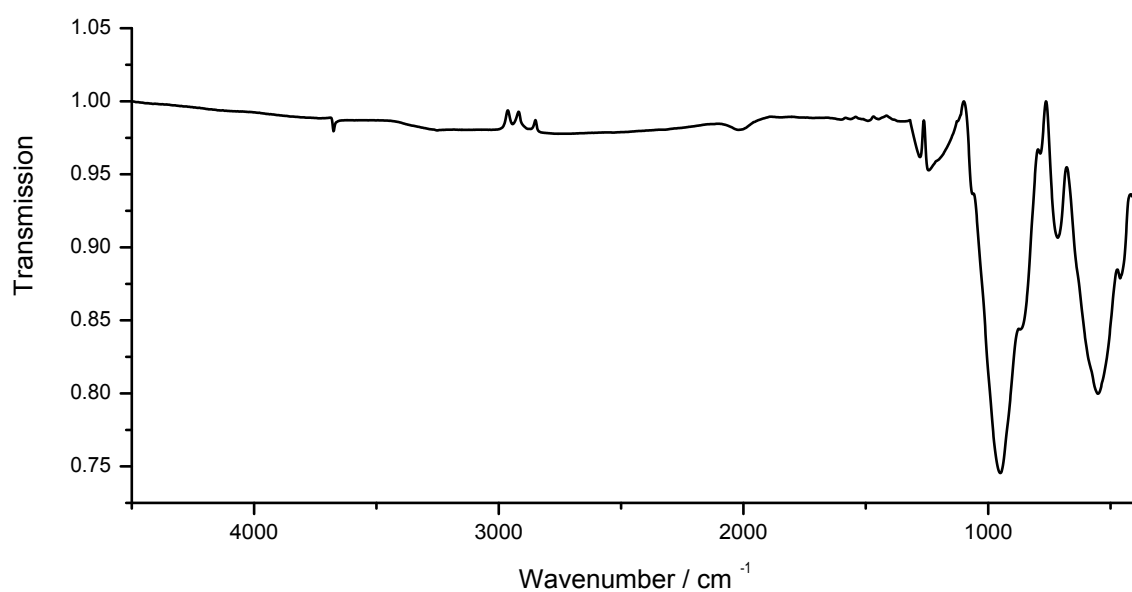


Figure 6.4: FTIR spectrum of $\text{Li}_{14}(\text{PON}_3)_2\text{O}$.

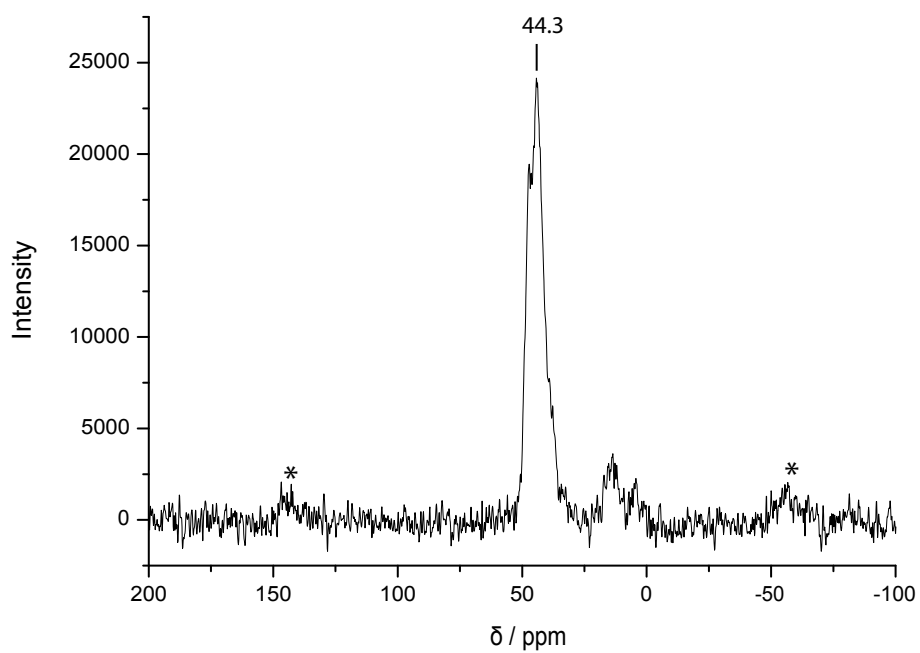


Figure 6.5: ^{31}P solid-state NMR spectrum of $\text{Li}_{14}(\text{PON}_3)_2\text{O}$ at 20 kHz MAS. Rotational sidebands are marked with asterisks.

single comparatively broad resonance can be attributed to the single crystallographic P site in the structural model. The large line width might be caused by cross-terms between the quadrupole interaction of the ^{14}N ($I=1$) and the dipolar coupling between ^{14}N and ^{31}P , which are in close proximity. The measured chemical shift is close to that observed for Li_7PN_4 ($\delta = 49.2, 54.6$ ppm).^[27] This suggests that the range of chemical shifts of *ortho*-(oxo)nitridophosphates is around 40–60 ppm. The ^7Li solid-state NMR spectrum (Figure E.1 in the supporting information) shows a single broad resonance at a chemical shift of 2.3 ppm that is a superposition of the crystallographically verified three distinct Li sites.

6.3 Conclusions

The crystal structure of $\text{Li}_{14}(\text{PON}_3)_2\text{O}$ was successfully elucidated using powder diffraction data. This is the first example of an *ortho*-oxonitridophosphate. Due to the chemical similarity to the *ortho*-nitridophosphate Li_7PN_4 , both compounds share structural similarities and can both be formally derived from the anti-fluorite structure type of Li_2O . The PON^{2-}_3 ion in this compound can be thought of as the full deprotonation product of phosphoric triamide $\text{PO}(\text{NH}_2)_3$. By varying the stoichiometric ratio of LiNH_2 and $\text{PO}(\text{NH}_2)_3$, a wide range of further lithium oxonitridophosphates with varying degrees of condensation might theoretically be accessible. The synthesis route of high-temperature deprotonation might thus be applicable for future synthesis of further new oxonitridophosphate materials. Since the related compounds Li_3N ^[28] and Li_7PN_4 ^[29] show significant lithium-ion conductivity, further investigations concerning the ionic conductivity of $\text{Li}_{14}(\text{PON}_3)_2\text{O}$ might be advisable in the future.

6.4 Experimental Section

6.4.1 General

All manipulations have been performed under exclusion of oxygen and moisture using either common air-free techniques in flame-dried glassware attached to a vacuum line or in an Ar-filled glove box (< 1 ppm O_2 , < 0.1 ppm H_2O , MBRAUN, Garching, Germany). Silica glass ampoules were sealed under dynamic vacuum using an oxyhydrogen torch. Phosphoric triamide $\text{PO}(\text{NH}_2)_3$ was synthesized from POCl_3 and liquid NH_3 according to the procedure described by Koch.^[30] 15 mL POCl_3 were slowly added to 150 mL of liquid NH_3 at -78 °C. The resulting suspension was further stirred for 1 h and the excess NH_3 was evaporated. In order to separate the mixture of $\text{PO}(\text{NH}_2)_3$ and NH_4Cl obtained in the previous step, it was refluxed with an excess of Et_2NH in CH_2Cl_2 until the evolution of NH_3 ceased. Pure $\text{PO}(\text{NH}_2)_3$ was then obtained by filtration from the suspension. The purity of the product was confirmed by powder X-ray diffraction. For the synthesis of $\text{Li}_{14}(\text{PON}_3)_2\text{O}$ $\text{PO}(\text{NH}_2)_3$ (23.8 mg, 0.25 mmol) and LiNH_2 (34.4 mg, 1.5 mmol, 95 %, Sigma-Aldrich) were thoroughly mixed in an agate mortar and filled into an evacuated silica glass ampoule. It was then placed in the center of a tube furnace. The temperature was raised to 550 °C at a rate of 15 K/h, held for 24 h and subsequently lowered to room temperature at 60 K/h. The product was obtained as a colorless, moisture sensitive powder.

6.4.2 Powder X-Ray Diffraction

Powder diffraction was carried out in parafocusing Debye-Scherrer geometry on a StadiP diffractometer (Stoe, Darmstadt, Germany) using Ge(111)-monochromated $\text{CuK}_{\alpha 1}$ -radiation and a linear PSD. The sample was enclosed in glass capillary ($\varnothing = 0.5$ mm). Structure solution and refinement on powder data were carried out using TOPAS Academic 4.1.^[31] Indexing of the powder pattern was achieved using the SVD-Algorithm.^[32] After intensity extraction using the Pawley method the structure was solved ab initio using the

charge flipping algorithm.^[33–35] During subsequent Rietveld refinement the peak shapes were modeled using the fundamental parameters approach (direct convolution of source emission profiles, axial instrument contributions and crystallite size and microstrain effects).^[36,37] The background was modeled as a Chebychev polynomial. Absorption effects are corrected by modeling a cylindrical sample with a packing density of 0.7. Preferred orientation was corrected by spherical harmonics functions of the 4th order.^[38] Further details of the crystal structure investigation can be obtained from the Fachinformations-Zentrum Karlsruhe, 76344 Eggenstein-Leopoldshafen, Germany (fax: (+49)7247-808-666; email: crysdata@fiz-karlsruhe.de) on quoting the depository number CSD-428737.

6.4.3 Spectroscopic Methods

FTIR spectroscopy was carried out on an IFS 66 v/S spectrometer (Bruker) using KBr disks. Solid-state NMR spectra were collected on a Bruker Avance III spectrometer equipped with an 11.7 T magnet and a 2.5 mm MAS probe at a spinning rate of 20 kHz, using direct excitation. Chemical shift values are referenced to 0.1% TMS in CDCl₃ (Sigma-Aldrich) as an external reference. Energy dispersive X-ray (EDX) spectroscopy was carried out on a Jeol JSM-6500F scanning electron microscope equipped with an Oxford Instruments Si/Li 7418 EDX detector.

6.5 References

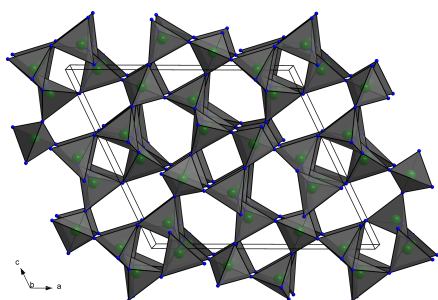
- [1] H. Rose, *Ann. Pharm.* **1834**, *11*, 129.
- [2] H. Rose, *Ann. Pharm.* **1834**, *11*, 139.
- [3] M. Gerhardt, *Ann. Chim. Phys.* **1846**, *18*, 188.
- [4] J. H. Gladstone, *Q. J. Chem. Soc.* **1862**, *14*, 121.

- [5] S. Horstmann, E. Irran, W. Schnick, *Angew. Chem. Int. Ed. Engl.* **1997**, 36, 1992; *Angew. Chem.* **1997**, 109, 2085.
- [6] S. Horstmann, E. Irran, W. Schnick, *Z. Anorg. Allg. Chem.* **1998**, 624, 221.
- [7] K. R. Waerstad, J. M. Sullivan *J Appl. Crystallogr.* **1976**, 9, 411.
- [8] W. Schnick, J. Lücke, *Z. Anorg. Allg. Chem.* **1992**, 610, 121.
- [9] A. L. Sauze, J. Haines, C. Chateac, J. M. Leger, R. Marchand, *Mater. Sci. Forum* **2000**, 325-326, 77.
- [10] J. M. Léger, J. Haines, C. Chateau, G. Bocquillon, M. Schmidt, S. Hull, F. Gorelli, A. Lesauze, R. Marchand, *Phys. Chem. Minerals* **2001**, 28, 388.
- [11] J. M. Léger, J. Haines, L. S. de Oliveira, C. Chateau, A. L. Sauze, R. Marchand, S. Hull, *J. Phys. Chem. Solids* **1999**, 60, 145.
- [12] D. Baumann, W. Schnick, *Angew. Chem. Int. Ed.* **2015**, 54, 4388; *Angew. Chem. Int. Ed.* **2015**, 127, 4463.
- [13] S. Sedlmaier, J. S. auf der Günne, W. Schnick, *Dalton Trans.* **2009**, 4081.
- [14] V. Schultz-Coulon, W. Schnick *Z. Anorg. Allg. Chem.* **1997**, 623, 69.
- [15] S. Sedlmaier, M. Eberspächer, W. Schnick, *Z. Anorg. Allg. Chem.* **2011**, 637, 362.
- [16] R. Conanec, W. Feldmann, R. Marchand, Y. Laurent, *J. Solid State Chem.* **1996**, 121, 418.
- [17] W. Schnick, U. Berger, *Angew. Chem. Int. Ed. Engl.* **1991**, 30, 830; *Angew. Chem.* **1991**, 103, 857.
- [18] W. Schnick, J. Lücke, *J. Solid State Chem.* **1990**, 87, 101.
- [19] J. Bates, N. Dudney, G. Gruzalski, R. Zuhr, A. Choudhury, C. Luck, J. Robertson, *J. Power Sources* **1993**, 43, 103.
- [20] Y. A. Du, N. Holzwarth, *Phys. Rev. B* **2010**, 81, 184106–1.

-
- [21] K. Senevirathne, C. S. Day, M. D. Gross, A. Lachgar, N. Holzwarth, *Solid State Ionics* **2013**, 233, 95.
- [22] A. Gudat, S. Haag, R. Kniep, A. Rabenau, *Z. Naturforsch. B: J. Chem. Sci.* **1990**, 45, 111.
- [23] J. Cabana, C. D. Ling, J. Oró-Solé, D. Gautier, G. Tobias, S. Adams, E. Canadelli, M. R. Palacín, *Inorg. Chem.* **2004**, 43, 7050.
- [24] G. Brachtel, R. Hoppe, *Z. Anorg. Allg. Chem.* **1978**, 438, 97.
- [25] R. D. Shannon, *Acta Crystallogr. Sect. A: Cryst. Phys. Diffr. Theor. Gen. Crystallogr.* **1976**, 32, 751.
- [26] G. J. Bullen, F. S. Stephens, R. J. Wade, *J. Chem. Soc. A* **1969**, 1804.
- [27] R. Lauterbach, Diplomarbeit, Universität Bayreuth, **1996**.
- [28] B. A. Boukamp, R. A. Huggins, *Mater. Res. Bull.* **1978**, 13, 23.
- [29] W. Schnick, J. Lücke, *Solid State Ionics* **1990**, 38, 271.
- [30] R. Klement, O. Koch, *Chem. Ber.* **1954**, 87, 333.
- [31] A. Coelho, *TOPAS-Academic Version 4.1*, Coelho Software: Brisbane, **2007**.
- [32] A. A. Coelho, *J. Appl. Crystallogr.* **2003**, 36, 86.
- [33] G. Oszlányi, A. Sütő, *Acta Crystallogr. Sect. A: Found. Crystallogr.* **2004**, 60, 134.
- [34] G. Oszlányi, A. Sütő, *Acta Crystallogr. Sect. A: Found. Crystallogr.* **2008**, 64, 123.
- [35] A. A. Coelho, *Acta Crystallogr. Sect. A: Found. Crystallogr.* **2007**, 63, 400.
- [36] R. W. Cheary, A. Coelho, *J. Appl. Crystallogr.* **1992**, 25, 109.
- [37] R. W. Cheary, A. A. Coelho, J. P. Cline, *J. Res. Natl. Inst. Stan.* **2004**, 109, 1.
- [38] M. Järvinen, *J. Appl. Crystallogr.* **1993**, 26, 525.

7 Summary

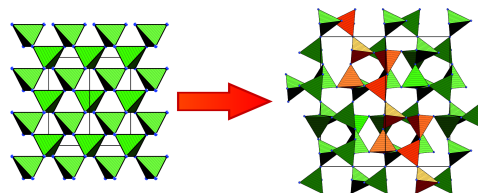
An Unprecedented AB_2 Tetrahedra Network Structure Type in a High-Pressure Phase of Phosphorus Oxonitride PON



A new polymorph of the phosphorus oxonitride PON has been synthesized in a Walker-type multi-anvil device at 12 GPa and 1250 °C. An amorphous precursor has been employed as the starting material. The crystal structure of the new polymorph δ -PON (space group $P2_1/c$ (no. 14), $a = 12.2472(2)$, $b = 4.83618(6)$, $c = 10.8604(2)$ Å, $\beta = 115.8026(8)^\circ$, $V = 579.12(2)$ Å³, $Z = 16$) is solved and refined on the basis of X-ray powder diffraction data. It can be described as a three-dimensional network of vertex-sharing $P(O,N)_4$ tetrahedra. δ -PON has been further characterized by FTIR and solid-state NMR spectroscopy. Topological analysis shows that δ -PON represents an entirely new AB_2 -type structure which has not yet been found in any other compound. Similarity to a predicted polymorph of SiO_2 through a common aristo-type is described.

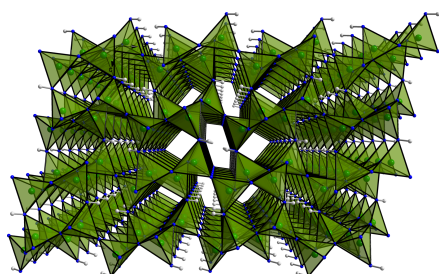
A High-Pressure Polymorph of Phosphorus Oxonitride PON with Coesite Structure

A new polymorph of the phosphorus oxonitride PON was prepared in a Walker-type multianvil device by heating cristobalite-type PON to 1300 °C at



15.5 GPa. *coe*-PON ($a = 6.95903(8)$, $b = 12.0610(2)$, $c = 6.96821(8)$ Å, $\beta = 120.0348(7)^\circ$, $V = 506.33(2)$ Å³, space group $C2/c$ (no. 15), $Z = 16$) is thoroughly characterized by X-ray powder diffraction, FTIR and NMR spectroscopy. Its crystal structure is compared to that of coesite SiO₂ and the unique angle of 180° is discussed in detail. Thermodynamic stability, theoretical transition pressure and bulk modulus are calculated using DFT calculations.

A High-Pressure Polymorph of Phosphorus Nitride Imide HP₄N₇ Representing a New Framework Topology

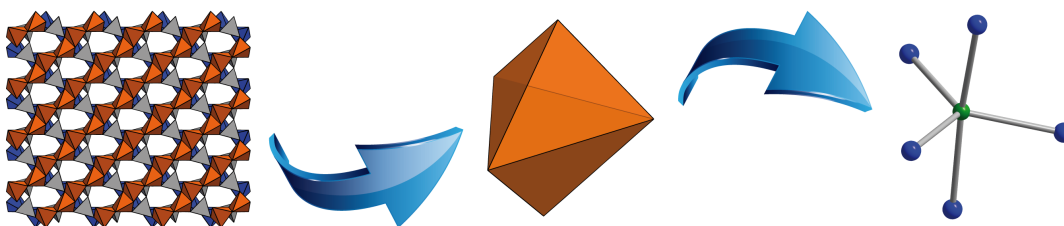


In order to investigate the structural behavior of phosphorus nitrides at high pressure, β -HP₄N₇, a new polymorph of the phosphorus nitride imide P₄N₆(NH), is investigated. It is prepared by the reaction of P₃N₅ and NH₄Cl between 800 °C and 1300 °C and 6 GPa in a Walker-type multianvil assembly.

Due to the presence of NH₄Cl as a mineralizer, single crystals of β -HP₄N₇ are accessible. The crystal structure (space group $C2/c$, no. 15, $a = 12.873(2)$, $b = 4.6587(4)$, $c = 8.3222(8)$ Å, $\beta = 102.351(3)^\circ$, $Z = 4$) is determined ab initio on the basis of single crystal X-ray diffraction data. The crystal structure of β -HP₄N₇ consists of a three-dimensional network of all-side vertex-sharing PN₄ tetrahedra. It is shown to be related to that of β -HPN₂

in the same way α -HP₄N₇ is related to α -HPN₂. The compound is further characterized by FTIR, MAS-NMR and UV-Vis spectroscopy as well as lattice energy calculations and topological analysis.

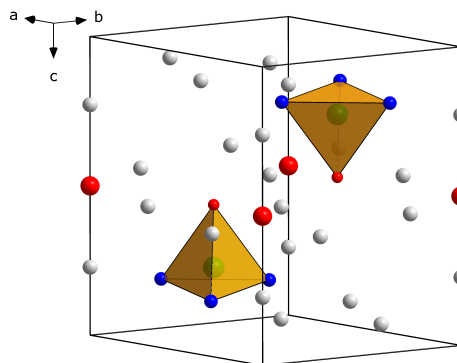
Pentacoordinated Phosphorus in a High-Pressure Polymorph of Phosphorus Nitride Imide P₄N₆(NH)



With γ -P₄N₆(NH), the first example of an inorganic network compound containing trigonal PN₅ bipyramids is described. This compound is accessible from P₃N₅ and NH₄Cl at 14 GPa and 1200 °C using the multianvil technique. Its crystal structure (space group *C2/c* (no. 15), $a = 6.8018(4)$, $b = 7.2204(5)$, $c = 8.9572(6)$ Å, $\beta = 111.231(2)^\circ$, $V = 410.05(5)$ Å³, $Z = 4$) is determined from single crystal X-ray diffraction data. It can be described as a network of perpendicular chains of edge-sharing PN₅ bipyramids interlinked by P₂N₇ double tetrahedra. This is the first occurrence of the structural motif of trigonal PN₅ bipyramids and the second occurrence of pentacoordinated P in phosphorus nitrides to date. The compound is further characterized by means of FTIR and MAS-NMR spectroscopy and lattice energy calculations.

$\text{Li}_{14}(\text{PON}_3)_2\text{O}$ – A Non-Condensed Oxonitridophosphate Oxide

$\text{Li}_{14}(\text{PON}_3)_2\text{O}$, the first *ortho*-oxonitridophosphate, is reported on. It was synthesized from LiNH_2 and $\text{PO}(\text{NH}_2)_3$ using a new high-temperature deprotonation approach in quartz glass ampoules. The crystal structure of $\text{Li}_{14}(\text{PON}_3)_2\text{O}$ (space group $P\bar{3}$ (no. 147), $a = 5.6880(5)$, $c = 8.0855(8)$ Å,



$V = 226.55(5)$ Å³, $Z = 1$) is elucidated by powder X-ray diffraction using charge-flipping and the Rietveld-method. The crystal structure can be described as a defect variant of the cubic anti-fluorite structure of Li_2O and is closely related to those of $\text{Li}_{14}\text{Cr}_2\text{N}_8\text{O}$ and $\text{Na}_{14}\text{Mn}_2\text{O}_9$. The crystal structure model is corroborated by FTIR and MAS NMR spectroscopic data.

8 Discussion and Outlook

8.1 High-Pressure Phases of Phosphorus Nitrides

The results presented in chapters 2 and 3 greatly expand the knowledge of the phase diagram of the phosphorus oxonitride PON (Figure 1.2b). Previous results had given no indication for the existence of further polymorphs other than the ones described in the literature. These are the ambient-pressure β -cristobalite-like PON^[1] and the high-pressure phases with α -quartz^[2] and moganite^[3] structures. All of these were described in detail by Marchand *et al.* While attempts were made to synthesize further polymorphs in large volume presses as well as diamond anvil cells, none are reported on. Experiments in laser-heated diamond anvil cells showed a gradual amorphization of PON at pressure in excess of 40 GPa.^[4,5]

A new synthetic approach utilizing an amorphous precursor, which has been used for the preparation of δ -PON (Chapter 2), shows promise in enabling the synthesis of further high-pressure polymorphs. In contrast to the classic high-pressure/high-temperature approach using crystalline starting materials it might be used to access thermodynamically metastable phases due to the lower reaction temperatures needed. The precursor used in the synthesis of δ -PON, called *amorphous* PON, has also been successfully used to synthesize the phosphorus nitride imide $\text{H}_3\text{P}_8\text{O}_8\text{N}_9$,^[6] which can be considered a step in the condensation process towards PON. The synthesis of δ -PON might therefore be a multistage reaction. First $\text{H}_3\text{P}_8\text{O}_8\text{N}_9$ is formed as an intermediate product, which then releases NH_3 to form PON. In accordance to Ostwald's step rule,^[7] this synthesis of the oxonitride in situ under high-pressure conditions should lead to less thermodynamically stable products. Coesite type PON, on the other hand, was synthesized using crystalline

cristobalite type PON as a starting material. This shows that even using the conventional high-pressure/high-temperature approach new phases of PON can be discovered. Therefore, both synthesis routes seem promising for the synthesis of further high-pressure polymorphs.

Classification of the crystal structures is greatly aided by topological analysis. Often simple comparison of the lattice parameters to established crystal structure databases is an easy way to determine that two compounds are isostructural. However, even small distortions can lead to differences in symmetry, which can prevent one from discovering similarities in this simple way. Topological analysis provides a valuable tool to classify crystal structures of extended solids without referring to unit cell or symmetry. The calculated point symbols are an easy way to establish whether two crystal structures can be considered equivalent.^[8] In the case of δ -PON, the crystal structure of the compound itself and that of the theoretically predicted polymorph of SiO_2 display the same connectivity of tetrahedra while their lattice parameters and space group differ greatly. Comparing the connectivity sequence of δ -PON to those of the entries of the PCOD (Predicted Crystallography Open Database)^[9] readily revealed this relationship. At the time of writing, the PCOD contains 11695 predicted crystal structures for SiO_2 and the isosteric AlPO_4 , predicted by the GRINSP^[10] software alone.^[11] It should therefore be safe to assume that most newly discovered AB_2 tetrahedra networks have already been predicted. For newly synthesized compounds consisting of SiO_2 -like frameworks and probably for many other compound classes (aluminates, borates, vanadates) it is an advisable strategy to look for related structures in the PCOD to allow easier structural classification.

The two new modifications of HP_4N_7 described in chapters 4 and 5 illustrate the structural relations of nitridophosphates and the structural evolution at high pressures. As described in section 4.3.2, the crystal structure of β - HP_4N_7 can be derived from that of β - HPN_2 in the same way that of α - HP_4N_7 can be derived from α - HPN_2 . This may indicate that certain structural motifs are energetically favored at different pressures. Possibly, the

close structural similarity may be indicative of certain reaction mechanisms. Both α - and β -HP₄N₇ can be synthesized from the more highly condensed P₃N₅ and NH₄Cl. A local excess of NH₃ around a grain of NH₄Cl in the reaction mixture could lead to intermediate formation of HPN₂. At the elevated reaction temperatures, this could further react topotactically to HP₄N₇, releasing NH₃ in the process. A mechanism like this would keep most of the structural motifs of the intermediately formed HPN₂ intact. On the other hand, the synthesis of β -HPN₂ from P₃N₅ and NH₄Cl might involve intermediate formation of β -HP₄N₇. In a second step, remaining NH₃ would selectively ammonolyse only certain P–N–P bonds. Therefore the crystal structure of β -HPN₂ would develop directly from that of β -HP₄N₇ without the formation of other intermediates.

The discovery of pentacoordinate phosphorus in γ -HP₄N₇, which is described in chapter 5, represents a significant advance for the solid-state chemistry of phosphorus nitrides. The previous discovery of γ -P₃N₅^[12,13] showed that coordination numbers higher than four are a possibility at elevated pressures and inspired further theoretical investigations.^[14] However, no predictions had been made for HP₄N₇. Interestingly, while both γ -P₃N₅ and γ -HP₄N₇ contain pentacoordinate phosphorus, the type of coordination polyhedron is different. This indicates that for the case of phosphorus coordinated only by nitrogen, quadratic pyramids and trigonal bipyramids differ only slightly in energy. Which one of those two coordination polyhedra allows for a better space-filling for a given compound is therefore probably more important than the absolute energy of those polyhedra, which can be expected to be in the same range. Both γ -P₃N₅ and γ -HP₄N₇ also still contain tetrahedrally coordinated phosphorus. One can reason that, due to the smaller size of the PN₄ tetrahedra, these mixed structures offer a more efficient packing.

As shown in chapter 3, DFT calculations can be a valuable tool in high-pressure chemistry. They can be used to establish the stability regions of newly discovered compounds as well as some of their mechanical properties such as the bulk modulus. For future investigations they can also be used to predict possible crystal structures and their synthesis

conditions. However, these will still rely on a trained chemist to choose suitable structure candidates. These are often chosen from the structures of heavier homologues or other similar crystal structures. However, in order to predict truly novel crystal structures, another approach will be necessary. Programs such as GRINSP^[10] and ZEFSA^[15–17] have been developed to predict new structure types by filling a given unit cell with vertex-sharing polyhedra in a chemically reasonable fashion. The thermodynamic stability of the crystal structures obtained in this way can then be investigated using DFT methods. Due to the large amount of possible crystal structures and the high computational cost, preselection of the structural candidates will be necessary. Furthermore, neither ZEFSA nor GRINSP have the ability to include edge-sharing polyhedra or triply bridging nitrogen. Both of these structural motifs are very common in phosphorus nitrides and nitridophosphates. It might therefore be necessary to modify these programs or develop an entirely new way of creating structural candidates.

Nevertheless, further exploratory investigations into high-pressure phases of phosphorus nitrides and oxonitrides should prove valuable in the future. Preliminary investigations show that further polymorphs of PON are accessible at pressures up to 20 GPa, which can be achieved using established multianvil techniques. At even higher pressures, which can be attained with diamond anvil cells, more exotic phases might be accessible. Considering the very close relation of PON and SiO₂, stishovite- and seifertite-like polymorphs containing hexacoordinate phosphorus should be accessible. The precursor approach used for the synthesis of δ -PON allows access to phases with entirely new structure types. Investigating these further might also yield insight into the high-pressure chemistry of SiO₂ in geological conditions.

8.2 Lithium Oxonitridophosphates

The high-temperature deprotonation approach used to synthesize the first *ortho*-oxonitridophosphate $\text{Li}_{14}(\text{PON}_3)_2\text{O}$, which is described as part of this thesis (Chapter 6), has shown to be a valuable tool in the synthesis of nitridophosphates and oxonitridophosphates. Conventional solid-state synthesis routes starting from highly condensed precursors like PON and P_3N_5 frequently lead to the formation of only a few select compounds, such as LiPN_2 . Nevertheless, recently Holzwarth *et al.* were able to synthesize the oxonitridophosphate $\text{Li}_2\text{PO}_2\text{N}$ from Li_2O , P_4O_{10} and P_3N_5 .^[18] Usage of highly condensed reactants like P_3N_5 may be the main problem in these classical syntheses due to the required high reaction temperatures. These lead to the formation of the few most thermodynamically stable compounds.

By using molecular precursors with a low degree of condensation, it is possible to circumvent this limitation. This synthesis, termed *high-temperature deprotonation*, uses molten amide salts. The NH_2^- ion displays a very high basicity ($\text{pK}_a(\text{NH}_3) \approx 41$)^[19,20], and readily deprotonates NH_2 and NH groups of phosphoric amides and related compounds. The continuous removal of gaseous NH_3 created by this reaction ensures that the equilibrium is shifted far to the product side, ensuring a complete reaction. In contrast to the classical solid-state syntheses described above, the full deprotonation of precursors containing amide and imide groups does not involve a change in the degree of condensation. Therefore, the wide range of molecular phosphorus imides and amides should be suitable as starting materials.

By varying the ratio of amide to precursor it is in theory furthermore possible to achieve degrees of condensation higher than those of the starting material. If the amount of molten amide is too small to completely deprotonate the starting material, remaining NH_2 and NH groups can participate in further condensation reactions, releasing NH_3 in the process. Phosphoric triamide ($\text{PO}(\text{NH}_2)_3$),^[21] one of the most simple precursors, can be used as

starting material for the completely deprotonated PON_3^{2-} ion in $\text{Li}_{14}(\text{PON}_3)_2\text{O}$ as well as the highly condensed phosphorus oxonitride PON .^[22] It is plausible that by varying the molar ratio of LiNH_2 to $\text{PO}(\text{NH}_2)_3$ between 0 and 6 one should be able to access many of the intermediate degrees of condensation.

While high-temperature deprotonation synthesis has many advantages over other synthesis routes, particularly for the synthesis of compounds with low degrees of condensation, there are some disadvantages that need to be considered. It requires that the metal of which salts are desired forms a congruently melting amide. It is also desirable that the melting point is lower than the temperature at which the condensation of the molecular precursor is completed. Conceivably, other highly basic salts with appropriate properties can also be used. Nevertheless, the lack of readily accessible amides with the desired properties limits this approach to mainly the alkali metal amides.^[23,24]

Usually, deprotonation syntheses are carried out in closed evacuated silica ampoules. Due to the large amount of NH_3 that is liberated during the reaction, the amount of sample that can be obtained from a single reaction is limited by the maximum pressure tolerated by the ampoule. For the case of $\text{Li}_{14}(\text{PON}_3)_2\text{O}$ this restricts the maximum amount of sample to about 50 mg. It may be possible to avoid this limitation by carrying out the reaction in open-ended flow tubes under a stream of dry NH_3 or an inert gas.

Considering the advantages detailed above, high-temperature deprotonation should be a suitable synthetic route towards many new compounds. Further experiments should aim at investigating the reaction of known phosphorus-containing molecular amides, such as $\text{P}(\text{NH})(\text{NH}_2)_3$,^[25] $\text{P}(\text{NH}_2)_4\text{Cl}$,^[26] $\text{HPO}_2(\text{NH}_2)_2$,^[27] $\text{H}_2\text{PO}_3(\text{NH}_2)$ ^[28,29] as well as the many oligomeric phosphorus amides. Deprotonation of $\text{P}(\text{NH}_2)_3$ ^[30] could also lead to nitridophosphates(III), a substance class that has not yet been reported on. Furthermore, it can be speculated that this route could also be of use for the synthesis of ternary nitrides of other elements, such as B, Si, Al, Ga or Ge. The main difficulty would be the accessibility of well-defined molecular amides.

8.3 References

- [1] J. M. Léger, J. Haines, C. Chateau, G. Bocquillon, M. W. Schmidt, S. Hull, F. Gorelli, A. Lesauze, R. Marchand, *Phys. Chem. Minerals* **2001**, *28*, 388.
- [2] J. M. Léger, J. Haines, L. S. de Oliveira, C. Chateau, A. L. Sauze, R. Marchand, S. Hull, *J. Phys. Chem. Solids* **1999**, *60*, 145.
- [3] J. Haines, C. Chateau, J. M. Léger, A. L. Sauze, N. Diot, R. Marchand, S. Hull, *Acta Crystallogr. Sect. B: Struct. Sci.* **1999**, *55*, 677.
- [4] J. M. Léger, J. Haines, L. S. de Oliveira, C. Chateau, A. L. Sauze, R. Marchand, *J. Phys.: Condens. Matter* **1996**, *8*, L773.
- [5] J. Léger, J. Haines, C. Chateau, R. Marchand, *J. Phys. Chem. Solids* **2000**, *61*, 1447.
- [6] S. J. Sedlmaier, V. R. Celinski, J. Schmedt auf der Günne, W. Schnick, *Chem. Eur. J.* **2012**, *18*, 4358.
- [7] R. A. Van Santen, *J. Phys. Chem.* **1984**, *88*, 5768.
- [8] V. A. Blatov, M. O’Keeffe, D. M. Proserpio, *CrystEngComm* **2010**, *12*, 44.
- [9] A. L. Bail, *Phys. Chem. Chem. Phys.* **2010**, *12*, 8521.
- [10] A. Le Bail, *J. Appl. Crystallogr.* **2005**, *38*, 389.
- [11] A. Le Bail, **2009**, <http://www.crystallography.net/pcod/update-2009/gri.html> (visited on 02/18/2015).
- [12] K. Landskron, H. Huppertz, J. Senker, W. Schnick, *Angew. Chem. Int. Ed.* **2001**, *40*, 2643; *Angew. Chem.* **2001**, *113*, 2713.
- [13] K. Landskron, H. Huppertz, J. Senker, W. Schnick, *Z. Anorg. Allg. Chem.* **2002**, *628*, 1465.
- [14] P. Kroll, W. Schnick, *Chem. Eur. J.* **2002**, *8*, 3530.

- [15] M. W. Deem, J. M. Newsam, *Nature* **1989**, 342, 260.
- [16] M. W. Deem, J. M. Newsam, *J. Am. Chem. Soc.* **1992**, 114, 7189.
- [17] M. Falcioni, M. W. Deem, *J. Chem. Phys.* **1999**, 110, 1754.
- [18] K. Senevirathne, C. S. Day, M. D. Gross, A. Lachgar, N. Holzwarth, *Solid State Ionics* **2013**, 233, 95.
- [19] D. Algrim, J. E. Bares, J. C. Branca, F. G. Bordwell, *J. Org. Chem.* **1978**, 43, 5024.
- [20] F. G. Bordwell, G. E. Drucker, H. E. Fried, *J. Org. Chem.* **1981**, 46, 632.
- [21] R. Klement, O. Koch, *Chem. Ber.* **1954**, 87, 333.
- [22] E. Steger, U. G. Mildner, *Z. Anorg. Allg. Chem.* **1964**, 332, 314.
- [23] F. W. Bergstrom, W. C. Fernelius, *Chem. Rev.* **1933**, 12, 43.
- [24] F. W. Bergstrom, W. C. Fernelius, *Chem. Rev.* **1937**, 20, 413.
- [25] M. Becke-Goehring, K. Niedenzu, *Chem. Ber.* **1957**, 90, 2072.
- [26] A. Schmidpeter, C. Weingand, E. Hafner-Roll, *Z. Naturforsch. B: Anorg. Chem. Org. Chem. Biochem. Biophys. Biol.* **1969**, 24, 799.
- [27] H. N. Stokes, *Amer. Chem. J.* **1894**, 16, 123.
- [28] H. N. Stokes, *Amer. Chem. J.* **1893**, 15, 198.
- [29] R. Klement, G. Biberacher, V. Hille, *Z. Anorg. Allg. Chem.* **1957**, 289, 80.
- [30] M. Becke-Goehring, J. Schulze, *Chem. Ber.* **1958**, 91, 1188.

A Supporting Information for Chapter 2

A.1 Experimental Details of the HP/HT-Synthesis of δ -PON

Amorphous phosphorus oxonitride imide with composition $\text{PO}_{0.88}\text{N}_{1.24}\text{H}_{0.56}$ has been prepared by heating a mixture of phosphoryl triamide $\text{PO}(\text{NH}_2)_3$ and NH_4Cl (ratio 1:3) in a fused silica boat at 300 and 620 °C in a continuous ammonia flow for 12 h. The mixture can be obtained by the reaction of POCl_3 (99 % Acros Organics, Geel, Belgium) with liquid NH_3 (5.0, Linde, Pullach, Germany) as described in the literature.^[1] δ -PON has been synthesized by high-pressure high-temperature treatment of $\text{PO}_{0.88}\text{N}_{1.24}\text{H}_{0.56}$ in a 1000 t hydraulic press (Voggenreiter, Mainleus, Germany) using a Walker-type multianvil assembly. Further information concerning the assembly can be found in the literature.^[2–6] Inside a glove box (Unilab, MBraun, Garching, Germany) the starting material was tightly packed into a hexagonal boron nitride capsule. The capsule was placed inside two graphite tubes, which themselves were placed inside a Cr-doped MgO-octahedron with an edge length of 14 mm (Ceramic Substrates and Components, Isle of Wight, UK). The octahedron was compressed between eight tungsten carbide cubes (Hawedia, Marklkofen, Germany) with a truncation edge length of 8 mm. The pressure on the sample was raised to 12 GPa and the sample was heated to approximately 1350 °C within 15 min. The temperature was held for 120 min and subsequently lowered to room temperature within 30 minutes. After decompression, the product was isolated.

A.2 Information on the Data Collection and Structure Elucidation of δ -PON

Powder diffraction measurements were conducted in parafocusing Debye-Scherrer geometry using a StadiP-diffractometer (Stoe & Cie, Darmstadt, Germany) using Ge(111) monochromated Cu-K $_{\alpha 1}$ -radiation and a position sensitive detector. Structure elucidation was carried out using TOPAS Academic 4.1.^[7] Reflections were indexed using the SVD-algorithm^[8] and their intensities extracted with the Pawley-method. The full structural model was obtained using the charge-flipping-algorithm.^[9–11] Final refinement was carried out using the Rietveld method, employing the fundamental parameters approach (direct convolution of source emission profiles, axial instrument contributions and crystallite size and microstrain effects).^[12] The anion positions were occupied equally with 0.5 for both O and N applying a common atomic displacement parameter. 3 % of moganite-type PON was additionally refined as side phase. Capillary absorption correction (inner diameter 0.28 mm) was carried out using the calculated absorption coefficient. The FTIR spectrum was collected on a Spectrum BX II-spectrometer (Perkin Elmer, Waltham MA, USA). Solid-state MAS NMR-experiments were carried out on a Avance III Spectrometer (500 MHz, 4.7 T, Bruker, Bellerica, USA). The chemical shift values refer to a deshielding scale. 85 % H₃PO₄ was used as a external reference. Energy dispersive X-ray analyses were performed using a JSM 6500F scanning electron microscope (Jeol, Tokyo, Japan) with an Oxford Instruments 7418 X-ray detector.

A.3 Crystallographic Data for δ -PONTable A.1: Crystal details for δ -PON.

formula	PON
formula mass / $\text{g} \cdot \text{mol}^{-1}$	60.98
crystal system / space group	monoclinic, $P2_1/c$
lattice parameters	$a = 12.2472(2) \text{ \AA}$
	$b = 4.83618(6) \text{ \AA}$
	$c = 10.8604(2) \text{ \AA}$
	$\beta = 115.8026(8)^\circ$
cell volume / \AA^3	579.12(2)
formula units per cell Z	16
X-ray density / $\text{g} \cdot \text{cm}^{-3}$	27.976
linear absorption coefficient / cm^{-1}	120.85
radiation	Cu-K $_{\alpha 1}$ ($\lambda = 154.059 \text{ pm}$)
monochromator	Ge(111)
diffractometer	Stoe StadiP
detector	linear PSD
2θ -range / $^\circ$	15–90
temperature / K	298(2)
data points	7500
number of observed reflections	474
number of parameters	90
constraints	8
program used	TOPAS Academic
structure solution	charge-flipping
structure refinement	Rietveld-Method
profile function	fundamental parameters model
background function	shifted Chebychev
R_{wp}	0.0491
R_{p}	0.03806
R_{Bragg}	0.01213
χ^2	1.447

Table A.2: Fractional atomic coordinates, isotropic thermal displacement parameters, and site occupancies for δ -PON.

atom	x	y	z	$U_{eq} / \text{\AA}^2$	occupancy
P1	0.4993(4)	0.3996(6)	0.3269(3)	0.0256(11)	1
P2	0.1306(3)	0.7784(9)	0.1439(3)	0.0266(12)	1
P3	0.6966(3)	0.0061(10)	0.0977(3)	0.0254(10)	1
P4	0.1342(3)	0.2235(9)	0.4920(3)	0.0301(13)	1
O1	0.4967(9)	0.2163(14)	0.2114(8)	0.0401(11)	0.5
N1	0.4967(9)	0.2163(14)	0.2114(8)	0.0401(11)	0.5
O2	0.1520(7)	0.588(2)	0.0396(8)	0.0401(11)	0.5
N2	0.1520(7)	0.588(2)	0.0396(8)	0.0401(11)	0.5
O3	0.2235(7)	0.7188(18)	0.2985(8)	0.0401(11)	0.5
N3	0.2235(7)	0.7188(18)	0.2985(8)	0.0401(11)	0.5
O4	0.0043(8)	0.234(2)	0.3603(7)	0.0401(11)	0.5
N4	0.0043(8)	0.234(2)	0.3603(7)	0.0401(11)	0.5
O5	0.2278(7)	0.2332(19)	0.9364(8)	0.0401(11)	0.5
N5	0.2278(7)	0.2332(19)	0.9364(8)	0.0401(11)	0.5
O6	0.3799(7)	0.3362(14)	0.3400(8)	0.0401(11)	0.5
N6	0.3799(7)	0.3362(14)	0.3400(8)	0.0401(11)	0.5
O7	0.1436(7)	0.099(2)	0.1126(8)	0.0401(11)	0.5
N7	0.1436(7)	0.099(2)	0.1126(8)	0.0401(11)	0.5
O8	0.6116(8)	0.1768(15)	0.9677(9)	0.0401(11)	0.5
N8	0.6116(8)	0.1768(15)	0.9677(9)	0.0401(11)	0.5

Table A.3: Interatomic distances / pm for δ -PON.

P1–(O,N)1	1.525(9)	P3–(O,N)8	1.575(9)
P1–(O,N)6	1.560(11)	P3–(O,N)3	1.525(9)
P1–(O,N)1'	1.593(8)	P3–(O,N)6	1.601(9)
P1–(O,N)8	1.592(10)	P3–(O,N)5	1.622(10)
P2–(O,N)2	1.568(10)	P4–(O,N)4	1.612(9)
P2–(O,N)3	1.592(9)	P4–(O,N)5	1.525(10)
P2–(O,N)7	1.610(11)	P4–(O,N)2	1.577(10)
P2–(O,N)4	1.647(11)	P4–(O,N)7	1.528(9)

Table A.4: Bond angles / ° for δ -PON.

(O,N)1–P1–(O,N)6	106.0(5)	(O,N)3–P3–(O,N)5	113.8(5)
(O,N)1–P1–(O,N)1'	109.6(5)	(O,N)5–P3–(O,N)6	103.2(5)
(O,N)1–P1–(O,N)8	110.8(5)	(O,N)4–P4–(O,N)5	105.4(5)
(O,N)1'–P1–(O,N)6	110.4(5)	(O,N)2–P4–(O,N)4	105.3(5)
(O,N)6–P1–(O,N)8	108.6(5)	(O,N)4–P4–(O,N)7	114.8(5)
(O,N)1'–P1–(O,N)8	111.2(5)	(O,N)2–P4–(O,N)5	103.9(5)
(O,N)2–P2–(O,N)3	112.8(5)	(O,N)5–P4–(O,N)7	118.2(5)
(O,N)2–P2–(O,N)7	110.5(5)	(O,N)2–P4–(O,N)7	107.9(5)
(O,N)2–P2–(O,N)4	112.6(5)	P1–(O,N)1–P1	141.4(6)
(O,N)3–P2–(O,N)7	107.8(5)	P2–(O,N)2–P4	139.1(7)
(O,N)3–P2–(O,N)4	104.7(5)	P2–(O,N)3–P3	146.7(6)
(O,N)4–P2–(O,N)7	108.1(5)	P2–(O,N)4–P4	128.3(5)
(O,N)3–P3–(O,N)8	105.7(5)	P3–(O,N)5–P4	142.2(7)
(O,N)6–P3–(O,N)8	111.6(5)	P1–(O,N)6–P3	133.0(5)
(O,N)5–P3–(O,N)8	112.9(5)	P2–(O,N)7–P4	138.1(6)
(O,N)3–P3–(O,N)6	109.8(5)	P1–(O,N)8–P3	134.2(5)

A.4 Solid-State NMR and FTIR Spectra

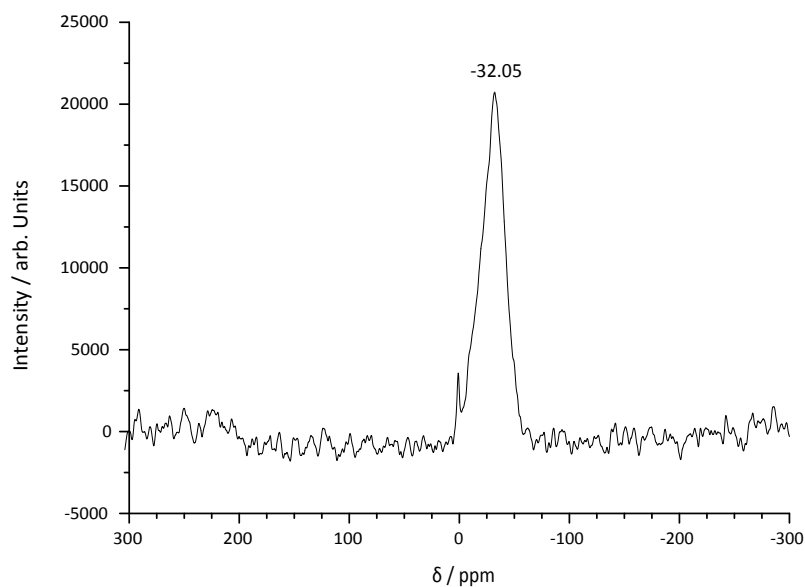


Figure A.1: ^{31}P -solid-state NMR-spectrum of δ -PON. The small peak at $\delta = 0$ ppm results from small amounts of hydrolysis products.

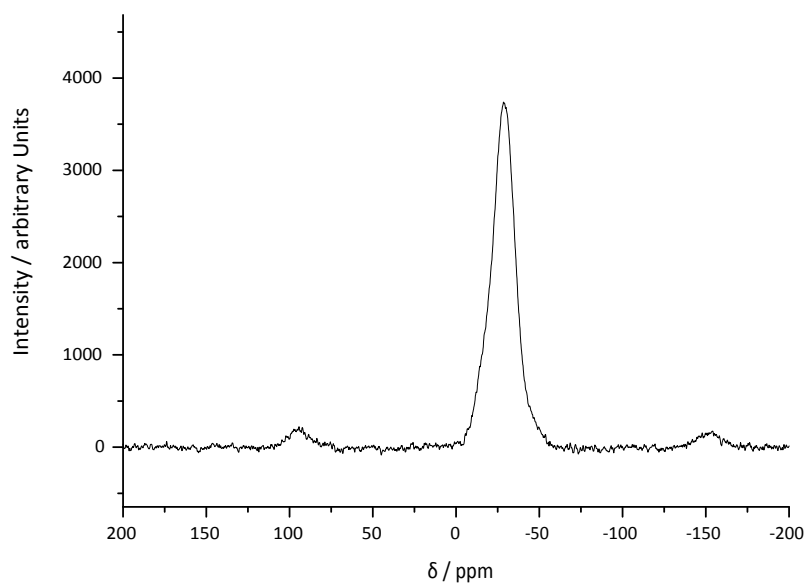
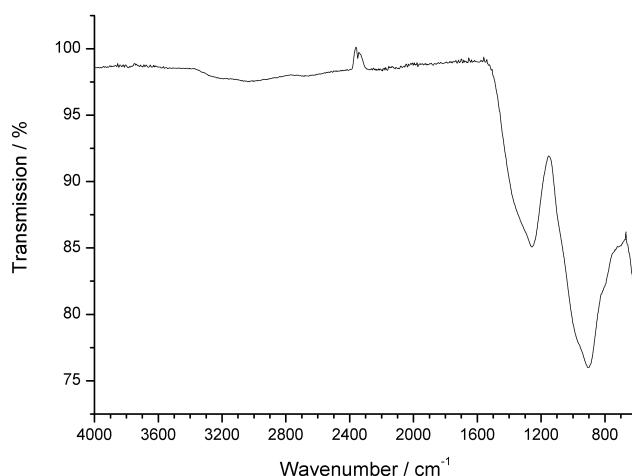


Figure A.2: ^{31}P -solid-state NMR-spectrum of cristobalite PON.

Figure A.3: FTIR spectrum of δ -PON.

A.5 Cycle Class Sequence of the δ -PON Network

Table A.5: Cycle class sequence of the network of δ -PON in comparison with the networks of the other PON polymorphs showing the prevalence of the $P_n(O/N)_n$ -rings.

n	2	3	4	5	6	7	8
δ -PON	0	0	6	0	12	0	68
Cristobalite	0	0	0	0	4	0	6
Quartz	0	0	0	0	3	0	21
Moganite	0	0	2	0	4	0	32

A.6 Symmetry Relationship to a Predicted SiO_2 Modification

Both compounds are related through a common aristotype in space group $Cmce$. The corresponding *Bärnighausen tree*,^[13,14] illustrating the symmetry reduction to the two hetto-types is shown in Figure A.3. The space groups of both structures are *translationengleiche* subgroups of index 2 of the space group of the aristotypes space group $Cmce$.

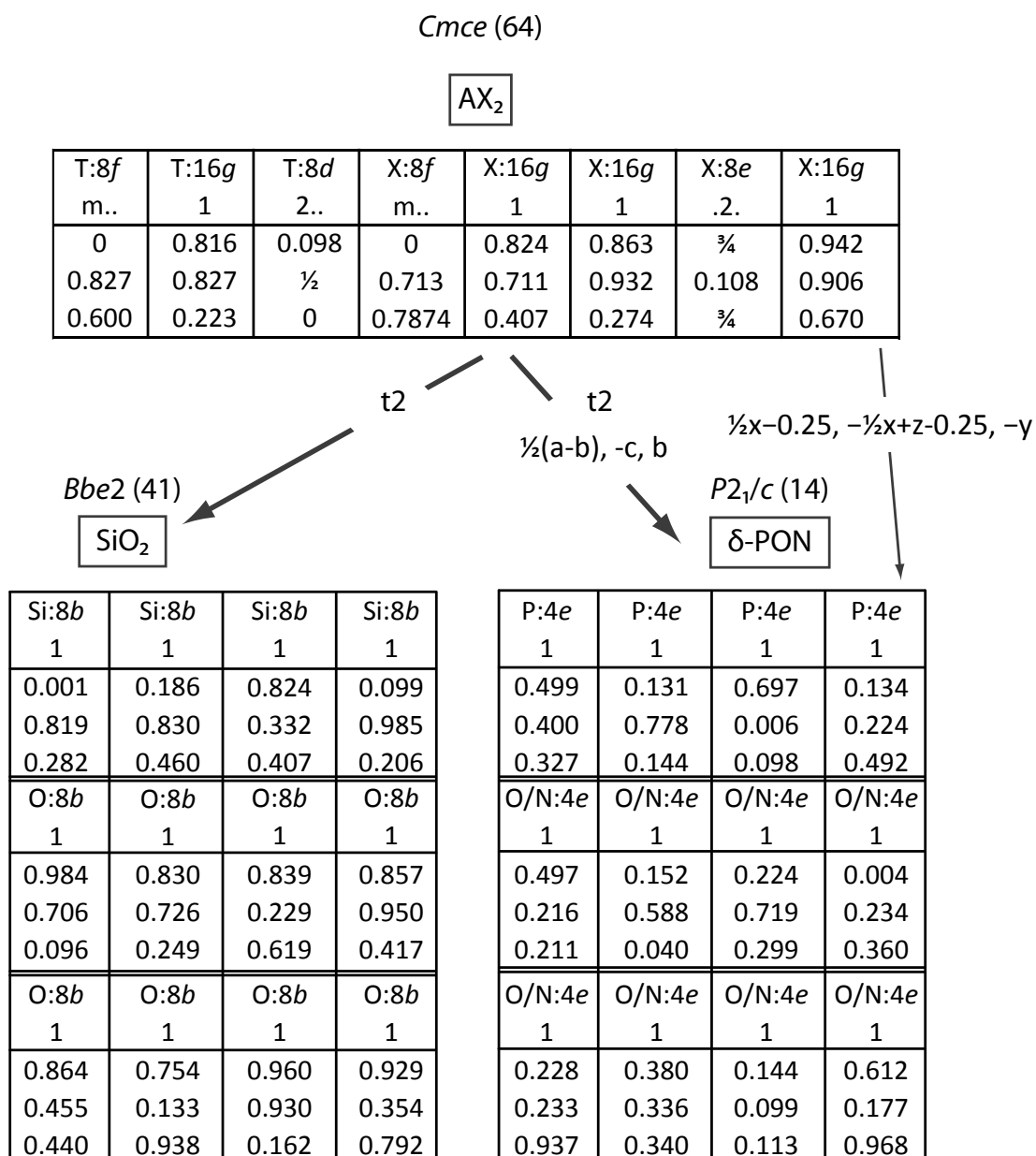


Figure A.4: Bärnighausen tree showing the symmetry relation between δ -PON and the predicted SiO_2 phase from the PCOD database.

A.7 References

- [1] R. Klement, O. Koch, *Chem. Ber.* **1954**, 87, 333.
- [2] N. Kawai, S. Endo, *Rev. Sci. Instrum.* **1970**, 41, 1178.
- [3] D. Walker, M. A. Carpenter, C. M. Hitch, *Am. Mineral.* **1990**, 75, 1020.
- [4] D. Walker, *Am. Mineral.* **1991**, 76, 1092.
- [5] D. C. Rubie, *Phase Transitions* **1999**, 68, 431.
- [6] H. Huppertz, *Z. Kristallogr.* **2004**, 219, 330.
- [7] A. Coelho, *TOPAS-Academic Version 4.1*, Coelho Software: Brisbane, **2007**.
- [8] A. A. Coelho, *J. Appl. Crystallogr.* **2003**, 36, 86.
- [9] G. Oszlányi, A. Sütő, *Acta Crystallogr. Sect. A: Found. Crystallogr.* **2004**, 60, 134.
- [10] G. Oszlányi, A. Sütő, *Acta Crystallogr. Sect. A: Found. Crystallogr.* **2008**, 64, 123.
- [11] A. A. Coelho, *Acta Crystallogr. Sect. A: Found. Crystallogr.* **2007**, 63, 400.
- [12] J. Bergmann, R. Kleeberg, A. Haase, B. Breidenstein, *Mater. Sci. Forum* **2000**, 347–349, 303.
- [13] H. Bärnighausen, *MATCH Commun. Math. Chem.* **1980**, 9, 139.
- [14] U. Müller, *Z. Anorg. Allg. Chem.* **2004**, 630, 1519.

B Supporting Information for Chapter 3

B.1 Experimental Details of the HP/HT-Synthesis of *coe*-PON

The starting material cristobalite PON was synthesized by a two-step condensation of phosphoric triamide. A mixture of $\text{PO}(\text{NH}_2)_3$ and NH_4Cl , obtained by reacting POCl_3 (99%, Sigma Aldrich) with liquid NH_3 (5.0, Air Liquide) as described in the literature,^[1] was heated to 620 °C for 5 h in a stream of dry ammonia. The resulting amorphous condensation product was crystallized for 7 days at 750 °C in evacuated fused quartz ampoules yielding pure cristobalite-type PON. *coe*-PON was synthesized by a high-pressure high-temperature reaction using a modified Walker-type multianvil assembly. The starting material cristobalite PON was tightly packed in a BN crucible which was in turn placed in a MgO octahedron (Ceramic Substrates & Components, Isle of Wight, UK) with an edge length of 10 mm. More details about the assembly can be found in the literature.^[2–6] The sample was compressed to 15.5 GPa between eight truncated tungsten carbide cubes (Hawedia, Marklkofen, Germany) using a 1000 t hydraulic press (Voggenreiter, Mainleus, Germany). The temperature was raised to 1300 °C within 15 min and held for 60 min. After quenching and decompression the sample was mechanically isolated and ground in an agate mortar.

B.2 Information on Data Collection and Structure Elucidation of *coe*-PON

X-ray powder diffraction measurements were conducted in parafocusing Debye-Scherrer geometry using a StadiP-diffractometer (Stoe & Cie, Darmstadt, Germany) using Ge(111) monochromated $\text{Cu-K}_{\alpha 1}$ -radiation and a MYTHEN 1K Si-strip detector (Dectris, Baden,

Switzerland). Structure elucidation was performed using TOPAS Academic 4.1.^[7] The powder pattern was indexed using the SVD-algorithm^[8] and the reflection intensities extracted with the Pawley-method. Structure solution was carried out with the charge-flipping algorithm.^[9–11] Final refinement was carried out using the Rietveld method, peak shapes being modelled by the fundamental parameters approach (direct convolution of source emission profiles, axial instrument contributions and crystallite size and microstrain effects).^[12,13] The anion positions were occupied equally with 0.5 for both O and N applying a common atomic displacement parameter. Capillary absorption correction (inner diameter 0.28 mm) was carried out using the calculated absorption coefficient. Preferred orientation was corrected using spherical harmonics functions of the 4th order.^[14] Temperature dependent X-ray powder diffraction measurements were carried out on a Stoe StadiP diffractometer that was equipped with a high-temperature graphite furnace using Ge(111) monochromated Mo-K_{α1} radiation ($\lambda = 0.70930$) and an image plate position sensitive detector. The sample was heated with a rate of 10 °C/min between measurements. The temperature was held constant for each 15 min measurement. The FTIR spectrum was collected on a Spectrum BX II-spectrometer (Perkin Elmer, Waltham MA, USA) in ATR geometry. The ³¹P-NMR spectrum was collected on a Bruker Avance III spectrometer, using a 11.7 T magnet and a 1.3 mm MAS probe. The sample was spun at a MAS rate of 50 KHz. The spectrum was acquired using a 90° pulse using a long recycle delay with T1 estimated to be > 30 min. The chemical shift values are referenced to 0.1% TMS in CDCl₃ (Sigma-Aldrich) as an external reference. Energy dispersive X-ray analyses were performed using a JSM 6500F scanning electron microscope (Jeol, Tokyo, Japan) with an Oxford Instruments 7418 X-ray detector.

B.3 Additional Crystallographic Data for *coe*-PON**Table B.1:** Fractional atomic coordinates, isotropic thermal displacement parameters, and site occupancies for *coe*-PON.

atom	Wyckoff Position	x	y	z	$U_{eq} / \text{\AA}^2$	occupancy
P1	<i>8f</i>	0.1434(4)	0.1066(2)	0.0753(4)	0.0193(6)	1
P2	<i>8f</i>	0.5037(5)	0.1613(2)	0.5376(3)	0.0132(4)	1
O1	<i>4a</i>	0	0	0	0.024(2)	0.5
N1	<i>4a</i>	0	0	0	0.024(2)	0.5
O2	<i>4e</i>	$\frac{1}{2}$	0.1121(7)	$\frac{3}{4}$	0.024(2)	0.5
N2	<i>4e</i>	$\frac{1}{2}$	0.1121(7)	$\frac{3}{4}$	0.024(2)	0.5
O3	<i>8f</i>	0.257(1)	0.1229(4)	0.9300(7)	0.012(2)	0.5
N3	<i>8f</i>	0.257(1)	0.1229(4)	0.9300(7)	0.012(2)	0.5
O4	<i>8f</i>	0.319(1)	0.1014(5)	0.334(1)	0.031(2)	0.5
N4	<i>8f</i>	0.319(1)	0.1014(5)	0.334(1)	0.031(2)	0.5
O5	<i>8f</i>	0.0178(8)	0.2109(4)	0.4831(7)	0.018(2)	0.5
N5	<i>8f</i>	0.0178(8)	0.2109(4)	0.4831(7)	0.018(2)	0.5

Table B.2: Interatomic distances / pm for *coe*-PON.

P1–O1/N1	155.0(2)	P2–O2/N2	160.7(4)
P1–O3/N3	157.5(7)	P2–O3/N3	163.5(8)
P1–O4/N4	159.6(7)	P2–O4/N4	153.6(7)
P1–O5/N5	159.6(6)	P1–O5/N5	154.9(5)

Table B.3: Bond angles / ° for *coe*-PON.

O1/N1–P1–O3/N3	109.3(2)	O5/N5–P2–O2/N2	114.1(4)
O1/N1–P1–O4/N4	110.4(3)	O5/N5–P2–O3/N3	109.8(3)
O1/N1–P1–O5/N5	108.4(3)	O2/N2–P2–O3/N3	104.7(2)
O3/N3–P1–O4/N4	112.7(4)	P1–O1/N1–P1	180
O3/N3–P1–O5/N5	104.6(3)	P2–O2/N2–P2	136.6(6)
O4/N4–P1–O5/N5	111.3(3)	P1–O3/N3–P2	138.6(3)
O4/N4–P2–O5/N5	112.7(3)	P2–O4/N4–P1	147.0(5)
O4/N4–P2–O2/N2	106.5(4)	P2–O5/N5–P1	137.5(4)
O4/N4–P2–O3/N3	108.6(4)		

B.4 Details of the Rietveld Refinement

Table B.4: Crystal details for *coe*-PON.

formula	PON
formula mass / $\text{g} \cdot \text{mol}^{-1}$	60.98
crystal system / space group	monoclinic, $C2/c$ (no. 15)
lattice parameters / $\text{\AA}, ^\circ$	$a = 6.95903(8)$
	$b = 12.0610(2)$
	$c = 6.96821(8)$
	$\beta = 120.0348(7)$
cell volume / \AA^3	506.33(2)
formula units per cell Z	16
X-ray density / $\text{g} \cdot \text{cm}^{-3}$	3.200
linear absorption coefficient / cm^{-1}	138.23
radiation	Cu- $K_{\alpha 1}$ ($\lambda = 154.059 \text{ pm}$)
monochromator	Ge(111)
diffractometer	Stoe StadiP
detector	MYTHEN 1K
2θ -range / $^\circ$	3–119.985
temperature / K	298(2)
data points	7800
number of observed reflections	385
number of parameters	65
constraints	0
program used	TOPAS Academic
structure solution	charge-flipping
structure refinement	Rietveld-Method
profile function	fundamental parameters model
background function	shifted Chebychev
R_{wp}	0.04069
R_{exp}	0.01927
R_{p}	0.02716
R_{Bragg}	0.00657
χ^2	2.111

B.5 Comparison of Coesite SiO_2 and PON**Table B.5:** Comparison of the atomic coordinates of coesite SiO_2 and PON. $|u|$ is the absolute distance between the equivalent atomic sites.

Wyckoff position	atom (SiO_2) ^a	x (SiO_2)	y (SiO_2)	z (SiO_2)	atom (PON) ^b	x (PON)	y (PON)	z (PON)	$ u $ / pm
8f	Si1	0.1403	0.1084	0.0723	P1	0.1434	0.1066	0.0753	3.07
8f	Si2	0.5066	0.1580	0.5405	P2	0.5037	0.1613	0.5376	4.64
4a	O1	0	0	0	(O,N)1	0	0	0	0
4e	O2	$\frac{1}{2}$	0.1161	$\frac{3}{4}$	(O,N)2	$\frac{1}{2}$	0.1121	$\frac{3}{4}$	4.87
8f	O3	0.2660	0.1232	0.9400	(O,N)3	0.2565	0.1229	0.9300	6.95
8f	O4	0.3110	0.1037	0.3280	(O,N)4	0.3191	0.1014	0.3342	5.95
8f	O5	0.0177	0.2119	0.4784	(O,N)5	0.0178	0.2109	0.4831	3.56

a) lattice parameters: $a = 7.17$, $b = 7.17$, $c = 12.38$ Å, $\beta = 120.0^\circ$ ^[15]b) lattice parameters: $a = 6.95903$, $b = 12.0610$, $c = 6.96821$ Å, $\beta = 120.0348^\circ$

B.6 Solid-State NMR and FTIR Spectra

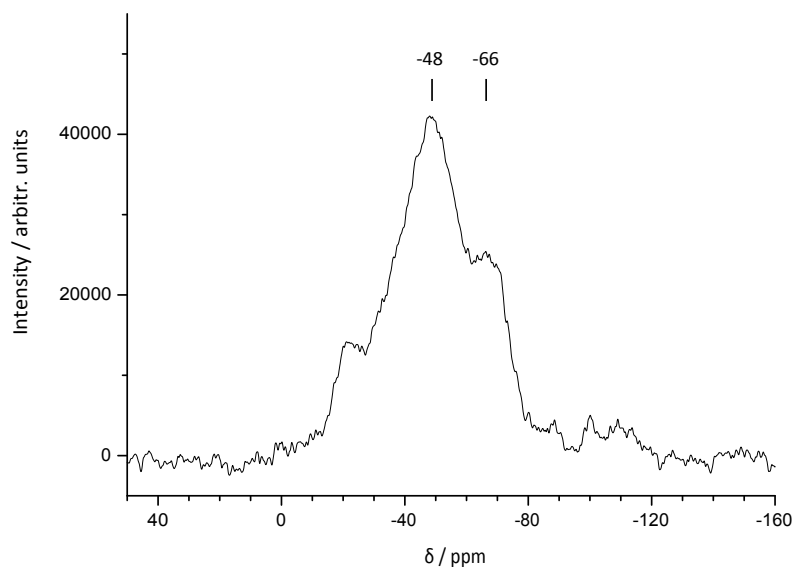


Figure B.1: ^{31}P -solid-state NMR spectrum of *coe*-PON. The signals at -20 and -100 ppm may be caused by small amounts of a high-pressure polymorph of $\text{P}_4\text{N}_6\text{O}$ with $\gamma\text{-HP}_4\text{N}_7$ -structure present in the sample used for the measurement.^[16]

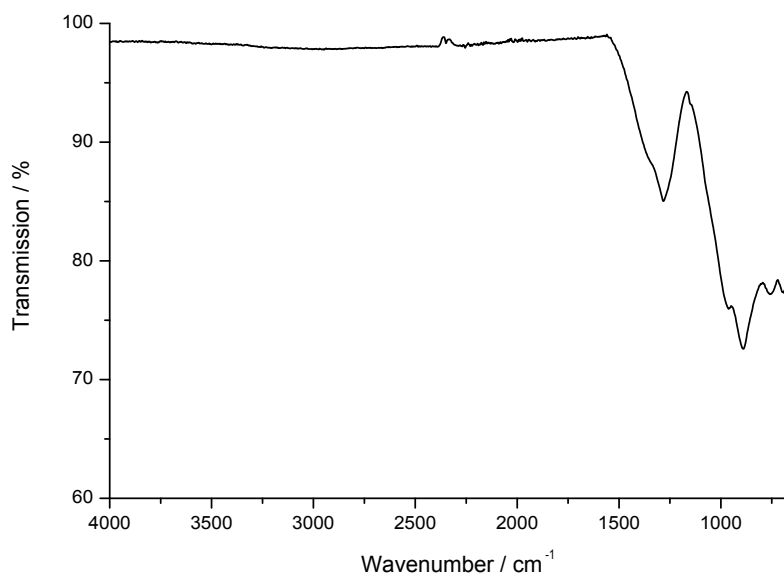


Figure B.2: FTIR spectrum of *coe*-PON.

B.7 Detailed Rietveld Plot

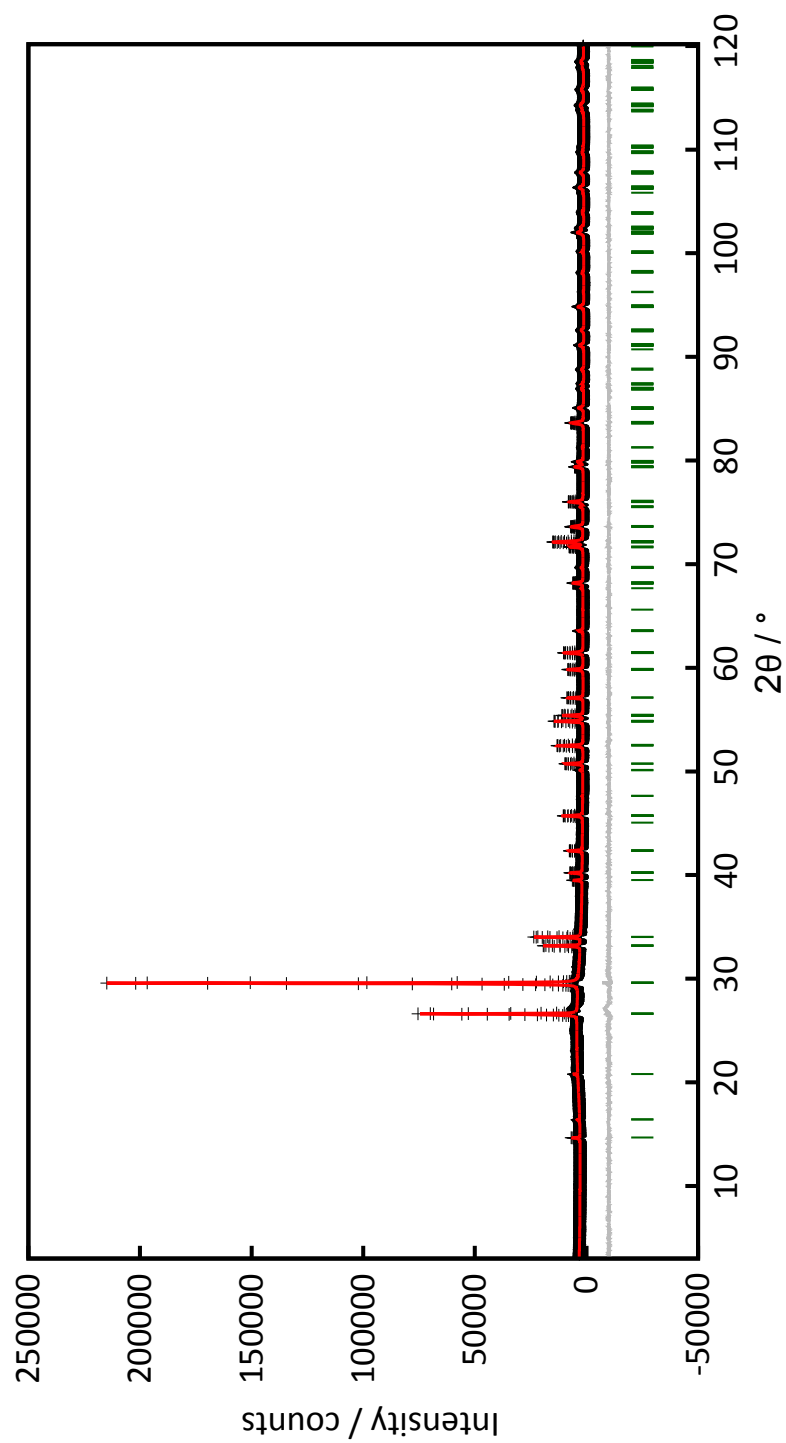
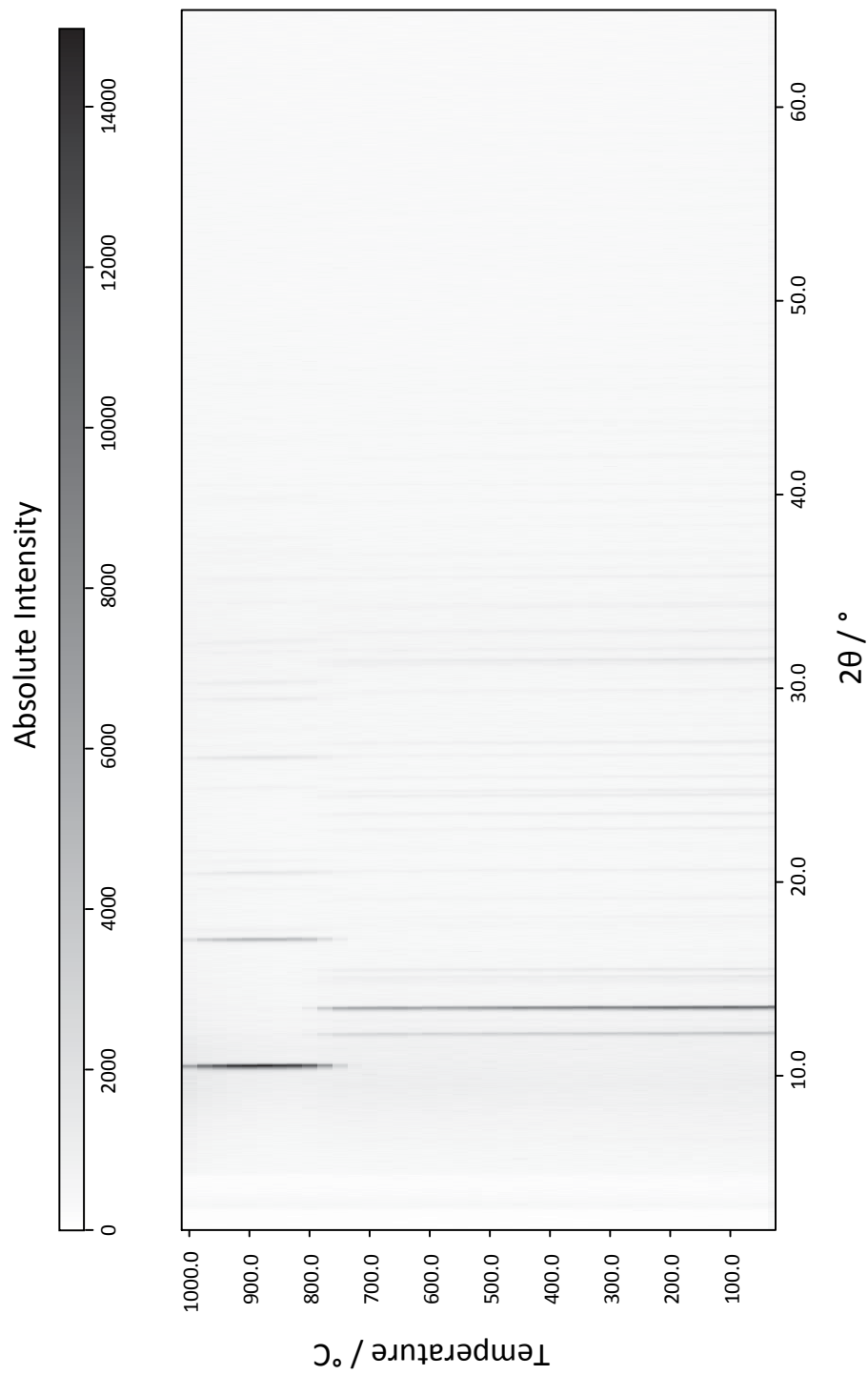


Figure B.3: Observed (crosses) and calculated (red line) powder diffraction pattern of *coe*-PON as well as positions of Bragg reflections (green) and difference profile (gray line).

B.8 Temperature Dependent Powder X-ray Diffraction

Figure B.4: Temperature dependent powder X-ray diffraction for *coe*-PON.

B.9 Details on the DFT Calculations

To corroborate the observed high pressure phase transition from β -cristobalite to coesite type for PON, ab initio calculations were performed for a variety of O/N ordering models of both structure types. Ordering models in P1 were considered, since it is not easily feasible to perform structure optimizations for statistical atom occupation, as has been proven to be the case for the O/N site of cristobalite PON, and which is also observed for the high-pressure coesite phase. Hence, to examine the trend in transition pressure, chemically reasonable ordering models, each containing PON tetrahedra with 2 O and 2 N atoms respectively, were created for both phases of PON. The different ordering variants for cristobalite and *coe*-PON are depicted in Figure B.5.

We calculated the total energies and atomic structures using density functional theory in the generalized gradient approximation (GGA) of Perdew, Burke, and Ernzerhof (PBE),^[17,18] together with the projector-augmented-wave (PAW) method,^[19,20] as implemented in the Vienna ab initio simulation package (VASP).^[21–23] The GGA was chosen over the LDA as it is typically superior in reproducing the transition pressures in solid-state materials.^[24,25] The structures of all PON models were completely optimized by relaxing all internal coordinates and cell parameters, while using a plane-wave cut-off of 535 eV. The Brillouin zone was sampled on a dense gamma centered k -mesh (cristobalite PON: $10 \times 10 \times 7$, *coe*-PON: $8 \times 5 \times 9$) produced from the method of Monkhorst and Pack^[26] to ensure high precision. The energy convergence criterion was set to 1×10^{-8} eV per unit cell to ensure accurate electronic convergence, while the residual atomic forces were converged below values of 2×10^{-3} eV/Å.

The total energies were calculated for all chosen ordering variants of cristobalite and *coe*-PON as depicted in Table B.6. As expected the difference in total energy between the ordering models is small and partly identical for cristobalite PON which is in agreement with the observed statistical ordering of N and O determined by neutron diffraction.^[27]

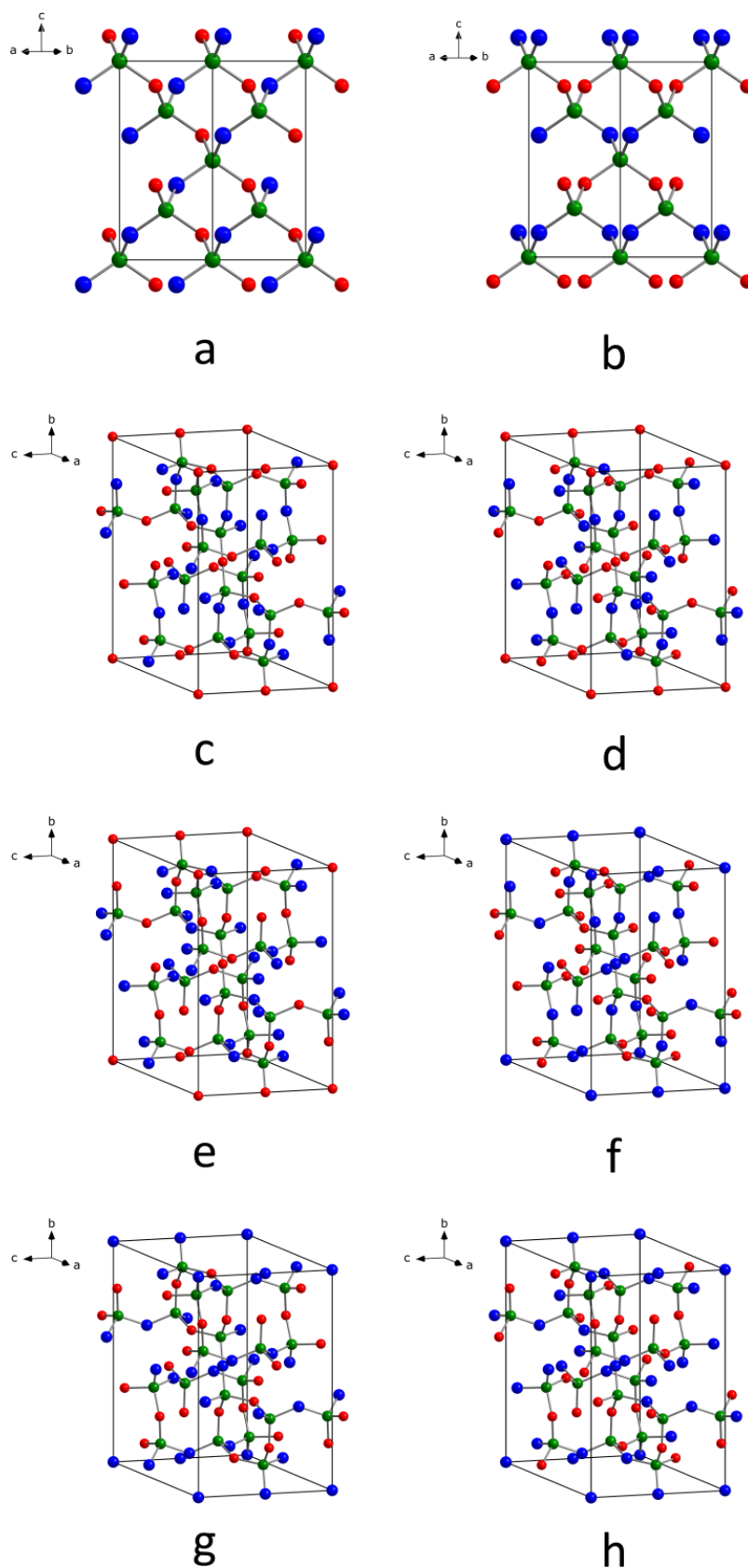


Figure B.5: Different O/N arrangements used for the DFT calculations. **a:** cristobalite PON N1N2O3O4N5N6O7O8, **b:** cristobalite PON N1O2N3O4O5N6N7O8. **c–h:** models used for *coe*-PON: **c:** O1O2O3N4N5, **d:** O1O2N3O4N5, **e:** O1O2N3N4O5, **f:** N1N2O3O4N5, **g:** N1N2O3N4O5, **h:** N1N2N3O4O5. Numbers reference the anion positions according to Table B.1.

Table B.6: Total energies per formula unit of PON for the chosen ordering models of cristobalite and *coe*-PON within the GGA.

Cristobalite-PON		<i>coe</i> -PON	
Ordering variant	Total energy (eV) / PON	Ordering variant	Total energy (eV) / PON
N1N2O3O4N5N6O7O8	−22.08301681	O1O2O3N4N5	−21.76608136
N1O2N3O4N5O6N7O8	−22.07427969	O1O2N3O4N5	−21.76171247
N1O2N3O4N5O6O7N8	−22.06690326	O1O2N3N4O5	−21.78091168
N1O2N3O4O5N6N7O8	−22.08155875	N1N2O3O4N5	−21.86939451
N1O2N3O4O5N6O7N8	−22.07427969	N1N2O3N4O5	−21.87634218
N1O2O3N4N5O6N7O8	−22.06690326	N1N2N3O4O5	−21.86940664
N1O2O3N4N5O6O7N8	−22.07427969		
N1O2O3N4O5N6N7O8	−22.07427969		
N1O2O3N4O5N6O7N8	−22.08155874		

To study the structural behavior at high pressures, the total energies were (re)calculated at constant volume for a uniform expansion of the lattice parameters to simulate an expansion and compression of volume between 103% and 96% (respectively 91% for cristobalite PON) of the originally relaxed structure, resulting in pressures up to 20 GPa. This was done only for the two energetically lowest ordering modifications of cristobalite PON, for we consider them the most fitting representation of the ambient pressure modification of cristobalite PON from which the transition is initiated in the experiment. For *coe*-PON on the other hand, all ordering variants were taken into account as the high pressure and temperature of the reaction might shift the relative stability of the ordering variants. The resulting energy-volume(E-V) curves are depicted in Figure B.6 and demonstrate further that cristobalite PON is energetically favored by about 0.2 eV compared to *coe*-PON and that a phase transition at higher pressure can be predicted. The fact that two sets of the ordering variants of *coe*-PON differ by 0.088 eV can possibly be explained by the fact that

within the three energetically lower ordering variants the (O,N)1 position, which is part of the 180° bond, is occupied by N instead of O.

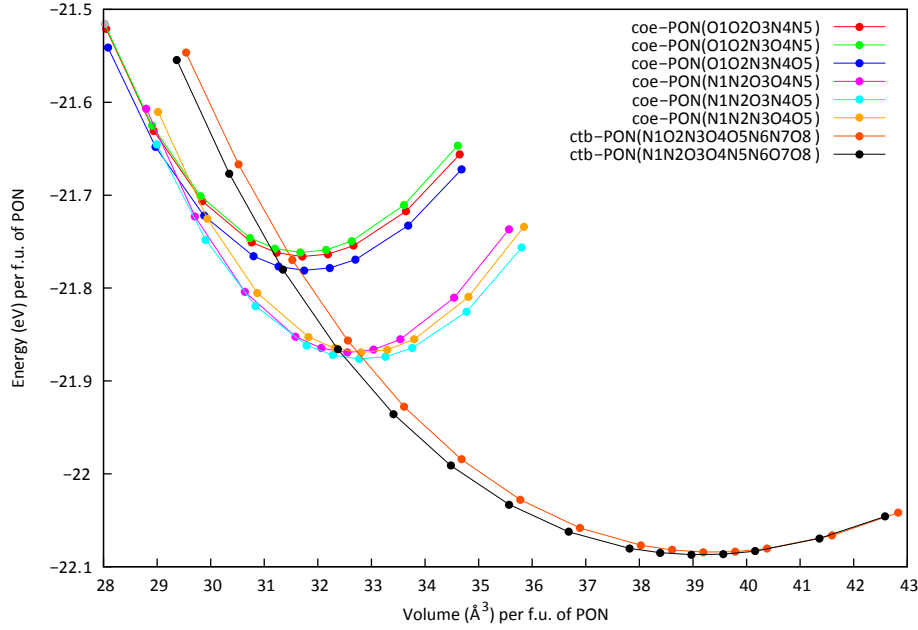


Figure B.6: Energy-volume diagram for anion ordering of the energetically lowest models of cristobalite(*ctb*)-PON and the different coesite(*coe*)-PON models. The results were obtained with GGA. Each point represents one structural optimization at constant volume. Energy and volume are given per formula unit (f.u.) of PON.

By fitting the total energies of the resulting E-V diagram with the Murnaghan equation of state (EOS)^[28] it is possible to obtain the bulk modulus B_0 as depicted in Table B.7 for the different coesite-PON models, and subsequently to create enthalpy-pressure diagrams.

Phase changes are dependent on the free energy $G = E + pV - TS$, where ΔG constitutes the driving force between the occurring transition. Due to the small difference in entropy between the crystal structures of two solid-state materials, this part of ΔG is usually neglected, reducing ΔG to ΔH , where $H = E + pV$, permitting for accurate estimations, depending only on the energy, volume and pressure of the system. By variation of the volume, the pressure can be extracted from the resulting E-V diagram by a simple numerical differentiation: $p = -\partial E / \partial V$. The enthalpy difference ΔH between two phases can, subsequently, be plotted in reference to the phase of interest, in this case with respect

to cristobalite PON. The enthalpy-pressure diagram is depicted in Figure B.7. The points of intersection for the different *coe*-PON curves with the chosen cristobalite PON curve indicate the pressure at which the free energy and enthalpy is identical for both phases and beyond which the phase transition to *coe*-PON becomes thermodynamically favored.

Table B.7: Results of the Murnaghan-EOS fit for the chosen ordering models of *coe*-PON.^[a]

Model	<i>coe</i> -PON (GGA)						\bar{x}
	O1O2O3- N4N5	O1O2N3- O4N5	O1O2N3- N4O5	N1N2O3- O4N5	N1N2O3- N4O5	N1N2N3- O4O5	
E_0	-21.76	-21.76	-21.78	-21.86	-21.87	-21.86	
V_0	31.70	31.67	31.74	32.55	32.76	32.80	
B_0	151.5	156.3	149.4	169.4	150.5	168.8	157.7
B'	3.3	2.7	3.1	1.9	1.5	1.7	

[a] Energy and volume are given in eV and \AA^3 , respectively. The bulk modulus B_0 for zero pressure is given in GPa. B' is the dimensionless derivative of the bulk modulus at zero pressure. \bar{x} is the arithmetic mean.

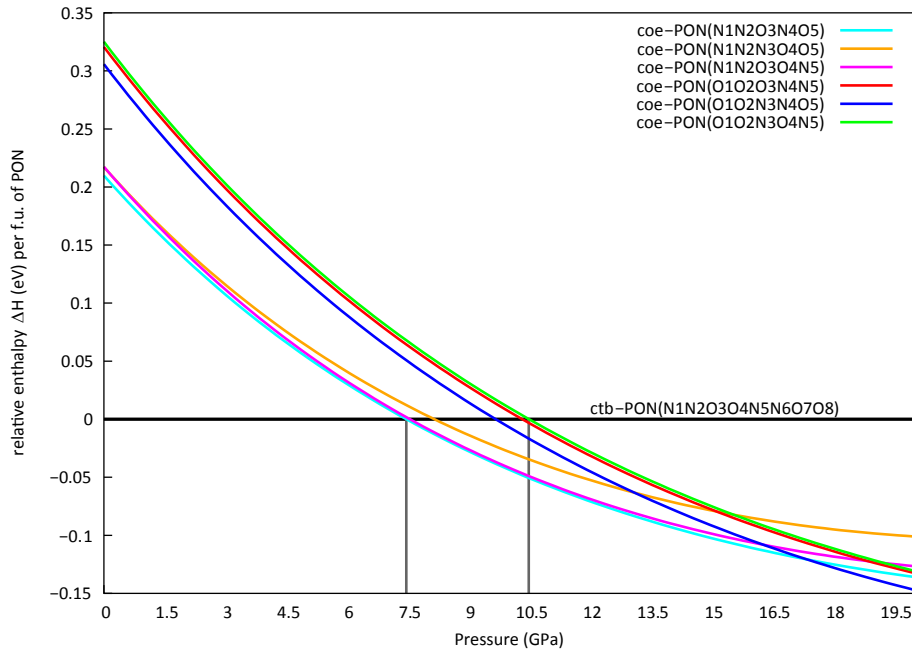


Figure B.7: Enthalpy-pressure diagram for the high pressure phase transition of PON from the energetically most stable cristobalite (*ctb*) model to the different coesite(*coe*) models as obtained by fitting the Murnaghan equation of state from the energy-volume diagram. The enthalpy is given per formula unit of PON relative to the *ctb* modification of PON. The approximate range of pressure for the transitions is indicated by the dotted lines.

From Figure B.7 a transition pressure for PON of about 7.5 GPa can be extracted for the transition of the energetically lowest cristobalite model to the energetically lowest coesite model, while the highest possible pressure is determined to about 10.5 GPa for the transition to the energetically most unfavorable coesite model. While we cannot guarantee having examined every possible modification for the ordering variants of coesite and cristobalite, the broad variety of chosen PO_2N_2 -tetrahedron-models are all in good agreement with the experimental observation on the formation of coesite-like PON at pressures of 15 GPa. The enthalpy curves of all models of *coe*-PON are energetically very close in terms of enthalpy, and do intersect each other beyond pressures of 12.5 GPa, further corroborating the observed statistical contribution of the O and N positions in *coe* PON.

B.10 References

- [1] R. Klement, O. Koch, *Chem. Ber.* **1954**, 87, 333.
- [2] N. Kawai, S. Endo, *Rev. Sci. Instrum.* **1970**, 41, 1178.
- [3] D. Walker, M. A. Carpenter, C. M. Hitch, *Am. Mineral.* **1990**, 75, 1020.
- [4] D. Walker, *Am. Mineral.* **1991**, 76, 1092.
- [5] D. C. Rubie, *Phase Transitions* **1999**, 68, 431.
- [6] H. Huppertz, *Z. Kristallogr.* **2004**, 219, 330.
- [7] A. Coelho, *TOPAS-Academic Version 4.1*, Coelho Software: Brisbane, **2007**.
- [8] A. A. Coelho, *J. Appl. Crystallogr.* **2003**, 36, 86.
- [9] G. Oszlányi, A. Sütő, *Acta Crystallogr. Sect. A: Found. Crystallogr.* **2004**, 60, 134.
- [10] G. Oszlányi, A. Sütő, *Acta Crystallogr. Sect. A: Found. Crystallogr.* **2008**, 64, 123.
- [11] A. A. Coelho, *Acta Crystallogr. Sect. A: Found. Crystallogr.* **2007**, 63, 400.
- [12] R. W. Cheary, A. Coelho, *J. Appl. Crystallogr.* **1992**, 25, 109.

-
- [13] R. W. Cheary, A. A. Coelho, J. P. Cline, *J. Res. Natl. Inst. Stand. Technol.* **2004**, 109, 1.
- [14] M. Järvinen, *J. Appl. Crystallogr.* **1993**, 26, 525.
- [15] G. Gibbs, C. Prewitt, K. Baldwin, *Z. Kristallogr. Kristallgeom. Kristallphys. Kristallchem.* **1977**, 145, 108.
- [16] D. Baumann, W. Schnick, *Angew. Chem. Int. Ed.* **2014**, 53, 14490; *Angew. Chem.* **2014**, 126, 14718.
- [17] J. P. Perdew, K. Burke, M. Ernzerhof, *Phys. Rev. Lett.* **1996**, 77, 3865.
- [18] J. P. Perdew, K. Burke, M. Ernzerhof, *Phys. Rev. Lett.* **1997**, 78, 1396.
- [19] P. E. Blöchl, *Phys. Rev. B* **1994**, 50, 17953.
- [20] G. Kresse, D. Joubert, *Phys. Rev. B* **1999**, 59, 1758.
- [21] G. Kresse, J. Hafner, *Phys. Rev. B* **1993**, 47, 558.
- [22] G. Kresse, J. Hafner, *Phys. Rev. B* **1994**, 49, 14251.
- [23] G. Kresse, J. Furthmüller, *Comput. Mater. Sci.* **1996**, 6, 15.
- [24] J. E. Jaffe, J. A. Snyder, Z. Lin, A. C. Hess, *Phys. Rev. B* **2000**, 62, 1660.
- [25] P. Kroll, W. Schnick, *Chem. Eur. J.* **2002**, 8, 3530.
- [26] H. J. Monkhorst, J. D. Pack, *Phys. Rev. B* **1976**, 13, 5188.
- [27] J. M. Léger, J. Haines, L. S. de Oliveira, C. Chateau, A. L. Sauze, R. Marchand, S. Hull, *J. Phys. Chem. Solids* **1999**, 60, 145.
- [28] F. D. Murnaghan, *Proc. Natl. Acad. Sci. USA* **1944**, 30, 244.

C Supporting Information for Chapter 4

C.1 Additional Crystallographic Data for β -HP₄N₇

Table C.1: Anisotropic displacement parameters for β -HP₄N₇ with standard deviations in parentheses.

atom	U ₁₁	U ₂₂	U ₃₃	U ₂₃	U ₁₃	U ₁₂
P1	0.0048(3)	0.0023(3)	0.0045(3)	0.0000(2)	0.0012(2)	−0.0001(2)
P2	0.0040(3)	0.0028(3)	0.0050(3)	−0.0005(2)	−0.0004(2)	−0.0003(2)
N1	0.0060(11)	0.0044(11)	0.0073(12)	0	−0.0012(9)	0
N2	0.0075(8)	0.0066(8)	0.0037(8)	0.0017(7)	0.0001(6)	−0.0015(7)
N3	0.0074(8)	0.0031(7)	0.0054(8)	−0.0013(7)	0.0025(6)	0.0002(6)
N4	0.0061(8)	0.0023(7)	0.0070(8)	−0.0008(6)	0.0028(7)	−0.0001(6)

Table C.2: Complete bond angles / ° for β -HP₄N₇.

N2–P1–N3	117.57(11)	N2–P2–N4	109.62(10)
N2–P1–N4	109.13(10)	N3–P2–N4	103.69(10)
N2–P1–N4	107.89(9)	P2–N1–P2	142.4(2)
N3–P1–N4	107.99(10)	P1–N2–P2	136.23(15)
N3–P1–N4	104.46(9)	P1–N3–P2	125.26(12)
N4–P1–N4	109.56(10)	P1–N4–P1	119.28(11)
N1–P2–N2	106.39(10)	P1–N4–P2	123.26(11)
N1–P2–N3	120.84(12)	P1–N4–P2	117.28(11)
N1–P2–N4	104.44(9)	P1–N2–H1	116(5)
N2–P2–N3	111.31(10)	P2–N2–H1	106(5)

C.2 Details of the Rietveld Refinement

Table C.3: Crystal details for β -HP₄N₇.

formula	HP ₄ N ₇
formula mass / g · mol ⁻¹	222.96
crystal system / space group	monoclinic, C2/c
lattice parameters	$a = 12.89455(9) \text{ \AA}$
	$b = 4.66185(3) \text{ \AA}$
	$c = 8.33451(6) \text{ \AA}$
	$\beta = 77.6404(6)^\circ$
cell volume / \AA^3	489.396(6)
formula units per cell Z	4
X-ray density / g · cm ⁻³	30.122
linear absorption coefficient / cm ⁻¹	137.29
radiation	Cu-K α_1 ($\lambda = 154.056 \text{ pm}$)
monochromator	Ge(111)
diffractometer	Stoe StadiP
detector	linear PSD
2θ -range / °	10–90
temperature / K	298(2)
data points	8000
number of observed reflections	202
number of parameters	60
constraints	0
program used	TOPAS Academic
structure refinement	Rietveld-Method
profile function	fundamental parameters model
background function	shifted Chebychev
R_{wp}	0.07725
R_{p}	0.05207
R_{Bragg}	0.018355
χ^2	3.705

C.3 Solid-State NMR Spectrum

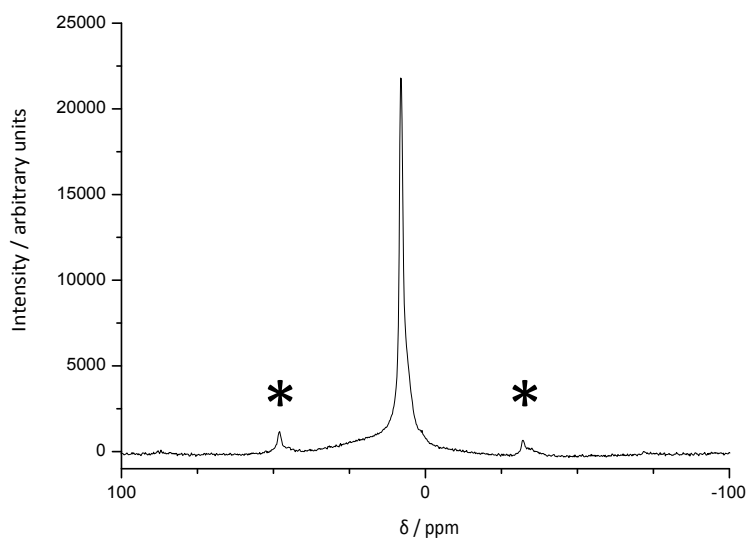


Figure C.1: ^1H -solid-state NMR-spectrum of $\beta\text{-HP}_4\text{N}_7$. Rotational sidebands are marked with asterisks.

C.4 Diffuse Reflectance Spectroscopy

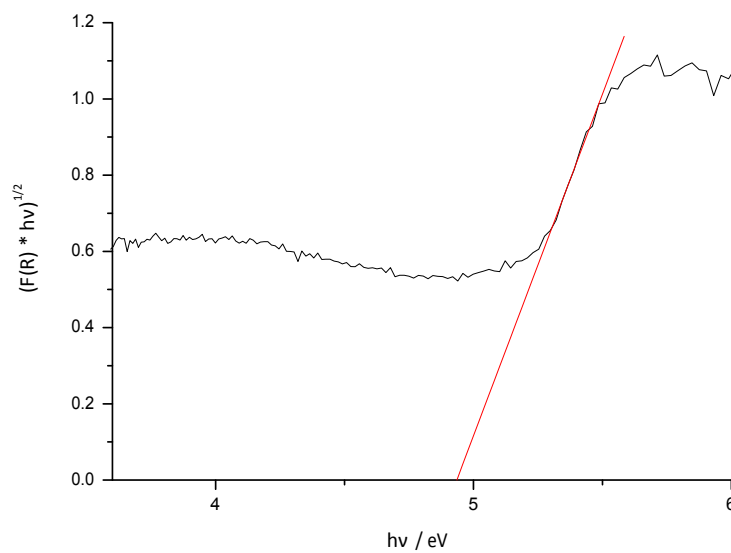


Figure C.2: Tauc Plot ($n = 1/2$) for $\beta\text{-HP}_4\text{N}_7$.

C.5 Detailed Rietveld Plot

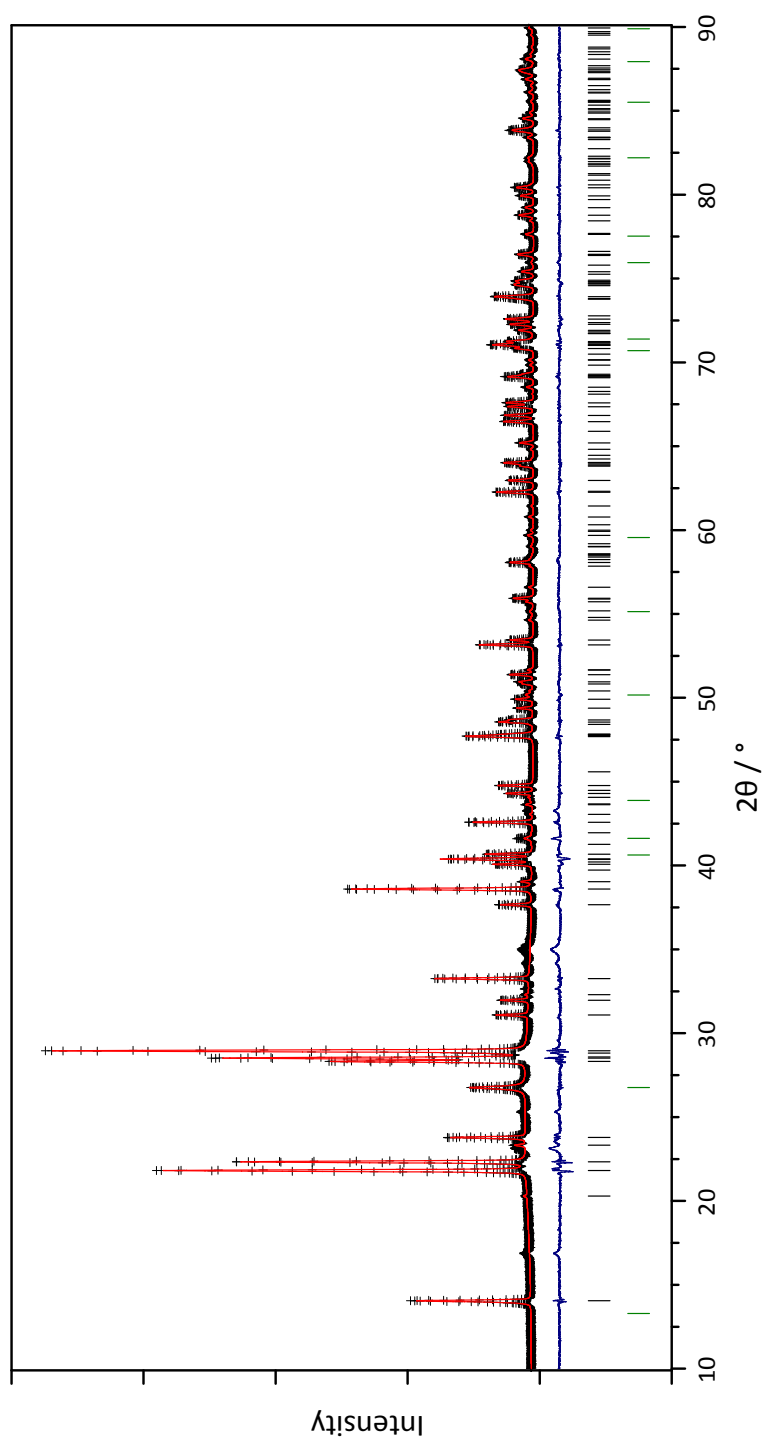
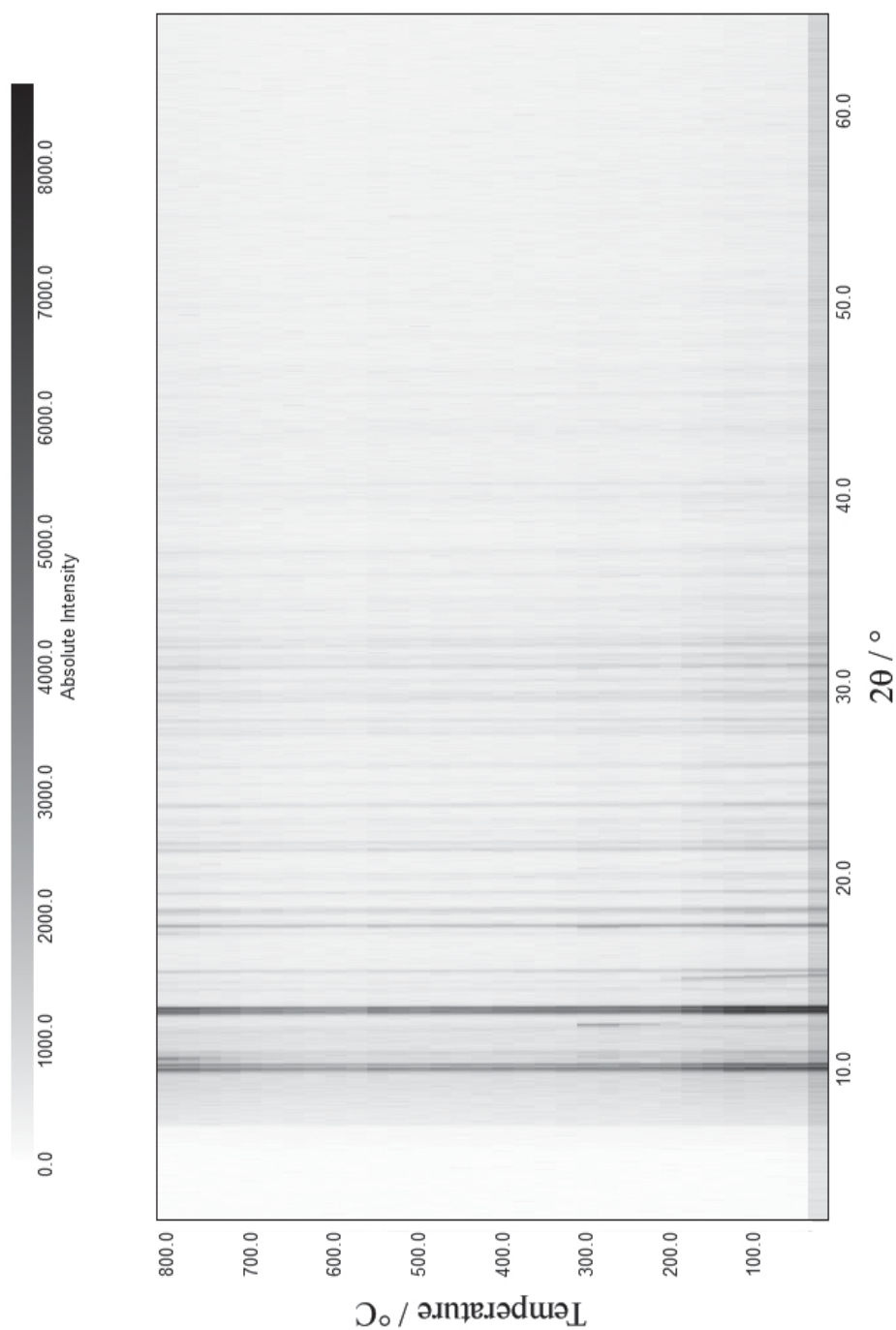


Figure C.3: Observed (crosses) and calculated (red line) powder diffraction pattern of β -HP₄N₇ as well as position of Bragg reflections (black: β -HP₄N₇; green: BN) and difference profile (blue line).

C.6 Temperature Dependent Powder X-ray Diffraction

Figure C.4: Temperature dependent powder X-ray diffraction for β -HPN₇.

D Supporting Information for Chapter 5

D.1 Experimental Details of the HP/HT-Synthesis of γ -HP₄N₇

Phosphorus nitride P₃N₅ was synthesized according to the procedure described by *Stock* and *Grüneberg*.^[1] Inside an open silica glass tube (outer diameter 3 cm, wall thickness 2 mm, length 30 cm), placed inside a larger silica glass flow tube P₄S₁₀ (8.0 g, 36 mmol, 99%, Sigma-Aldrich) was saturated with dry NH₃ gas (99.98%, Air Liquide) in a continuous flow for 4 h at room temperature. This resulted in a noticeably exothermic reaction. In the second reaction step the temperature was raised to 850 °C at a rate of 3 °C/min while maintaining the gas flow. After 8 h the product was cooled, ground and washed successively with 1M HCl deionized water, ethanol and acetone to remove soluble byproducts. After drying the product at 100 °C P₃N₅ is obtained as a yellow-brown solid. γ -HP₄N₇ was synthesized by reacting P₃N₅ (10 mg, 61 μ mol) with NH₄Cl (0.8 mg, 15 μ mol, 99.5 %, Sigma-Aldrich) at a pressure of 14 GPa and a temperature of approximately 1200 °C. The reaction was carried out in a Walker-type multianvil assembly placed inside a 1000 t hydraulic press (Voggenreiter, Mainleus, Germany), details of which can be found in the literature.^[2–6] The reactants were thoroughly ground in an agate mortar and tightly packed into a hexagonal boron nitride crucible, which was in turn placed inside two concentric graphite heater tubes. This assembly was placed in a Cr³⁺-doped MgO octahedron with an edge length of 10 mm (Ceramic Substrates and Components, Isle of Wight, UK). The whole assembly was compressed between eight tungsten carbide cubes (Hawedia, Marklkofen, Germany) with a truncation edge length of 5 mm. Compression was performed during 270 min. Then the temperature was raised to approximately 1200 °C within 60 min. After holding the temperature for 120 min the sample was cooled within 60 min. After decom-

pression the sample was isolated and mechanically separated from the crucible material. The sintered pellet was broken up in an agate mortar and the sample was washed with deionized water, ethanol and acetone successively. After drying at 100 °C the sample was obtained as a light gray crystalline air-stable solid.

D.2 Information on the Data Collection and Structure Elucidation of γ -HP₄N₇

A single crystal ($0.011 \times 0.026 \times 0.026$ mm³) for the structure analysis was selected in paraffin oil under an optical microscope. The crystal was mounted on a micromount (aperture size 20 μ m, MiTeGen, Ithaca, USA). Data collection was carried out on a Bruker D8 Venture (Bruker, Bellerica, USA) diffractometer equipped with a rotating anode generator and multilayer optics (Mo-K α , $\lambda = 71.073$ pm). A multi-scan absorption correction was carried out using SADABS (Bruker). The crystal structure was solved with direct methods using SHELXS-97. Subsequent full-matrix least squares refinement was carried out on F^2 using SHELXL-97.^[7] Powder diffraction data was collected in parafocusing Debye-Scherrer geometry (0.28 mm capillary inner diameter) on a Stoe StadiP diffractometer (Stoe & Cie, Darmstadt, Germany) using Cu-K α_1 radiation. The diffractometer was equipped with a Ge(111) monochromator and a MYTHEN 1K microstrip detector (DeCTRIS, Baden, Switzerland). Rietveld refinement was carried out using TOPAS-Academic 4.1.^[8] The structure model from the single crystal structure determination was used as a starting model. Peak shapes were modeled using the fundamental parameters approach (direct convolution of source emission profiles, axial instrument contributions and crystallite size and microstrain effects).^[9] The measured data was corrected for absorption using the linear absorption coefficient of the refined substance mixture.

D.3 Crystallographic Data for γ -HP₄N₇**Table D.1:** Fractional atomic coordinates, isotropic thermal displacement parameters, and site occupancies for γ -HP₄N₇.

atom	Wyckoff position	x	y	z	$U_{eq} / \text{\AA}^2$	occupancy
P1	$8f$	0.2341(2)	0.2579(1)	0.29712(8)	0.0045(2)	1
P2	$8f$	0.3378(2)	0.0819(1)	0.02327(8)	0.0035(2)	1
N1	$8f$	0.2074(4)	0.0603(3)	0.5943(3)	0.0034(4)	1
N2	$8f$	0.2941(4)	0.2814(3)	0.1312(3)	0.0032(4)	1
N3	$4e$	0	0.1915(5)	$\frac{1}{4}$	0.0057(6)	1
N4	$8f$	0.3990(4)	0.0898(3)	0.3984(3)	0.0036(4)	1

Table D.2: Anisotropic displacement parameters / \AA^2 for γ -HP₄N₇.

atom	U_{11}	U_{22}	U_{33}	U_{23}	U_{13}	U_{12}
P1	0.0042(3)	0.0051(3)	0.0044(3)	0.0006(2)	0.0018(2)	0.0007(2)
P2	0.0031(3)	0.0035(3)	0.0035(3)	0.0003(2)	0.0008(2)	0.0005(2)
N1	0.0040(9)	0.003(1)	0.0047(9)	−0.0018(8)	0.0026(8)	0.0003(8)
N2	0.0044(9)	0.004(1)	0.0022(9)	0.0010(8)	0.0018(8)	0.0019(8)
N3	0.002(2)	0.007(2)	0.008(2)	0	0.002(2)	0
N4	0.0026(9)	0.0037(9)	0.0038(9)	0.0019(8)	0.0003(8)	−0.0002(8)

Table D.3: Interatomic distances / \AA for γ -HP₄N₇.

P1–N1	1.596(2)	P2–N2'	1.818(2)
P1–N2	1.686(2)	P2–N4	1.671(2)
P1–N3	1.567(2)	P2–N4'	1.817(2)
P1–N4	1.678(2)	P2–P2'	2.667(2)
P2–N1	1.629(2)	P2'–P2	2.670(2)
P2–N2	1.672(2)		

Table D.4: Bond angles / ° for γ -HP₄N₇.

N3–P1–N1	114.9(2)	N2–P2–P2	111.03(9)
N3–P1–N4	109.9(2)	N4–P2–P2	38.14(7)
N1–P1–N4	107.2(2)	N2–P2–P2	137.58(9)
N3–P1–N2	109.90(9)	N1–P2–P2	111.00(9)
N1–P1–N2	111.6(2)	N4–P2–P2	112.64(9)
N4–P1–N2	102.8(2)	N2–P2–P2	42.15(8)
N1–P2–N4	120.6(2)	N4–P2–P2	135.53(9)
N1–P2–N2	119.4(2)	N2–P2–P2	38.10(7)
N4–P2–N2	120.0(2)	P2–P2–P2	136.66(5)
N1–P2–N4	95.1(2)	P1–N1–P2	134.9(2)
N4–P2–N4	80.3(2)	P2–N2–P1	124.1(2)
N2–P2–N4	93.9(2)	P2–N2–P2	99.8(2)
N1–P2–N2	94.3(2)	P1–N2–P2	121.8(2)
N4–P2–N2	96.1(2)	P1–N3–P1	144.4(2)
N2–P2–N2	80.3(2)	P2–N4–P1	131.1(2)
N4–P2–N2	170.5(2)	P2–N4–P2	99.7(2)
N1–P2–P2	112.32(9)	P1–N4–P2	124.6(2)
N4–P2–P2	42.20(8)		

Table D.5: Details of the single crystal X-ray refinement for γ -HP₄N₇.

formula	HP ₄ N ₇
formula mass / g · mol ⁻¹	222.96
crystal system / space group	monoclinic, C2/c (no. 15)
lattice parameters / Å, °	$a = 6.8018(4)$
	$b = 7.2204(5)$
	$c = 8.9572(6)$
	$\beta = 111.231(2)$
cell volume / Å ³	410.05(5)
formula units per cell Z	4
X-ray density / g · cm ⁻³	3.612
linear absorption coefficient / mm ⁻¹	1.734
radiation	Mo-K _α ($\lambda = 71.073$ pm)
diffractometer	Bruker D8 Venture
2 θ -range / °	4.28–30.48
temperature / K	298(2)
$F(000)$	436
observed reflections	5565
independent reflections ($> 2\sigma$)	628 (555)
number of parameters	51
R_{int} ; R_σ	0.0273; 0.0174
final R indices [$I > 2\sigma(I)$]	$R_1 = 0.0252$
	$wR_2 = 0.0788^{[a]}$
final R indices (all data)	$R_1 = 0.0301$
	$wR_2 = 0.0814^{[a]}$
Goodness of fit	1.197

[a] $w = 1/[\sigma^2(F_o^2) + (0.0458 P)^2 + 2.3837 P]$, with $P = (F_o^2 + 2F_c^2) / 3$

D.4 Details of the Rietveld Refinement

Table D.6: Details of the Rietveld refinement for γ -HP₄N₇.

formula	HP ₄ N ₇
formula mass / g · mol ⁻¹	222.96
crystal system / space group	monoclinic, C2/c (no. 15)
lattice parameters / Å, °	$a = 6.82983(5)$
	$b = 7.24537(6)$
	$c = 8.96504(7)$
	$\beta = 111.5557(3)$
cell volume / Å ³	412.604(5)
formula units per cell Z	4
X-ray density / g · cm ⁻³	3.572
linear absorption coefficient / cm ⁻¹	1.628
radiation	Cu-K _{α1} ($\lambda = 154.056$ pm)
monochromator	Ge(111)
diffractometer	Stoe StadiP
detector	MYTHEN 1K
2 θ -range / °	3–110.385
temperature / K	298(2)
data points	7160
number of observed reflections	268
number of parameters	68
constraints	0
program used	TOPAS Academic
structure refinement	Rietveld-Method
profile function	fundamental parameters model
background function	shifted Chebychev
R_{wp}	0.03457
R_p	0.02487
R_{Bragg}	0.01742
χ^2	3.118

D.5 Solid-State NMR and FTIR Spectra

Solid-state NMR spectra were collected on an Avance III spectrometer (Bruker) under MAS conditions using a 1.2 mm probe. The chemical shift values are referenced to 0.1% TMS in CDCl_3 (Sigma-Aldrich) as an external reference. The FTIR spectrum was collected on a IFS 66 v/S spectrometer (Bruker) using KBr disks prepared in an Ar filled glovebox.

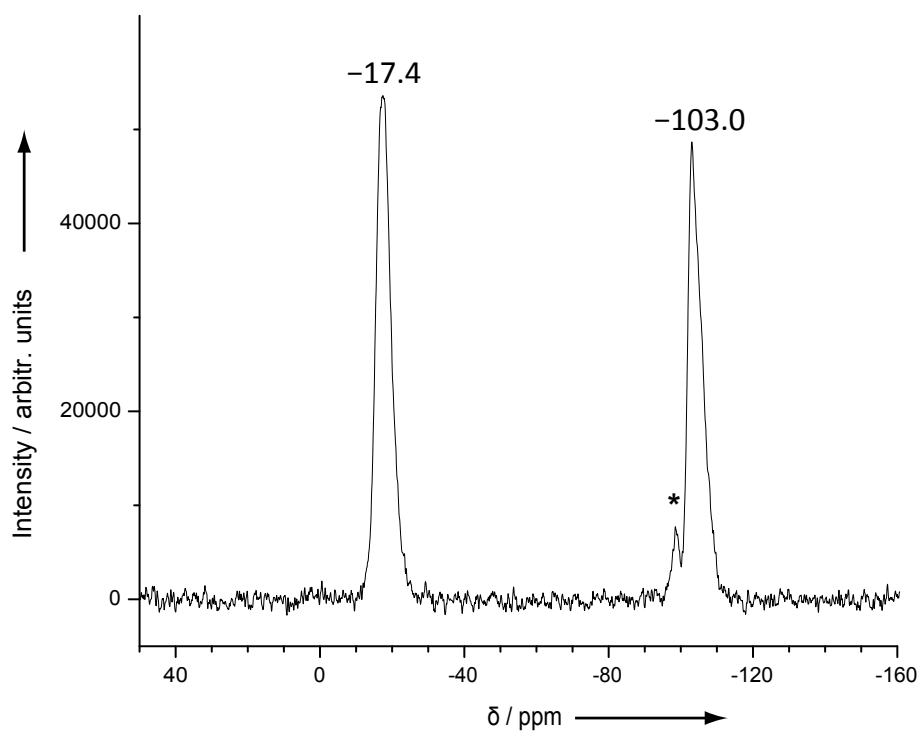


Figure D.1: ^{31}P -solid-state NMR-spectrum of $\gamma\text{-HP}_4\text{N}_7$. Rotational sidebands are marked with asterisks.

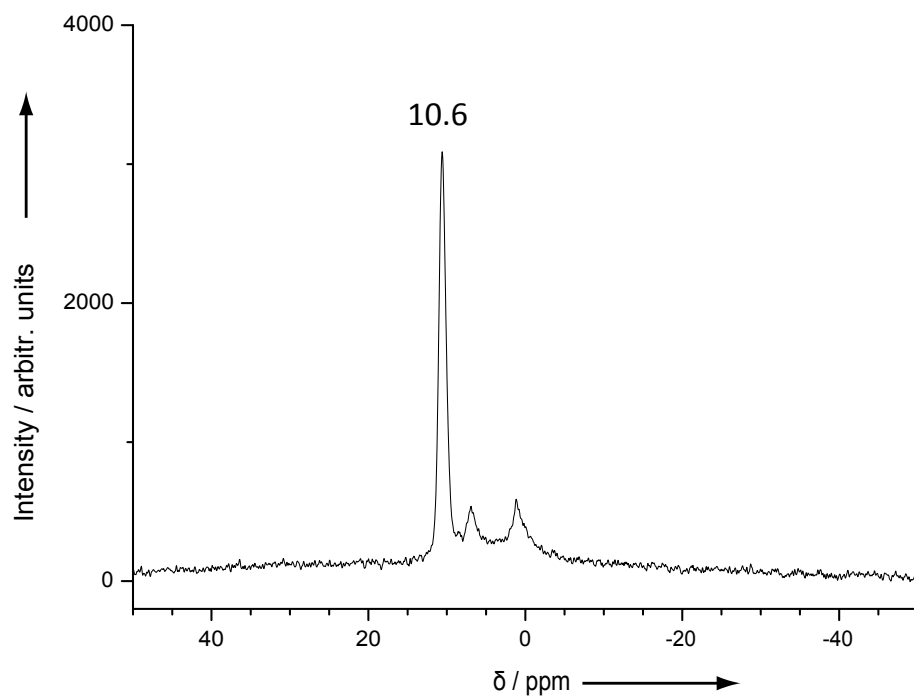


Figure D.2: ¹H-solid-state NMR-spectrum of γ -HP₄N₇.

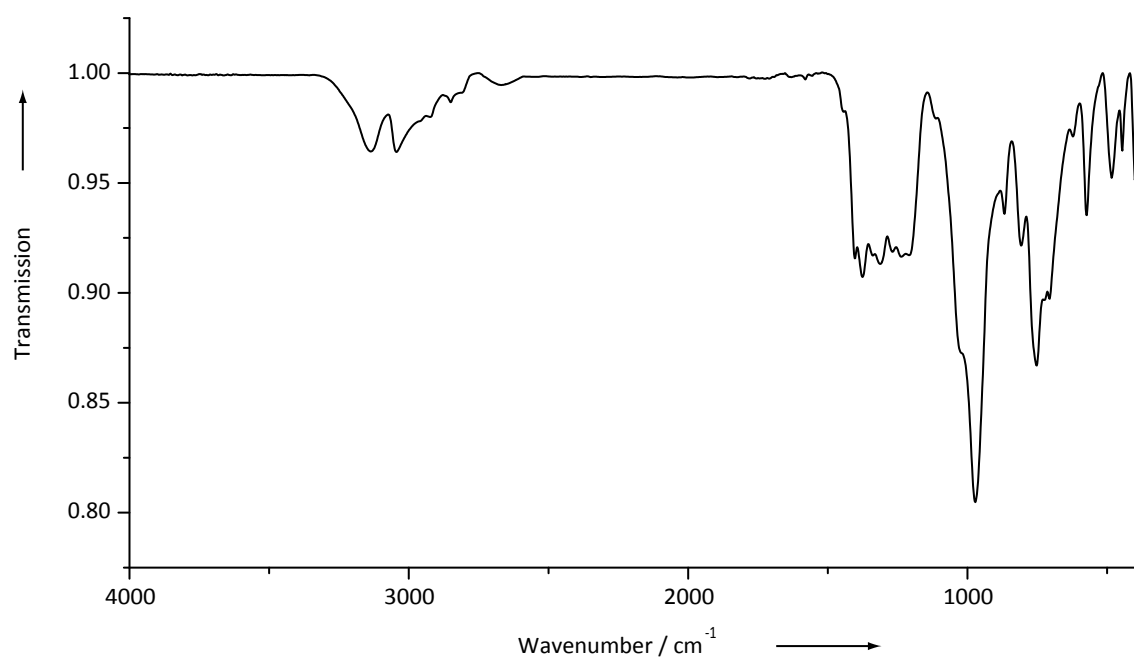


Figure D.3: FTIR spectrum of γ -HP₄N₇.

D.6 Energy Dispersive X-Ray Spectroscopy

The sample was prepared by dusting the sample on a conductive adhesive film and sputtering the surface with carbon using a BAL-TEC MED 020 evaporator (Bal-Tec AG, Liechtenstein). The analysis was performed using a EOL JSM-6500F field emission scanning electron microscope using an accelerating voltage of 10 kV.

Table D.7: Results of energy dispersive X-Ray spectroscopy.

	P / atom %	N / atom %	O / atom %
expected for HP_4N_7	36	64	0
measured	33	63	4

D.7 References

- [1] A. Stock, H. Grüneberg, *Ber. Dtsch. Chem. Ges.* **1907**, 40, 2573.
- [2] N. Kawai, S. Endo, *Rev. Sci. Instrum.* **1970**, 41, 1178.
- [3] D. Walker, M. A. Carpenter, C. M. Hitch, *Am. Mineral.* **1990**, 75, 1020.
- [4] D. Walker, *Am. Mineral.* **1991**, 76, 1092.
- [5] D. C. Rubie, *Phase Transitions* **1999**, 68, 431.
- [6] H. Huppertz, *Z. Kristallogr.* **2004**, 219, 330.
- [7] G. M. Sheldrick, *Acta Crystallogr. Sect. A: Found. Crystallogr.* **2008**, 64, 112.
- [8] A. Coelho, *TOPAS-Academic Version 4.1*, Coelho Software: Brisbane, **2007**.
- [9] R. Cheary, A. Coelho, *J. Appl. Crystallogr.* **1992**, 25, 109.

E Supporting Information for Chapter 6

E.1 Additional Crystallographic Data for $\text{Li}_{14}(\text{PON}_3)_2\text{O}$

Table E.1: Bond lengths / pm for $\text{Li}_{14}(\text{PON}_3)_2\text{O}$.

P1–O1	170.0(9)	Li2–O2	181(1)
P1–N1	172.8(7)	Li2–N1	196(2)
Li1–N1	178(2)	Li2–O1	205(2)
Li1–N1'	211(2)	Li2–O1'	231(2)
Li1–N1''	216(2)	Li3–N1	198(2)
Li1–N1'''	227(2)	Li3–O2	219(9)

E.2 ^7Li Solid-State NMR Spectrum

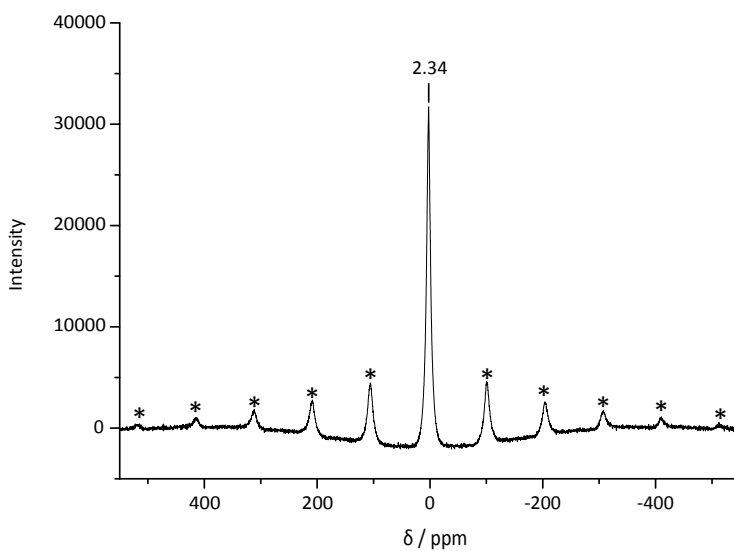


Figure E.1: ^7Li -solid-state NMR-spectrum of $\text{Li}_{14}(\text{PON}_3)_2\text{O}$. Rotational sidebands are marked with asterisks.

E.3 Detailed Rietveld Plot

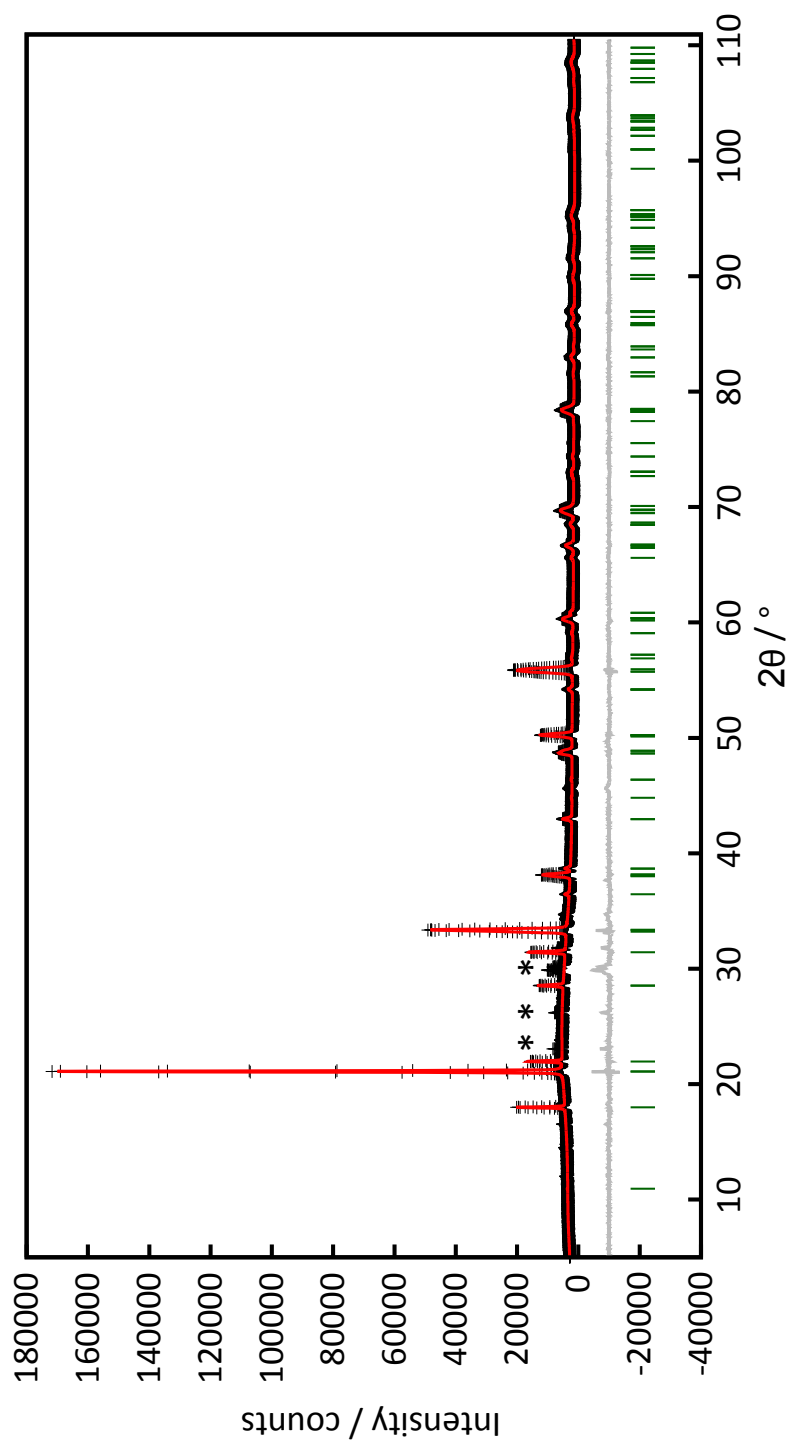


Figure E.2: Observed (crosses) and calculated (red line) powder diffraction pattern of $\text{Li}_{14}(\text{PON}_3)_2\text{O}$ as well as position of Bragg reflections (green) and difference profile (gray line). Reflections from an unknown side phase are marked with asterisks.

F Miscellaneous

F.1 List of Publications

The results compiled in this thesis were published in scientific journals as detailed in the following list. Publications exceeding the scope of this thesis are not included in the previous chapters and are compiled in a separate list.

F.1.1 Publications Within this Thesis

1. An Unprecedented AB₂ Tetrahedra Network Structure Type in a High-Pressure Phase of Phosphorus Oxonitride PON

Dominik Baumann, Stefan J. Sedlmaier, Wolfgang Schnick

published in: *Angew. Chem. Int. Ed.* **2012**, 51, 4707. DOI: 10.1002/anie.201200811

published in: *Angew. Chem.* **2012**, 121, 4785. DOI: 10.1002/ange.201200811

Writing the manuscript, synthesis of the samples, literature and database research, topological analysis, MAPLE calculations and creation of graphical material was done by Dominik Baumann. Evaluation of analytical data, structure elucidation and Rietveld refinement were performed by Dominik Baumann and Stefan J. Sedlmaier in close collaboration. Wolfgang Schnick directed and supervised the work. All authors revised the manuscript.

2. A High-Pressure Polymorph of Phosphorus Oxonitride PON with Coesite Structure

Dominik Baumann, Robin Niklaus, Wolfgang Schnick

published in: *Angew. Chem. Int. Ed.* **2015**, 54, 4388. DOI: 10.1002/anie.201410526

published in: *Angew. Chem.* **2015**, 127, 4463. DOI: 10.1002/ange.201410526

Writing the main parts of the manuscript, creation of graphical material, literature research, synthesis of the sample, structure elucidation, evaluation of spectroscopic data and topological analysis were performed by Dominik Baumann. DFT calculations and evaluation thereof were performed by Robin Niklaus. Wolfgang Schnick directed and supervised the work. All authors revised the manuscript.

3. A High-Pressure Polymorph of Phosphorus Nitride Imide HP_4N_7 Representing a New Framework Topology

Dominik Baumann, Wolfgang Schnick

published in: *Inorg. Chem.* **2014**, 53, 7977. DOI: 10.1021/ic500767f

For this publication, literature research, writing the manuscript, creation of graphical material, synthesis of the samples, structure elucidation, Rietveld refinement, evaluation of spectroscopic data, topological analysis and MAPLE calculations were performed by Dominik Baumann. Wolfgang Schnick directed and supervised the work. All authors revised the manuscript.

4. Pentacoordinated Phosphorus in a High-Pressure Polymorph of Phosphorus Nitride Imide $\text{P}_4\text{N}_6(\text{NH})$

Dominik Baumann, Wolfgang Schnick

published in: *Angew. Chem. Int. Ed.* **2014**, 53, 14490. DOI: 10.1002/anie.201406086

published in: *Angew. Chem.* **2014**, 126, 14718. DOI: 10.1002/ange.201406086

Literature research, creation of graphical material, writing the manuscript, synthesis of the samples, structure elucidation, Rietveld refinement, MAPLE calculations, evaluation of spectroscopic data and topological analysis were performed by Dominik Baumann. Wolfgang Schnick directed and supervised the work. All authors revised the manuscript.

5. $\text{Li}_{14}(\text{PON}_3)_2\text{O}$ – A Non-Condensed Oxonitridophosphate Oxide

Dominik Baumann, Wolfgang Schnick

published in: *Eur. J. Inorg. Chem.* **2015**, 617. DOI: 10.1002/ejic.201403125

Literature research, creation of graphical material, writing the manuscript, synthesis of the samples, structure elucidation, Rietveld refinement and evaluation of spectroscopic data were performed by Dominik Baumann. Wolfgang Schnick directed and supervised the work. All authors revised the manuscript.

F.1.2 Publications Beyond this Thesis

1. Materials Properties of Ultra-Incompressible Re_2P

Sebastian B. Schneider, Dominik Baumann, Ashkan Salamat, Zuzana Konôpková, Wolfgang Morgenroth, Hanns-Peter Liermann, Marcus Schwarz, Lkhamsuren Bayarjargal, Alexandra Friedrich, Björn Winkler, Wolfgang Schnick

published in: *Chem. Mater.* **2012**, 24, 3240. DOI: 10.1021/cm3016885

For this article, writing the main part, image editing, synthesis of the sample, literature screening, analyses of high-pressure PXRD data, determination of bulk moduli, interpretation of magnetic and electric conductivity measurements, as well as analysis of

thermal expansion coefficients were carried out by Sebastian B. Schneider. Measurements and analyses of Vickers hardness as well as chemical analysis were performed by Marcus Schwarz. In close collaboration, Sebastian B. Schneider, Dominik Baumann, Ashkan Salamat, Zuzana Konôpková, Wolfgang Morgenroth, Hanns-Peter Liermann, Lkhamsuren Bayarjargal, and Alexandra Friedrich loaded the diamond-anvil cells with samples, pressure transmitting media and standards for pressure determination upon in situ HP-investigations. All theoretical investigations were performed by Björn Winkler. Wolfgang Schnick directed and supervised the work. All authors also revised the manuscript.

2. Reversible High-Pressure Phase Transition in LaN

Sebastian B. Schneider, Dominik Baumann, Ashkan Salamat, Wolfgang Schnick

published in: *J. Appl. Phys.* **2012**, 111, 093503. DOI: 10.1063/1.4709392

For this contribution, writing the main part, image editing, literature screening, as well as the determination of bulk moduli of ambient LaN and its high-pressure polymorph were performed by Sebastian B. Schneider. Both, Sebastian B. Schneider and Dominik Baumann, measured and analyzed high-pressure PXRD data, including the identification of the high-pressure polymorph. Sebastian B. Schneider, Dominik Baumann, and Ashkan Salamat, loaded the diamond-anvil cells with samples, pressure transmitting media and standards for pressure determination. Wolfgang Schnick directed and supervised the work. All authors also revised the manuscript.

F.2 Contributions to Conferences

1. $\text{Li}_{14}\text{P}_2\text{N}_6\text{O}_3$ – Ein Lithiumoxonitridophosphat-oxid (oral presentation)

D. Baumann, W. Schnick

Hirschegg-Seminar on Solid State Chemistry 2012, Hirschegg, Austria

2. **High-pressure synthesis of novel N-based binary and multinary phases** (oral presentation)

Sebastian B. Schneider, Dominik Baumann, Wolfgang Schnick

High-Pressure Synthesis of Novel (Oxo-)Nitridosilicates, (Oxo-)Nitridophosphates and Related Binary and Multinary Phases (poster presentation)

Sebastian B. Schneider, Dominik Baumann, Wolfgang Schnick

5th Berichtskolloquium of the DFG Priority Program 1236 "Strukturen und Eigenschaften von Kristallen bei extrem hohen Drücken und Temperaturen" 2012, Bad Salzschlirf, Germany

3. **Pentacoordinated Phosphorus in a High-Pressure Polymorph of Phosphorus Nitride Imide HP_4N_7** (poster presentation)

D. Baumann, W. Schnick

8th International Symposium on Nitrides 2014, Wildbad Kreuth, Germany

F.3 Deposited Crystallographic Data

Crystallographic data for the compounds synthesized as part of this work were deposited at the Fachinformationszentrum (FIZ) Karlsruhe, Germany (fax: +49-7247-808-666, e-mail: crysdata@fiz-karlsruhe.de) and are available on quoting the following CSD depository numbers.

Compound	CSD-Number
δ -PON	423589
<i>coe</i> -PON	428382
β -HP ₄ N ₇	427230
γ -HP ₄ N ₇	427650
Li ₁₄ (PON ₃) ₂ O	428737

F.4 Curriculum Vitae

Personal Details

Name	Dominik Oskar Baumann
Date of Birth	03/05/1985
Place of Birth	München, Germany
Nationality	German

Education

since 03/2011	Research assistant in the group of Prof. Dr. Wolfgang Schnick (Department of Chemistry, <i>Ludwig-Maximilians-Universität München, Germany</i>) Doctoral thesis entitled: " <i>Structural classification of novel phosphorus (oxo)nitrides at extreme conditions</i> "
8/2010–2/2011	Master thesis (Inorganic Chemistry) <i>Ludwig-Maximilians-Universität München, Germany</i> (Prof. Dr. Wolfgang Schnick) Master thesis entitled: " <i>Synthesis and Characterization of New Phosphorus Oxonitrides</i> "
11/2008–2/2011	Master of Science (Chemistry) <i>Ludwig-Maximilians-Universität München, Germany</i>

- 7/2008–11/2008 **Bachelor thesis** (Inorganic Chemistry)
Ludwig-Maximilians-Universität München, Germany (PD Dr. Klaus Müller-Buschbaum) Bachelor thesis entitled: "*Synthese und Charakterisierung neuer Seltenerd- und Erdalkalimetallimidazolate*"
- 10/2005–11/2008 **Bachelor of Science** (Chemistry and Biochemistry)
Ludwig-Maximilians-Universität München, Germany
- 10/2004–6/2005 Civilian Service
Vereinigung Integrationsförderung e.V.
- 06/2004 **Allgemeine Hochschulreife**
- 09/1995–06/2004 Secondary School
Ludwigsgymnasium München
- 09/1991–07/1995 Primary School
Gilmschule München